AN ELECTROCHEMICAL REDUCTION PROCESS FOR THE RECOVERY OF COPPER POWDER FROM A REFINERY EFFLUENT STREAM

Chandon Bezuidenhout

Masters in Chemical Engineering - Hydrometallurgy

University of Cape Town

February 2014

DECLARATION

I know the meaning of plagiarism and declare that all the work in the document, save for that which is properly acknowledged, is my own.

C. Bezuidenhout

EXECUTIVE SUMMARY

In recent years a significant amount of research has gone into the development of a feed pre-treatment process for the concentrate refined at Anglo American Platinum's Precious Metals Refiners (PMR). Such a process has the potential to significantly simplify the downstream refining process and reduce the number of unit processes required for purification. One of the considered options involves a high temperature oxidative roast process followed by a high temperature hydrochlorination process to volatilise base metal chlorides and other impurities. The resulting precious group metal (PGM) concentrate is cleaner and thus requires significantly less process steps to final product.

The off-gas from hydrochlorination contains predominantly silver, copper, nickel and iron. This off-gas undergoes a quench-scrub to condense the base metal chlorides. The quench-scrub liquor undergoes a dechlorination process with sulfuric acid to precipitate AgCl(s). The filtrate from this process then undergoes an electrochemical reduction process to recover copper metal concentrate.

The objectives of this study were to:

i. Determine the operating conditions for an electrochemical reduction process aimed at recovering copper as a copper powder from a sulfuric acid stream containing copper, nickel and iron.

ii. Develop a conceptual flowsheet for a batch electrochemical process and estimate the capital cost and operating cost.

Bench-scale experimental work was conducted using two 4 L electrochemical reactors with titanium cathodes and dimensionally stable anodes. Synthetic solutions were made up to the anticipated feed concentrations of 30 g/L copper, 10 g/L nickel, 6 g/L iron and 1 mol/L sulfuric acid. Solutions were treated at high current densities (≈1 000 A/m^2) to promote the formation of copper powder. After seven hours of electrochemical reduction the electrolyte and solids were removed from the cell, filtered and washed. In order to determine the optimal operating conditions and impact of feed variability on the process, the following parameters were varied: applied current; initial acidity; initial copper concentration; initial nickel concentration; and initial iron concentration.

It was found that after seven hours of electrochemical reduction near-complete reduction of Cu^{2+}(aq) to Cu(s) could be achieved for all experimental runs. The Cu(s) that formed did not adhere to the cathode surface and gravitated to the bottom of the cell for subsequent recovery. After filtration and washing of the solids, various degrees of copper powder re-dissolutions were observed.

During the electrochemical reduction the nickel and iron in solution did not reduce to metallic form. However, under mass transport limited conditions it was observed that ferric ions were reduced to ferrous ions and re-oxidised to ferric ions, thus reducing the current efficiency of the process. During electrochemical reduction hydrogen gas evolved at the cathode and oxygen gas evolved at the anode.

For a Cu electrochemical reduction process targeting a process yield of 95% at a current density of 1 000 A/m^2, the required processing time was determine to be 4.5 hours with an overall current efficiency of 86.4%, cell voltage of 3.06-4.91 V and specific energy consumption of 12.37 kWh/kg Cu.

Lower initial acidities (0.5 mol/L H^+) and initial copper concentrations (3 g/L Cu) resulted in higher cell voltage, elevated electrolyte temperature and higher degrees of copper powder re-dissolutions during filtration and washing. A similar degree of copper powder re-dissolution was observed for a solution containing higher initial copper concentrations (50 g/L).

Feed solutions with higher acidities (1-4 mol/L H^+) and feed solutions with variation in nickel concentration (5-20 g/L) or iron concentration (1-12 g/L) had no detrimental impact on the electrochemical reduction of copper.

It was found that the current applied during the electrochemical reduction process impacted on the rate of copper recovery and the specific energy consumption of the process. Based on a targeted process yield of 95% the optimum current density was found to be 1 000 A/m^2.

A conceptual flowsheet was developed for a batch electrochemical reduction process to treat an anticipated feed solution of 22.40 kg/h Cu. The capital cost of the process was estimated at R 15.9 million and the operating cost was estimated at R 3.8 million per annum. Based on a discounted rate of 11.5% the project has a net present value (NPV) of R 26.9 million and an internal rate of return (IRR) of 37.6% over 5 years.

The main recommendations from this study are to:

1. Perform larger scale piloting and demonstration of the integrated process on actual process solutions. This includes an investigation into a suitable solids handling process to convert copper powder into a saleable product and characterisation of the morphology and quality of copper solids. A detailed costing and economic evaluation study should then be done based on the pilot plant results. The main factors to consider during design of the pilot plant include: batch vs. continuous operation; optimisation of anode and cathode materials of construction; optimisation of electrode spacing; hydrodynamics of electrochemical cell; conditions for removing copper deposits; solid purity; particle size distribution; solids morphology and filtration flux.

2. Perform a detailed economic evaluation to compare the OPEX and CAPEX for the electrochemical reduction process to that of the alternative hydrometallurgical processes considered. This includes further study to determine the operating conditions and economic parameters for a suitable process to recover nickel from the copper spent electrolyte.

TABLE OF CONTENTS

LIST OF TABLES

LIST OF FIGURES

NOMENCLATURE

Acronyms

EC	Electrochemical cell
FL	Filter
MMO	Mixed metal oxide
PGM	Precious group metals
PMR	Precious Metals Refiners
PP	Pump
RBMR	Rustenburg Base Metals Refiners
SB	Sample board
TK	Tank
VA	Vacuum receiver

Parameters

A	Cell electro-active area, m^2
A_s	Electro-active area per unit volume, m^2
c	Concentration, mol/L
E_{CELL}	Cell voltage, V
E_e	Equilibrium potential, V
E_e^0	Formal potential, V
E_e^C	Equilibrium potential for the cathode, V
E_e^A	Equilibrium potential for the anode, V
F	Faraday constant, 96 485 C/mol
i	Current density, A/m^2
I	Current, A
i_L	Limiting current density, A/m^2
M	Mass, kg
n_0	Initial molar amount, mol
n_t	Molar amount at time t, mol
n	Number of electrons
q	Charge passed
Q	Volumetric flow rate, m^3/h
R	Universal gas constant, 8.314 J/(mol.K)
R_{CELL}	Resistance of cell, Ω
$R_{CIRCUIT}$	Resistance of circuit, Ω
T	Temperature, K
V_R	Effective reactor volume, m^3
X_A	Process yield of A, %

ϕ_i	Instantaneous current efficiency, %
ϕ	Overall current efficiency, %
η_A	Anode overpotential, V
η_C	Cathode overpotential, V
τ	Mean residence time, s

Other

e^-	Electrons
(aq)	Aqueous phase
(s)	Solid phase
(g)	Vapour phase

Units

A	Ampere
g	Gram
h	Hour
K	Kelvin
kg	Kilogram
kW	Kilowatt
L	Litre
mol	Mole
mm	Millimetre
mL	Millilitre
min	Minute
m	Metre
s	Second
V	Volt
Ω	Ohm
°C	Degrees Celsius

1 INTRODUCTION

1.1 BACKGROUND

Anglo American Platinum Ltd. is the largest producer of refined platinum in the world. In 2012 a total of 2.38 million ounces of platinum and 4.64 million ounces of precious group metals (PGMs) were refined at the Precious Metals Refiners (PMR) [1].

The PMR receives final concentrate from the Rustenburg Base Metal Refiners (RBMR). This concentrate is produced in a slow-cooling and magnetics separation process and typically contains 50-70% precious metals (platinum, palladium, rhodium, iridium, ruthenium, osmium, gold and silver). Typical impurities include base metals (cobalt, copper, nickel and iron), amphoteric metals (selenium, tellurium) and other impurities (lead, zinc, arsenic, antimony, bismuth, tin, silver) [2,3].

The refining processes applied at the PMR involves a series of separation and purification processes to produce high purity PGM products (>99.9%). Separation processes such as solvent extraction and distillation are used to separate specific PGMs from impurities and the remainder of PGMs. These streams are then purified through crystallisation, precipitation, hydrolysis and metal reduction [2].

In recent years a significant amount of research has gone into the development of a feed pre-treatment process to remove amphoterics, base metals and other impurities from the feed concentrate refined at the PMR. The removal of these impurities from the feed concentrate has the potential to significantly improve the separation efficiencies of the overall process. It further has the potential to significantly simplify the downstream PGM refining process and reduce the number of unit processes required for purification [3].

US patent 2013/0177487 A1 [3] describes a process for the upgrading of this PGM concentrate where near-complete removal of base metals and other impurities is achieved. The patent describes a high temperature oxidative pre-treatment process followed by a high temperature hydrochlorination process to volatilise base metal chlorides and other impurities. The aim of the oxidative pre-treatment process is to convert metals to metal oxides. The metal oxide solids are then contacted with a hydrochlorination agent (at a controlled HCl/H_2O ratio) at elevated temperatures to produce metal chlorides and water as shown in the following reaction [3]:

$$MO + 2HCl \rightarrow MCl_2 + H_2O \quad (1)$$

The above-mentioned reaction is thermodynamically favourable over the direct hydrochlorination of metal to form metal chlorides and hydrogen gas, and thus requires a lower stoichiometric excess of HCl(g) to volatilise an equivalent amount of base metal chlorides. Selective volatilisation of base metal chlorides and other impurities over PGM chlorides is achieved by controlling the temperature and HCl/H_2O ratio during the hydrochlorination process [3].

During the oxidative pre-treatment process sulfur, selenium, tellurium and osmium species are volatilised to the off-gas. The species are scrubbed using a suitable off-gas scrubbing system.

The off-gas from the hydrochlorination process contain predominantly HCl(g), H_2O(g) and base metal chlorides of silver, copper, nickel and iron. This off-gas undergoes a quench-scrub process with 33% HCl to condense the base metal chlorides and recycle HCl(g). At 33% HCl the scrub solution is saturated with HCl and minimal absorption of HCl(g) is expected. This HCl(g) stream is routed to an appropriate HCl recovery process to regenerate pure HCl(g) for reuse in the hydrochlorination

process. The quench-scrub solution is bled to a base metal handling process for subsequent recovery value in the form of silver, copper and nickel.

Figure 1 illustrates a conceptual block flow diagram for the oxidative pre-treatment process and off-gas scrubbing, hydrochlorination process with off-gas quench-scrub, HCl recovery process and base metal handling process.

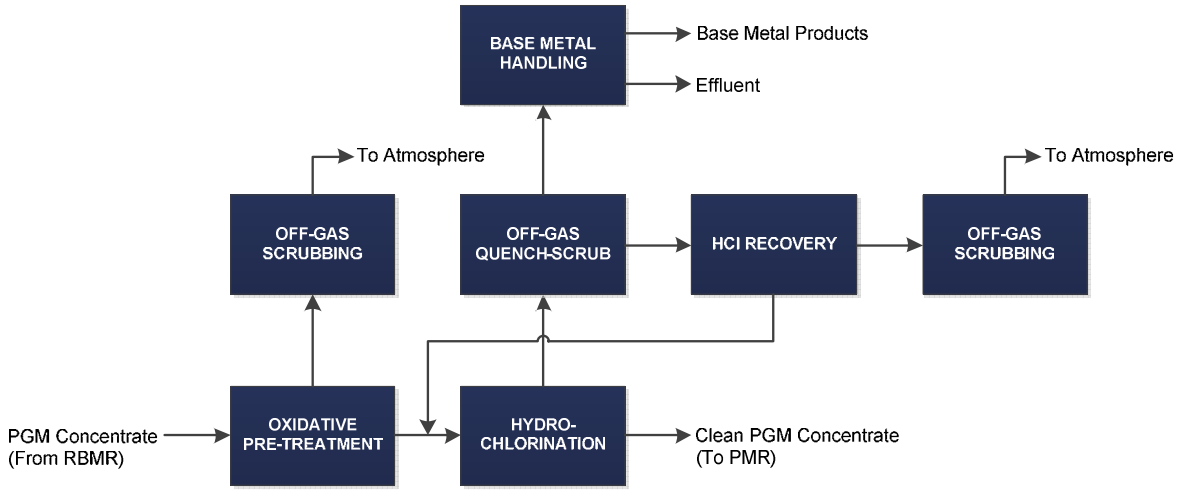

Figure 1: Potential feed pre-treatment for PGM concentrate to PMR.

Within base metal handling a process for the precipitation of silver chloride has been considered. This involves a dechlorination processes with sulfuric acid at elevated temperatures, followed by back-dilution with water and filtration to recover the silver chloride concentrate. The resulting filtrate would then be concentrated and treated with a suitable hydrometallurgical process to recover copper and nickel, respectively. Hydrometallurgical process options that have been considered include the following:

1. Recycling of the base metal solution to RBMR for leaching, purification and electrowinning to produce copper cathode and nickel cathode.
2. Electrochemical reduction of copper powder followed by a suitable precipitation processes to recover nickel.
3. Electrochemical reduction copper powder followed by the electrochemical reduction of nickel powder.
4. Production of a suitable concentrate for toll-refining.

Techno-economic evaluations for each of the above-mentioned process options will be done in order to develop a suitable business cases for the overall project. This study will focus on the electrochemical reduction of copper powder.

1.2 PROBLEM STATEMENT

Given the relatively small stream resulting from the dechlorination process (≈720 L/h) it was considered that the sulfate solution containing approximately 30 g/L copper, 10 g/L nickel and 6 g/L iron could be rerouted to the RBMR for electrowinning of copper and nickel cathodes. However, in the event that this is impractical or not feasible, suitable processes would be required at PMR to recover both copper and nickel. Such processes would involve the production of copper and nickel concentrates that can either be recycled to Waterfall Smelter or converted into saleable products.

Based on the current London Metal Exchange prices the value of the respective streams are estimated to be in the order of R 15.7 million per annum of copper and R 10.2 million per annum for nickel [4,5].

Electrochemical processes with high process yields (in the order of 90-95%) were proposed where powders, rather than cathodes were produced. Due to the order of reducibility of these metals, and the different operating conditions required for the electrochemical production, two separate electrochemical processes would be considered. Firstly, the electrochemical recovery of copper powders from acidic sulfate solutions and secondly, the electrochemical reduction of nickel powder under less acidic sulfate conditions. The spent electrolyte from electrochemical recovery of nickel would then be sent for effluent treatment.

The conventional copper electrowinning processes applied at RBMR typically have feed solutions in the order of 50-80 g/L Cu and the process is operated at a copper bite (ΔCu) of approximately 20 g/L to produce saleable copper cathodes. However, for the proposed electrochemical reduction process for PMR it is required that effectively all copper be removed from solution in the form of a copper powder.

The upfront hydrochlorination and dechlorination processes would be operated as batch, and it is thus required that the copper and nickel electrochemical processes also be operated as batch.

Research and development work is required on an electrochemical process for the selective recovery of copper from a sulfuric acid solution containing predominantly copper, nickel and iron. Typical aqueous concentrations have been estimated at 30 g/L copper, 10 g/L nickel and 6 g/L iron at an acidity of 2 mol/L.

The feasibility of an electrochemical process for the recovery of copper is dependent on the estimated capital and operating cost of the process to treat the required inputs. It is therefore required that experimental work be conducted to determine the operating conditions for such a process. Once the required operating conditions have been established it is required that a conceptual flowsheet be developed and estimates for the capital cost and operating cost of the process be provided.

1.3 OBJECTIVES

The objectives of this study were to:

i. Determine the operating conditions for an electrochemical reduction process aimed at recovering copper as a copper powder from a sulfuric acid stream containing copper, nickel and iron.

ii. Develop a conceptual flowsheet for a batch electrochemical process and estimate the capital cost and operating cost.

1.4 METHODOLOGY

The methodology followed for this study was as follows:

i. A literature study was conducted on the recovery of copper from effluents streams and processes for the recovery of copper powders. This included hydrometallurgical processes for the recovery of copper from effluent streams, commercial processes for the recovery of copper powders and a study on the factors that impact electrochemical reduction of powders.

ii. Bench-scale experimental work was conducted using synthetic solutions made up to the anticipated feed concentrations. Parameters such as feed concentrations, feed acidity and applied current were varied to determine the impact of each on the operating conditions of the process.

iii. A conceptual flowsheet was developed based on the experimental operating conditions of the electrochemical process.

iv. Estimates for capital cost and operating cost were determined based on mechanical equipment, reagent and utility costs for the current PMR and Lang factors estimation.

1.5 HYPOTHESIS

It was hypothesised that for a feed electrolyte containing 30 g/L copper, 10 g/L nickel and 6 g/L iron at an acidity of 2 mol/L, copper powder could be produced using an electrochemical reduction process at high current densities (≈1 000 A/m^2). $Cu^{2+}(aq)$ is cathodically reduced to Cu(s) that is poorly adhered to the cathode surface. The metallic copper powder can then be separated by solid-liquid separation.

2 LITERATURE SURVEY

A literature study was conducted on the recovery of copper from effluents streams and processes for the recovery of copper powders. This included hydrometallurgical processes for the recovery of copper from effluent streams, commercial processes for the recovery of copper powders and a study on the factors that impact electrochemical reduction of powders.

2.1 THE RECOVERY OF COPPER FROM EFFLUENT STREAMS

Agrawal and Sahu [6] studied processes for the recovery of copper from copper electrorefining bleed streams, solid wastes, scraps, and by-products from other processes containing significant amounts of Cu, Ni, Co. A number of pyrometallurgical- and hydrometallurgical processes were considered. Pyrometallurgical processes are generally used when the metal to be recovered is high (up to approximately 65% of the feed material), and are not suited for feeds containing less than 5% of required metal. The pyrometallurgical methods that are generally used to recover copper are the Outokumpu process, the Ausmelt smelting process and ISASMELT technology [6]. Hydrometallurgical processes for the treatment of copper ores and concentrates account for approximately 20% of global primary copper production. These processes consist of sulfate-, sulfate/chloride or chloride (and bromide) based leaching processes that are coupled with combinations of solvent extraction and electrowinning technologies. Although widely used for primary ores, hydrometallurgical processes for the recovery of copper from secondary sources have not found large application due to poor economic feasibilities [6].

Agrawal *et al*. [7] studied three different hydrometallurgical approaches to recover copper from copper bleed streams. These were as follows:

i. Synthesis of copper sulfate powder by evaporative crystallisation;
ii. Synthesis of pure copper powder by direct hydrogen reduction; and
iii. Synthesis of electrolytic grade copper powder.

Large and bench scale experimental work was conducted on synthetic solutions (38.42 g/L Cu 19.37 g/L Ni and 171.5 g/L H_2SO_4) and actual copper bleed stream solutions from an Indian copper smelter (39.86 g/L Cu, 9.58 g/L Ni, 0.26 g/L Fe, 0.108 g/L Bi, 0.007 g/L As, 0.055 g/L Sb and 198.04 g/L H_2SO_4).

In the synthesis of copper sulfate powder by evaporative crystallisation, copper bleed stream solutions were evaporated and crystallised to produce copper sulfate and mixed copper-nickel sulfate. It was found that the fractional recovery of copper crystal increases with increasing evaporation. At 55% evaporation the formation of nickel crystals became significant and a mixed copper-nickel salt was crystallised [7].

In the synthesis of pure copper powder by direct hydrogen reduction approximately 99.4% copper powder recovery could be achieved in 2 hours using an 1 L capacity titanium lined autoclave. The autoclave was operated at 453 K and 80 bar at a stirring speed of 400 rpm. The copper powder produced from actual copper bleed stream solutions had a purity of 99.4% [7].

Agrawal *et al.* [8] demonstrated the recovery of copper powder from copper bleed streams containing copper, nickel and other impurities (Fe, Bi, As, Sb) in sulfuric acid. The process comprised decopperisation, crystallisation, solvent extraction and electrochemical treatment. For electrochemical treatment a large scale (9 L) undivided cell with two cylindrical stainless steel cathodes and two lead-antimony (6%) anodes was used. An electrolyte of 38.13 g/L Cu and 90 g/L H_2SO_4 yielded a 95% copper powder recovery after eight hours at a current density of 700 A/m^2. The morphology of the

copper powder was found to be dendritic in nature with a particle size of approximately 50% passing 150 µm. After annealing with H_2 gas a copper powder with purity of 99.95% was produced.

Agrawal *et al.* [9] then went on to demonstrate the quantitative and selective recovery of nickel powder from the solvent extraction raffinate produced from the above-mentioned process. The same 9 L undivided cell was used. An electrolyte of 10 g/L Ni, 40 g/L $(NH_4)_2SO_4$, 10 g/L H_3BO_3 and 0.2 g/L thiourea yielded a 87% nickel recovery at a current density of 5 000 A/m^2 and feed pH of 5.25. Additional runs with electrolyte solution of 20 g/L Ni yielded 99% nickel recovery at a pH of 4.66. The nickel powder was dendritic and after annealing with H_2 gas, a purity of 99.89% was achieved.

Based on the above-mentioned studies it has been established that relatively high purity copper powder could be produced from effluent streams containing relatively low concentrations of copper. Furthermore, given the hydrometallurgical process options evaluated in recent studies, it is possible that electrochemical production could be considered for both copper and nickel production.

2.2 COMMERCIAL PROCESSES FOR THE PRODUCTION OF COPPER POWDER

Industrial processes for the production of granular copper powder typically involve an atomisation, electrochemical, hydrometallurgical, or solid state reduction process [10,11]. Table 1 provides a summary of the properties of copper powder produced by the various commercial processes [12].

Table 1: Properties of copper powder by various industrial processes [11,12].

Property	Atomisation	Electrochemical	Hydro-metallurgical	Solid state reduction
Copper (%)	99-99.5	99-99.5	99-99.5	98-99
Weight loss in H_2 (%)	0.1-0.75	0.1-0.75	0.1-0.75	0.1-0.75
Acid insoluble (%)	0.5-0.1 max	0.03 max	0.03 max	0.3 max
Apparent density (g/cm^3)	2-4	1.5-4	1.5-2.5	2-4
Flow (sec/50 g)	20-35	30-40	none	20-35
Green strength (psi)	0-2500	400-6000	0-10,000	0-2500
MPa	0-17.2	2.8-41.3	0-68.9	0-17.2
-325 Mesh (%)	25-80	5-90	60-95	25-50

From Table 1 it can be seen that similar copper powder purities are achieved for all copper powder production processes. However, it should be noted that for processes involving atomisation and solid state reduction it is required that the feed material have a purity greater than 99%. Electrolytic and hydrometallurgical processes selectively recover copper from the feed material, and are thus more suited when further refining is required. Similar weight losses in hydrogen (a measure of the oxygen content of the powder) are seen for all processes. Copper powder produced through electrochemical and hydrometallurgical processes were found to be less soluble in mineral acid, and typically had lower apparent densities [10].

2.2.1 Atomised Copper Powder

Atomisation involves contacting a molten copper stream with a gas or liquid jet-stream to form metal droplets that solidify into copper powder particles. Inert gas atomisation processes produce spherical particles, whilst water atomisation processes produce particles that vary from irregular to spherical by controlling the flow rates, water pressure, design configuration and interaction conditions between the

water jets and the metal stream. Scanning electron micrographs (SEM) of typical copper powder particles produced through nitrogen atomisation and water atomisation are shown in Figure 2 [10,11].

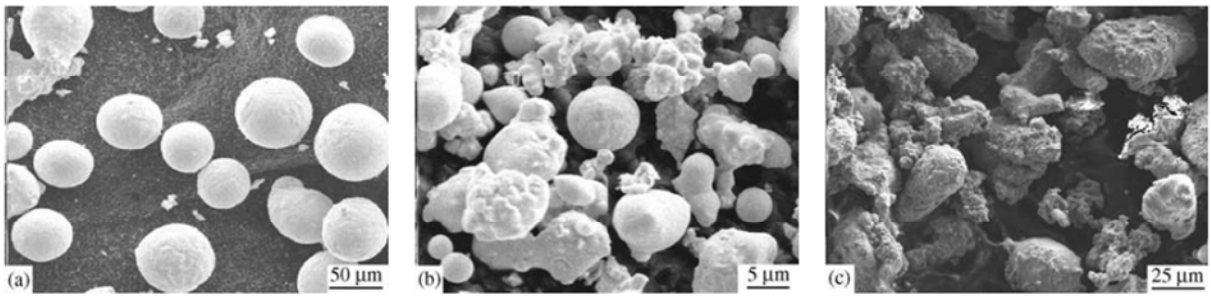

Figure 2: Typical copper powders particles formed in (a) a nitrogen atomised process and (b,c) water atomised processes [11].

Commercial atomisation processes involve superheating copper above its melting point (typically 1 230-1 280°C). The stream is then directed through a nozzle at a flowrate of approximately 28 kg/min. Water pressure of 10-14 MPa is typically used to produce copper powder with a particle size of less than 150 µm. Impurities in the copper melt have a significant impact on the conductivity of the copper powder and care is taken to eliminate contamination in the smelt preparation. Control of oxygen is also required to control the shape and compactibility of the copper powder. This is done by introduction of hydrogen [9].

After atomisation the copper powder is annealed in a reducing atmosphere (temperatures of approximately 800°C), milled, classified and blended to the required particle size distribution [10]. Figure 3 illustrates a flow diagram for a water atomisation process to produce copper powders.

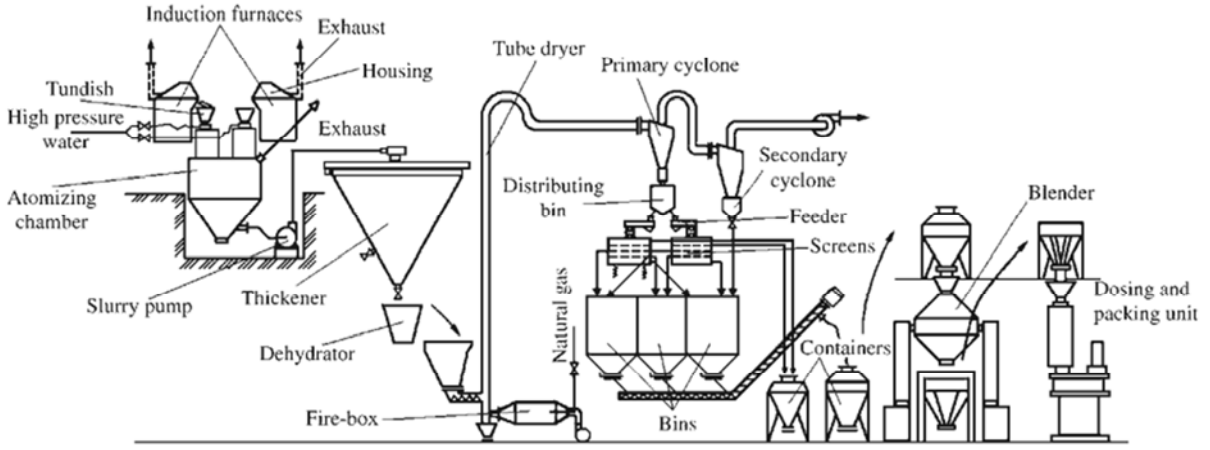

Figure 3: Flow diagram for a water atomisation process for production of copper powder [11].

Atomised copper powder is suited for most powder metallurgy applications as a result of its high flow and good strength. It is typically used in electronic and electrical applications that require high conductivity [10].

2.2.2 Electrochemical Copper Powder

Electrochemical copper powder production involves an electrodeposition process under conditions to promote the formation of a spongy powder deposit at the cathode. Electrochemical copper powder production is done by passing current through an electrolyte with low copper ion concentration, high

acidity and high cathode current density. Copper anodes are used to facilitate the formation of the copper powder and additives (e.g. glucose) are added to promote uniform copper deposition. In order to meet commercial requirements control of the following parameters is required: type and quantity of additive; electrolyte temperature; electrolyte circulation rate; type and size of the anodes and cathodes; electrode spacing; and brush-down interval of cathodes [10,11]. Figure 4 illustrates a process route for electrochemical copper powder production.

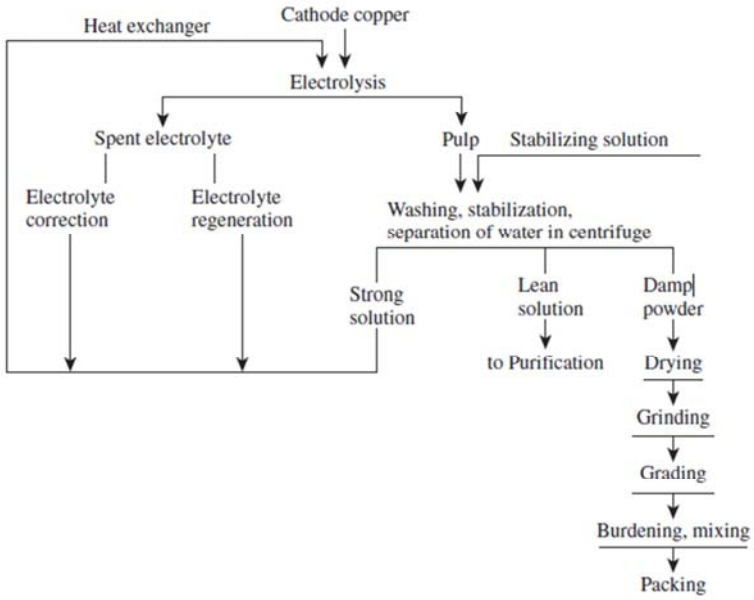

Figure 4: Process route for electrochemical copper powder production [11].

Electrochemical processes for the production of copper powder requires low copper content in the electrolyte to prevent adherent deposits. For electrolyte containing 23-33 g/L copper the maximum current efficiency is approximately 92%. Copper concentrations greater than 33 g/L result in both lower current efficiencies and more adherent copper deposits. Apparent density and particle size of the copper powder increases with increasing copper concentration, but decreases with increasing acidity. A maximum current efficiency is achieved at a concentration of 120 g/L sulfuric acid. Beyond this acidity the current efficiency decreases and leads to passivation [11,13]. The impact of copper concentration and sulphuric acid concentration on current efficiency and apparent density of the copper powder is illustrated in Figure 5.

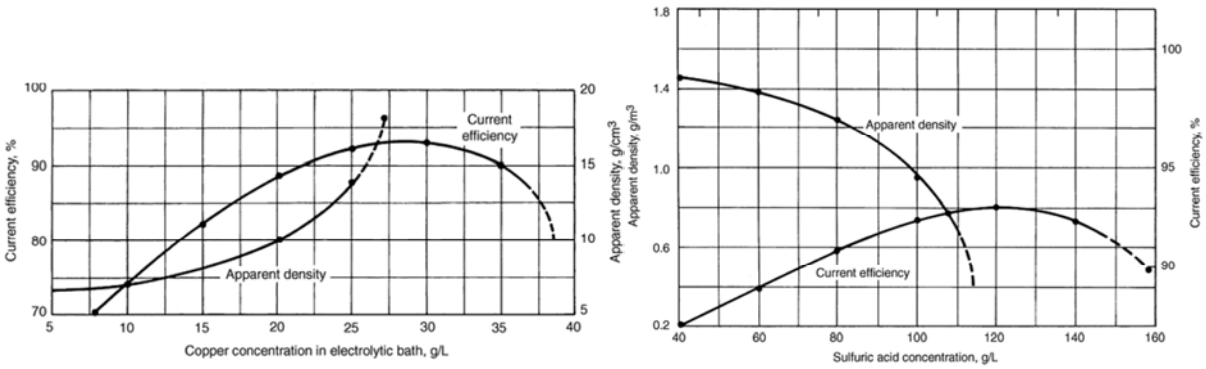

Figure 5: Current efficiency and apparent density for copper powder as a function of (a) copper concentration and (b) sulfuric acid concentration [13].

A high current density increases the rate of powder formation and decreases the particle size of the copper powder. For a solution containing 25 g/L copper and 120 g/L sulfuric acid the particle size fraction passing 53 µm increases from 20% to 96% with an increase in current density from 600 A/m^2 to 1000 A/m^2. Increased operating temperature results in higher current efficiency, reduced cell voltage and coarser powders. However at temperatures greater than 60°C operation of the electrochemical cell becomes problematic [11,13].

Removal of the copper powder deposit from the cathode is done by mechanical brushing or shaking. The brush-down interval impacts the particle size and extended brush-down intervals generally results in coarser particles and increased apparent densities [11,13].

An electrochemical cell for the production of copper powders is illustrated in Figure 16. Each electrochemical cell consists of an arrangement of anodes and cathodes in a rubber-lined or plastic electrochemical bath. Electrolyte is introduced at the top of the cell and exits at the bottom of the cell. During electrochemical treatment dendritic copper powder is formed at the cathode and is periodically brushed. On completion of the harvesting cycle the current to the cells is stopped, spent electrolyte is drained and the copper powder slurry is removed. The copper powder slurry is filtered, washed and treated with an aqueous solution (e.g. gelatine) to prevent oxidation. This is followed by a annealing process at 480-760°C under reducing conditions. The resulting powder is then milled, classified and blended to the required particle size distribution.

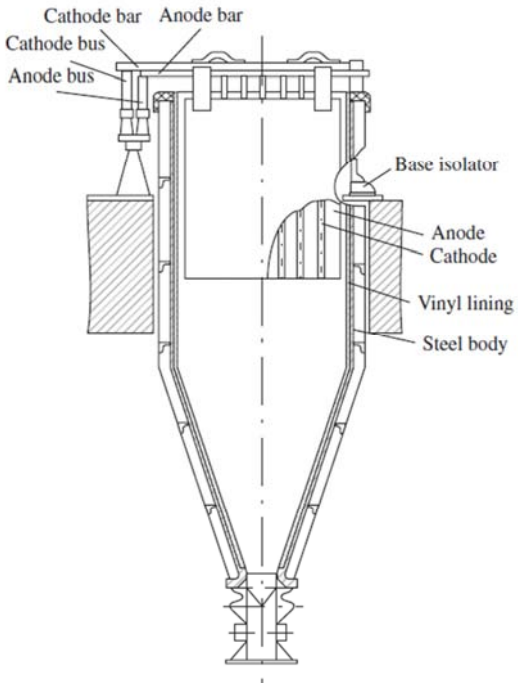

Figure 6: Electrochemical cell for production of copper powder [11].

The particle shape of dendritic copper powder after electrochemical treatment and after subsequent treatment is given in Figure 7a and Figure 7b, respectively. After thermo-mechanical treatment the initial dendrites particle size increases by welding of smaller particles [11].

A number of commercial processes for the electrochemical production of copper powder are given in Table 2.

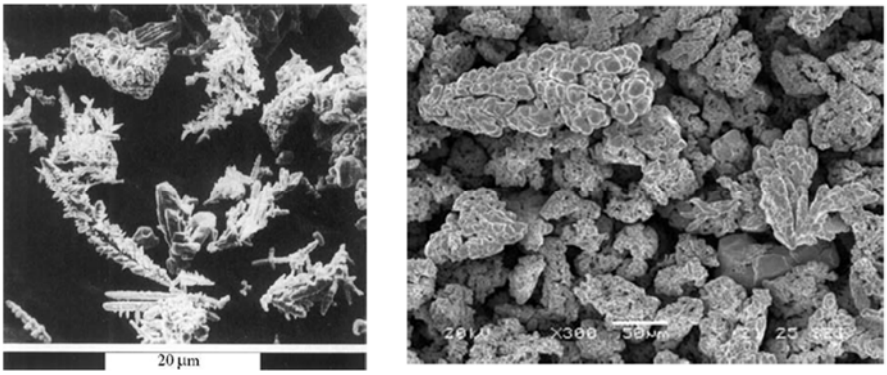

(a) (b)

Figure 7: Dendritic structures of copper particles after (a) electrochemical treatment and (b) subsequent thermo-mechanical treatment [11].

Table 2: Electrochemical methods for copper powder production (adapted from [11]).

Mode	Electrolyte	Current density (A/m^2)	Temperature (°C)	Process parameters and conditions
Electrolysis of aqueous solution	7-35 g/L Cu 50-100 g/L H_2SO_4	500-900	25-57	Current efficiency 80-99%; particle size 20-100 µm; brush down interval 15-60 min.
Electrolysis of aqueous solution	4-24 g/L Cu 163 g/L H_2SO_4	1 000-2 000	40	Current efficiency 75-96%; particle size 5-60 µm; apparent density 0.8-2.2 g/cm^3.
Electrolysis of aqueous solution	5-35 g/L Cu 120-150 g/L H_2SO_4	500-600	42-60	Current efficiency 60-98%; apparent density 0.8-2.5 g/cm^3; specific surface 500-1800 cm^2/g.
Electrolysis of aqueous solution	25-30 g/L Cu 90 g/L NH_2HSO_3	1 500-4 000	-	Current efficiency 90-93%; particle size 80 µm; circulation 1L(A.h).
Electrolysis of aqueous solution	6.4 g/L Cu 50 g/L H_2SO_4	-	14-50	Permanent overvoltage 0.3-0.7 V; particle size 2- 200 µm.
Electrolysis of aqueous solution	16-30 g/L Cu 160 g/L H_2SO_4	450-2 000	50	Current efficiency 100%; permanent overvoltage 0.3-0.5 V; apparent density 2.7 g/cm^3.
Electrolysis of aqueous solution	12-15 g/L Cu 160 g/L H_2SO_4	20-4 700	50	Current efficiency 100%; linear current variation; particle size 20-100 µm.
Electrolysis of aqueous solution	6.4 g/L Cu 50 g/L H_2SO_4	-	25	Pulsing voltage with amplitude 600 mV; frequency 1-100 Hz; particle size 50 -200 µm.
Electrolysis of aqueous solution	10-12 g/L Cu 150-200 g/L H_2SO_4	600	30-35	Current efficiency 98-99%; Pulse current; full period; pulse 10:1; particle size 50 µm; apparent density 1.5 g/cm^3 .
Electrolysis of double layered cell	3.2 g/L Cu, H_2SO_4 0.02-1% oleic acid	2 500	20	Drum rotation 10-40 rpm; dendrite size 0.3-3 µm.
Electrolysis of double layered cell	3.2 g/L Cu, Carbon acids in toluene	2 500	20	Current efficiency 93%; rotation 10-40 rpm; oleic acid changed to stearine to decrease Cu_2O yield.
Reduction of solid phase	5.3-10.6 g/L Na_2CO_3	1 000	70	Current efficiency 67-69%; raw material – CuO with particle size 0.25 mm; copper cathode; coal anode; particle size 0.5 mm.
Melt electrolysis	0.2-10 wt% CuCl KCl-NaCl	10-20 000	447-897	Two dimensional twin dendrites at 447-567°C; three dimensional dendrites at 897°C.
Cementation	12-15 g/L NaF H_2SO_4, pH 3.3-3.6	-	90-95	Drum rotation 3–5 rpm; cementing agent is aluminium.
Cementation	3-4 g/L Cu H_2SO_4	-	27-37	Cementing agent is zinc powder; mixing (Reynolds number = 10^3-10^4)

Copper powders produced through electrochemical processes typically exceed purities of 99.5%. Electrochemical copper powder is suited for powder metallurgy applications where high electrical and thermal conductivities are required and is typically used for electrical and electronic applications [10,11].

2.2.3 Hydrometallurgical Copper Powder

Hydrometallurgical processes for copper powder production typically involve leaching of copper sulphide and copper oxide ores with either sulfuric acid or ammoniacal solutions. The pregnant leach solution is filtered and the filtrate undergoes precipitation of the metal from solution. Typical precipitation processes include hydrogen reduction, cementation and electrowinning [10,11]. Figure 8 illustrates a process route for hydrometallurgical copper powder production.

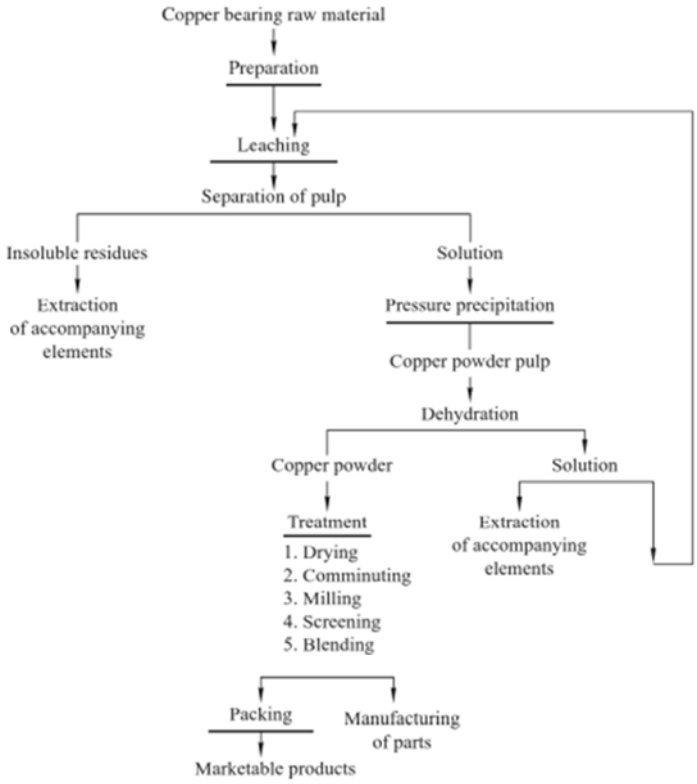

Figure 8: Process route for hydrometallurgical copper powder production [11].

Copper powder precipitation by means of a reduction with hydrogen, carbon monoxide or sulfur dioxide can be done with both sulfurous and ammoniacal solutions. The reduction processes are done under pressure and at elevated temperatures. The following reactions describe the precipitation of copper from solution using a reduction process [11]:

$$Cu^{2+} + H_2 \rightarrow Cu + 2H^+ \quad (2)$$

$$Cu^{2+} + CO + H_2O \rightarrow Cu + CO_2 + 2H^+ \quad (3)$$

$$Cu^{2+} + SO_2 + 2H_2O \rightarrow Cu + SO_4^{2-} + 4H^+ \quad (4)$$

$$Cu(NH_3)_2^{2+} + H_2 \rightarrow Cu + 2NH_4^+ \quad (5)$$

$$Cu(NH_3)_2^{2+} + CO + H_2O \rightarrow Cu + CO_2 + 2NH_4^+ \quad (6)$$

$$Cu(NH_3)_2^{2+} + SO_2 + 2H_2O \rightarrow Cu + SO_4^{2-} + 2NH_4^+ + 2H^+ \quad (7)$$

Precipitation with hydrogen is considered to be the most effective.

Copper powder precipitation by cementation involves the addition of a less noble metal such as zinc or iron. The cementation reactions for copper with zinc powder and iron powder are given by the following reactions [11]:

$$Cu^{2+} + Zn \rightarrow Zn^{2+} + Cu \quad (8)$$

$$Fe + CuSO_4 \rightarrow Cu + FeSO_4 \quad (9)$$

In zinc cementation feed solutions containing 50 g/L copper are treated with a stoichiometric excess of zinc powder (particle size of 100-400 µm). This is done in a well-mixed tank at a temperature of 50°C. Copper powder purities of 97.0-98.5% are achieved. After cementation the slurry is filtered, washed, stabilised and dried. For iron cementation processes scrap iron is used which result in lower copper powder purities (75-85%) [11].

Electrowinning processes for the recovery of copper from leach solutions are used for solutions containing 25 g/L copper (or greater). The electrochemical process is operated at cathode current densities of 1 350-2 700 A/m^2 and an electrolyte temperature of 60°C. Once a copper concentration of 15 g/L is reached, the electrolyte is drained and the copper powder is filtered, washed, stabilised and dried. Copper purities greater than 99.9% are achieved [11].

A second electrowinning process for the recovery of copper powder involves the electrochemical regeneration of titanium in a divided cell [11]. Titanium acts as a reductant for copper based on the following reaction:

$$Cu^{2+}(aq) + 2Ti^{3+}(aq) \rightarrow Cu(s) + 2Ti^{4+}(aq) \quad (10)$$

The above-mentioned process is operated at a temperature of 25°C with cathode current density of 50 A/m^2 and anode current density of 400 A/m^2 [11].

Hydrometallurgical copper powder is typically used in friction materials due to its fine particle sizes, low apparent density and high strength [10].

2.2.4 Solid State Reduced Copper Powder

Solid state reduction involves a process where copper oxide is reduced to copper at elevated temperatures by a reducing gas. This process yields a sintered porous cake that is subsequently ground to a powder [9].

Raw material in the form of copper mill scale, cement copper or high purity chopped scrap and atomised powder is oxidised to either cuprous oxide or cupric oxide. This is done either in a rotary kiln or fluidised bed with air at temperatures greater than 650°C. The oxidation reactions for the formation of cuprous oxide and cupric oxide are as follows [11,13]:

$$2Cu(s) + \tfrac{1}{2}O_2(g) \rightarrow Cu_2O(s) \quad (11)$$

$$Cu(s) + \tfrac{1}{2}O_2(g) \rightarrow CuO(s) \quad (12)$$

The oxidised metal is melted in a fuel-fired or induction furnace with hydrogen, cracked ammonia or carbon monoxide at 425-650°C. The reduction reactions for copper oxide by hydrogen and carbon monoxide are given by the following reactions [11,13]:

$$Cu_2O(s) + H_2(g) \rightarrow 2Cu(s) + H_2O(g) \quad (13)$$

$$Cu_2O(s) + CO(g) \rightarrow 2Cu(s) + CO_2(g) \quad (14)$$

$$CuO(s) + H_2(g) \rightarrow Cu(s) + H_2O(g) \quad (15)$$

Control of impurities such as aluminium, silica, tin and lead is important to prevent formation of abrasive powders, clogging of the furnace equipment and reduction in the electrical and thermal conductivity of the copper powder. The molten copper then undergoes an atomisation process with either air or water [11].

Copper powder by solid state reduction is suited for most powder metallurgy applications as a result of its high flow and good strength. Its most importance application is for self-lubricating bronze bearings [10,11].

2.3 ELECTROCHEMICAL METHODS FOR PRODUCING METAL POWDERS

Electrochemical methods can be used to produce metal powders in a variety of purities, particle shapes, particle sizes and degrees of compressibility. By varying the process parameters for these electrochemical methods, it is possible to control the crystallisation of metal powders that are formed. The electrochemical methods that are generally employed to produce metal powders (copper, nickel, cobalt, cadmium, zinc, silver) from aqueous solutions are differentiated into two deposition classes. The first class involves direct deposition of a friable or spongy deposit that disintegrates into fine particles. The second class involves deposition of a dense, smooth, brittle layer that can be ground into a powder. Both deposition classes are achieved by controlling or manipulating the following process parameters [11]:

i. Concentration of metal and pH of the electrolyte
ii. Current density
iii. Cathode potential
iv. Temperature and rate of circulation of electrolyte
v. Type and size of anode and cathode and their distance from each other
vi. Type and quantity of additional agents
vii. Conditions of removing deposits at the electrodes

Electrochemical metal powders are mainly produced as loose dendritic deposits. However, depending on the conditions of the electrochemical process and nature of the metal, powders in the form of flakes, needles, fibrous or spongy forms are observed [11].

Orhan *et al.* studied the effect of electrochemical parameters on the morphology of copper powder in both an electrochemical plate cell [14] and a rotating cylinder electrode cell [15]. In both studies the effect of copper concentration, electrolyte temperature and current density were evaluated in a sulfuric acid solution.

With an electrochemical plate cell it was found that the morphology of the copper powder was dependent on the copper concentration and the electrolyte temperature. Electrochemical treatment of an electrolyte containing 0.12 mol/L Cu and 0.5 mol/L H_2SO_4 at a current density of 1 500 A/m^2 and potential of 1 000 mV resulted in the formation of porous and disperse copper powder. With increasing copper concentration from 0.12 to 0.63 mol/L Cu, the morphology changed from porous, disperse to cauliflower-like, coral-like, shrub-like and stalk-stock-like [14]. SEM photomicrographs for the copper powder particles obtained at the various copper concentrations are given in Figure 9.

The cauliflower-like structure obtained at high current densities and high overpotentials was found to be indicative of the limiting diffusion current density where the hydrogen evolution rate is high. As the

hydrogen evolution rate becomes lower (with increasing copper concentration) the morphology of the powder particles change as depicted in Figure 9. Furthermore, it was found that increasing temperature from 30°C to 45°C and 60°C resulted in an increased surface area and lower apparent density of copper powder solids [14].

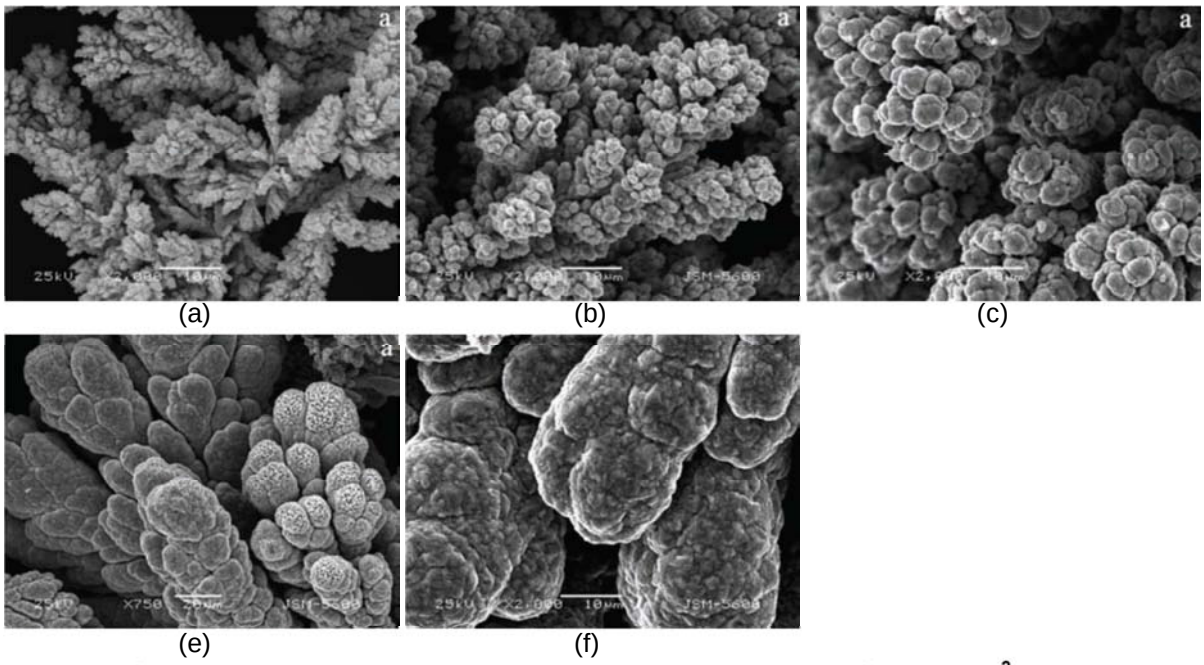

Figure 9: Copper powder particles produced at a current density of 1 500 A/m^2 and increasing various copper concentrations. (a) porous-disperse, (b) cauliflower-like, (c) coral-like, (d) shrub-like and (e) stalk-stock-like [14].

With a rotating disk electrode cell it was found that an increase in current density or decrease in electrolyte temperature resulted in a reduction in the size of the copper powder particles, thus promoting dendritic structures. Increasing copper concentration or cathode rotation speed increased the size of the particles which promoted cauliflower-like morphology [15].

A number of authors have studied the morphology of copper powder through electrochemical processes, and its correlations with hydrogen evolution [16-22]. Nikolić *et al.* determined three morphology groups for copper powder in sulfate solutions based on the average current efficiency of hydrogen evolution, $\phi_{avg,H2}$ [22]. These are as follows:

i. $\phi_{avg,H2}$ = 0-10%. Branch dendrites, independently formed cauliflower-like forms and possible formation of holes due to detached hydrogen bubbles (dish-like holes).
ii. $\phi_{avg,H2}$ = 10-20%. Mixture of dish-like holes and holes constituting honeycomb-like structures with independently formed copper grain agglomerates. Mixture of holes and cauliflower-like forms. Mixture of holes and branchy dendrites.
iii. $\phi_{avg,H2}$ >20%. Mixture of holes and cauliflower-like copper grain agglomerates that are formed around holes. No dendrites appear.

Wang *et al.* [23] studied the electrochemical production of copper powder under a super gravity field in an attempt to enhance the kinetics of the process. Under the experimental conditions it was found that the current efficiency of the process increased by 20% relative to normal gravity conditions. This was attributed to disturbance of the electrode/electrolyte interface which resulted in enhanced mass transfer of Cu^{2+}. Lower cell voltages were recorded and it was found that particle size decreased with increasing gravitation force. The use of a super gravity force furthermore facilitated the detachment of copper powders from the electrode surface.

3 FUNDAMENTALS

This section outlines the chemistry, thermodynamics and kinetics of the electrochemical reduction process.

3.1 CHEMISTRY

The electrochemical reduction of copper in acidic solutions is achieved at the cathode. This is associated with hydrogen gas evolution at the cathode and oxygen gas evolution at the anode. The main reactions for the electrochemical process are given as follows:

At the cathode:

$$Cu^{2+}(aq) + 2e^{-} \rightarrow Cu(s) \quad (16)$$

$$2H^{+}(aq) + 2e^{-} \rightarrow H_2(g) \quad (17)$$

At the anode:

$$2H_2O(aq) \rightarrow O_2(g) + 4H^{+}(aq) + 4e^{-} \quad (18)$$

Under mass transport limited conditions for copper it is possible for ferric to be reduced to ferrous at the cathode, which is subsequently oxidised back to ferric at the anode. This is given by the following reactions:

At the cathode:

$$Fe^{3+}(aq) + e^{-} \rightarrow Fe^{2+}(aq) \quad (19)$$

At the anode:

$$Fe^{2+}(aq) \rightarrow Fe^{3+}(aq) + e^{-} \quad (20)$$

The above-mentioned electrochemical system is illustrated in Figure 10.

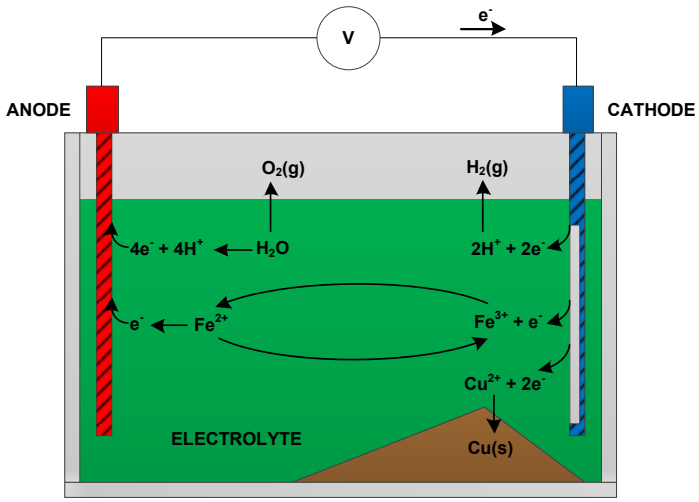

Figure 10: Electrochemical system for the reduction of copper in acidic solution.

Reduction of nickel is not expected to take place due to the significantly lower reduction potential relative to that of copper (See Section 3.2.1).

3.1.1 The Effect of Current Density

The current density (*i*) of metal deposition affects the morphology of the deposit. As current density (or the ratio of i/i_L) increases, the mean size of the crystallites making up the deposit decreases. Thus, the rate of nucleation increases. Figure 11 indicates the typical effect of current density on the nature of metal deposits [24, 25].

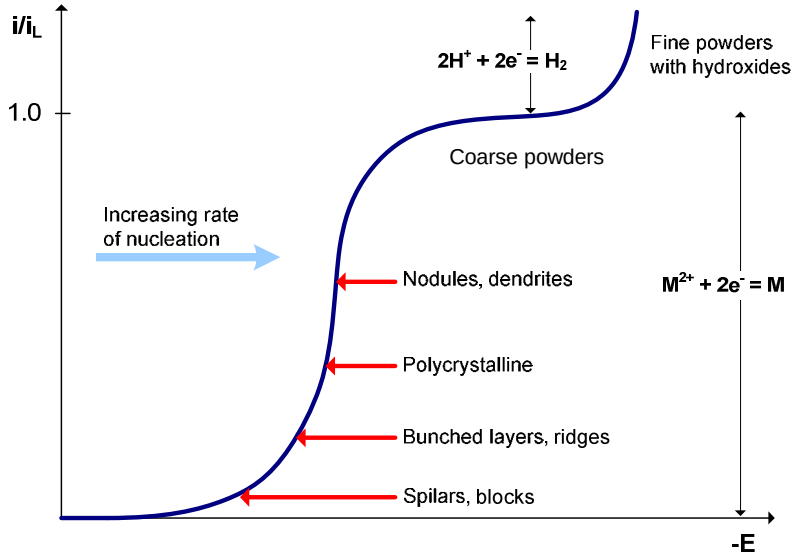

Figure 11: Effect of current density on the nature of metal deposits [24,25].

For industrial electrowinning applications, the maximum current density that is typically applied is 30-40% of the limiting current density. Thus, in order to produce a powdery deposit, the current density should be operated in the range of 50-100% of the limiting current density.

3.1.2 The Effect of Feed Copper Concentration

The copper ion concentration in the electrolyte affects the morphology and power consumption of the process. As the copper ion concentration decreases, the mean size of the crystallites making up the deposit decreases, thus forming smaller, weak deposits.

Low metal concentrations in the electrolyte result in low electrical conductivity. This, in turn, causes high electrical power consumption. At low copper concentrations, the overall rate-determining step of the deposition of copper is mass transport controlled.

Higher metal concentrations could result in anode passivation and excessively high metal concentrations could increase the electrolyte viscosity, which results in increased solids suspension.

3.1.3 The Effect of Feed Nickel Concentration

The nickel ion concentration in the electrolyte affects the morphology and power consumption of the process for elements such as copper.

Low metal concentrations in the electrolyte result in low electrical conductivity. This, in turn, causes high electrical power consumption.

Higher metal concentrations could result in anode passivation and excessively high metal concentrations could increase the electrolyte viscosity, which results in increased solids suspension.

3.1.4 The Effect of Feed Iron Concentration

The presence of iron affects the current efficiency for copper electrowinning. As the iron concentration increases, the current efficiency generally decreases. Thus, the power consumption increases. This is mainly driven by the reduction of ferric ions in solution or produced by oxidation of iron at the anode. The ferric ions are reduced at their mass transport controlled rates at the potential of the cathode. Figure 12 schematically depicts current-potential curves for the cathodic processes for copper electrowinning in the presence of iron and oxygen [24-26].

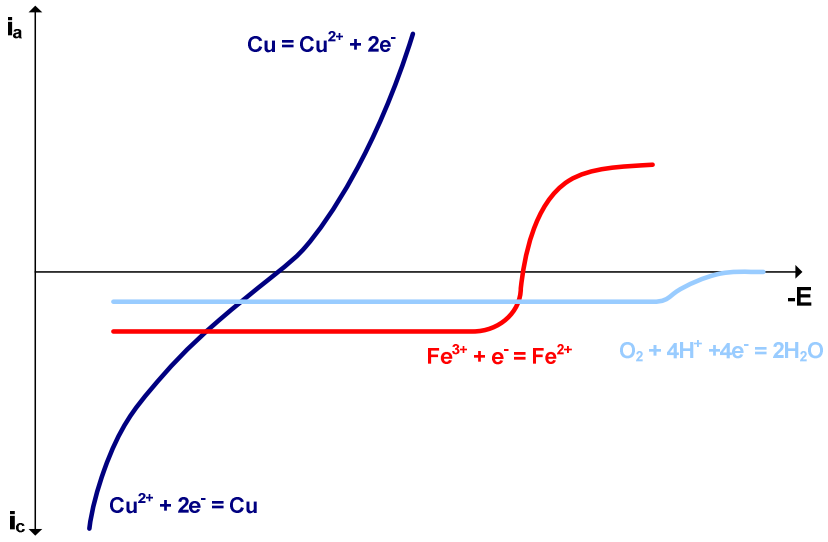

Figure 12: Schematic current-potential curves for iron competing during copper electrowinning [24-26].

3.2 THERMODYNAMICS

The following parameters were evaluated in order to illustrate the thermodynamic properties of the electrochemical process:

i. The thermodynamic order of reducibility for metal ions in solution.
ii. The effect of complexation on redox potentials for metal ions in solution.

3.2.1 The Thermodynamic Order of Reducibility

The equilibrium potential for an electrode is calculated using the Nernst equation:

$$E_e = E_e^0 + \frac{RT}{nF} \ln\left(\frac{c_{M^{2+}}^{\infty}}{c_M^{\infty}}\right) \qquad (21)$$

where E_e is the equilibrium potential (V), E_e^0 is the formal potential for the M^{2+}/M couple in the electrolyte (V), R is the universal gas constant 8.314 (J/(mol.K)), T is the temperature (K) and c^{∞} is concentration (mol/L).

A selection of standard half-reaction potentials in acid solutions is given Appendix A [27]. Based on these values, the thermodynamic order of reducibility for metal ions in standard solutions can be determined. Using the Nernst equation the order of reducibility can be determined for non-standard solutions.

The order of reducibility for both standard and non-standard solutions is given in Figure 13. This was calculated using the standard half-reaction potentials (Appendix A) and the Nernst equation. Non-standard solutions were based on an acidic sulfate solution at a temperature of 60 °C with 30 g/L copper, 10 g/L nickel, 9 g/L iron with 20 mg/L impurities (gold, iridium, silver and rhodium).

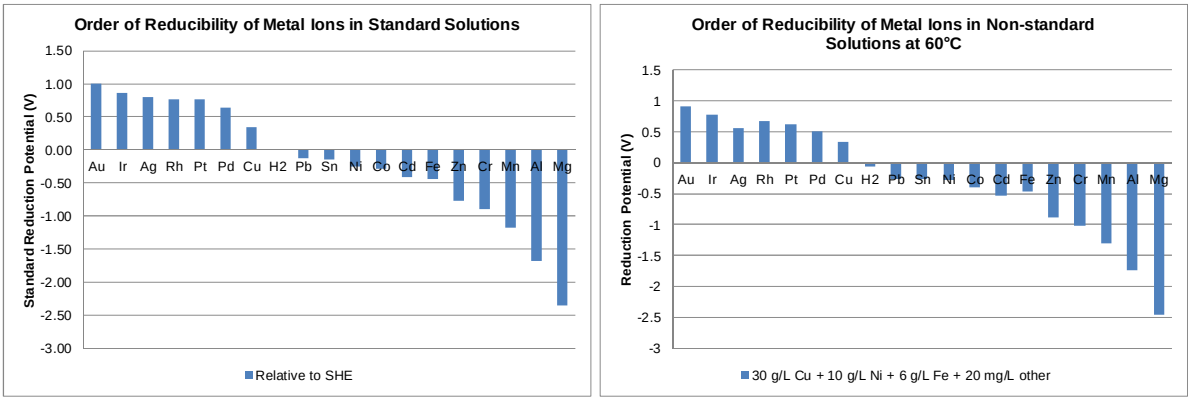

Figure 13: Thermodynamic order of reducibility of metal ions in standard solutions and non-standard solutions.

From Figure 13 it can be seen that the reduction potentials of gold, iridium, silver, rhodium, platinum and palladium are greater than copper for both standard and non-standard solutions. Thus, based on thermodynamics it is expected that these metals will co-deposit with copper during the electrochemical reduction. Conversely metals such as nickel and iron will not co-deposit.

3.2.2 The Effect of Complexation on Redox Potentials

The formation of complexes between a metal ion and a ligand can have significant effects on the reduction potential for electrochemical couples involving the metal ion. In general, complexation reduces the activity of the free metal ion. Thus a more negative potential is required to reduce the metal ion. In order to quantify the effect of complexation under different conditions, the speciation of a metal-containing aqueous solution is evaluated in the form of species distribution diagrams.

Metals in aqueous solutions are generally present in the form of soluble species such as free ions, neutral and charged complexes. The speciation of these aqueous solutions is dependent on the total concentration of each metal, the solution acidity, redox potential, temperature and pressure.

Thermodynamic modelling of the chemical equilibria for the $CuSO_4$-H_2SO_4-H_2O system [28] in the concentration range of 0-200 g/L H_2SO_4, 0-50 g/L Cu(II) and temperature range of 15-70°C, have indicated that a number of species can be formed at various pH and temperature values. The predominant species that are present in solution are as follows: HSO_4^- H^+, SO_4^{2-}, Cu^{2+} and $CuSO_4$(aq). At pH values lower than 1 it was found that sulfuric acid speciates as bisulfate ion (HSO_4^-) and hydrogen ion (H^+).

The following aqueous equilibrium reactions were considered for the $CuSO_4$-H_2SO_4-H_2O system:

$$Cu^{2+} + SO_4^{2-} \leftrightarrow CuSO_4(aq) \quad (22)$$

$$H^+ + SO_4^{2-} \leftrightarrow HSO_4^- \quad (23)$$

Similar results have been obtained for the $NiSO_4$-H_2SO_4-H_2O [29] system with the following aqueous equilibrium reactions:

$$Ni^{2+} + SO_4^{2-} \Leftrightarrow NiSO_4(aq) \quad (24)$$

$$H^+ + SO_4^{2-} \Leftrightarrow HSO_4^- \quad (23)$$

Thermodynamic modelling of the chemical equilibria for the Fe(II)-Fe(III)-H_2SO_4-H_2O system in concentrated solutions (2.2 M H_2SO_4 and 1.3 M Fe) at temperatures of 25°C and 50°C were also studied [30]. In aqueous sulfuric acid solutions iron is distributed as Fe(II) and Fe(III) species in the form of free ions (Fe^{2+}, Fe^{3+}) or complex compounds ($FeSO_4^0$, $FeSO_4^+$, $Fe(SO_4)_2^-$.The concentration of the these species are highly dependent on the solution concentration and temperature. It was found that the predominant species under the indicated conditions are as follows: HSO_4^-, H^+, Fe^{2+} and $FeH(SO_4)_2^0$. Due to the high concentration of bisulfate ion (HSO_4^-) in solution, it was proposed that aqueous solutions under these conditions demonstrate higher buffer effects. The following aqueous equilibrium reactions were considered for the Fe(II)-Fe(III)-H_2SO_4-H_2O system:

$$Fe^{2+} + SO_4^{2-} = FeSO_4^0 \quad (25)$$

$$Fe^{3+} + SO_4^{2-} = FeSO_4^+ \quad (26)$$

$$Fe^{3+} + 2SO_4^{2-} = Fe(SO_4)_2^- \quad (27)$$

$$H^+ + SO_4^{2-} = HSO_4^- \quad (23)$$

Species distribution diagrams for 0.47 M $CuSO_4$, 0.17 M $NiSO_4$ and 0.05 M $Fe_2(SO_4)_3$ solutions at 60°C with increasing acidity are illustrated in Figure 14 [31].

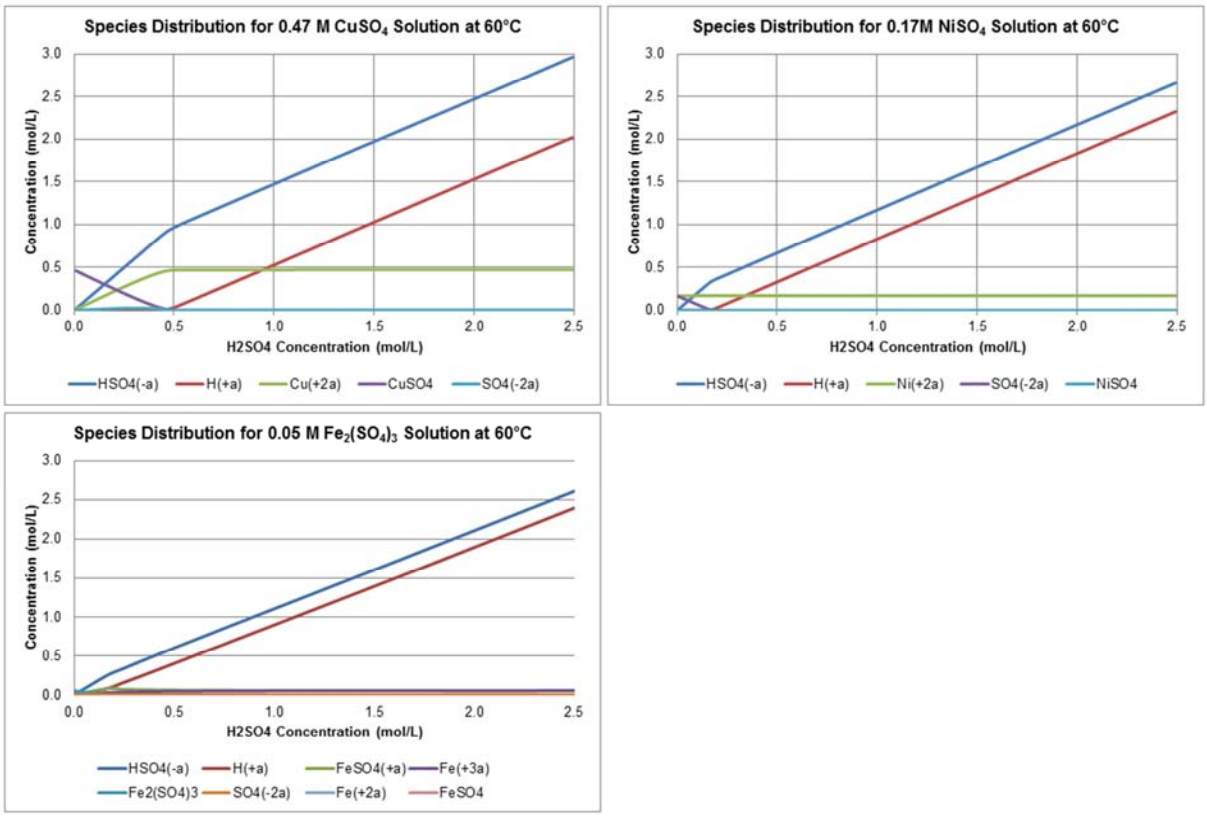

Figure 14: Species distribution diagrams for 0.47 M $CuSO_4$, 0.17 M $NiSO_4$ and 0.05 M $Fe_2(SO_4)_3$ solutions at 60°C (generated in HSC [31]).

From Figure 14 it can be seen that the metal ions for the considered solution (30 g/L Cu, 10g/L Ni and 6 g/L Fe) are all present as free metal ions (Cu^{2+}, Ni^{2+}, Fe^{3+} and Fe^{2+}) when the sulfuric acid concentration is in excess of 0.5 mol/L. Thus for a solution containing 30 g/L copper, 10 g/L nickel, 6 g/L iron and 1 mol/L sulfuric acid there will be no complexes between the metal ions and complexing ligand (SO_4^{2-}) and thus no impact on the reduction potential for electrochemical couples involving the metal ions.

3.3 ELECTROCHEMICAL PROCESS PARAMETERS

The following section outlines electrochemical process parameters that were used to evaluate the electrochemical process [32].

3.3.1 Process Yield

The process yield, X, for a metal A in an electrochemical batch process is given as:

$$X_A = \frac{n_0 - n_t}{n_0} \tag{28}$$

where X_A is the process yield of A, n_0 is the initial molar amount of A (mole), and n_t is the molar amount of A at time t (mole).

3.3.2 Current Efficiency

The current efficiency of an electrochemical process is given as the ratio of electrical charge used to form the desired product over the total charge passed during the electrochemical process. This is given by the following equation based on Faraday's Law:

$$\phi = \frac{n_0 nF}{q} \tag{29}$$

where n_0 is the molar amount of starting material (mole), n is the number of electrons involved in the electrode reaction, F is the Faraday constant (96 485 C/mol), and q is charge passed (C.s).

Instantaneous current efficiency (ϕ_i) is based on the charge passed for a specific time interval, whilst overall current efficiency (ϕ) is calculated based on the cumulative charge passed from time 0 to time t.

3.3.3 Cell Voltage

Cell voltage for an electrochemical cell is given as follows:

$$E_{CELL} = E_e^C - E_e^A - |\eta_C| - |\eta_A| - IR_{CELL} - IR_{CIRCUIT} \tag{30}$$

where E_e^A and E_e^C relates to the equilibrium potential for the anode an cathode reactions (V), η relates to the anode and cathode overpotential (V), I is the current applied (A); and R_{CELL} and $R_{CIRCUIT}$ are the overall resistance of the cell and circuit (Ω), respectively.

3.3.4 Electrical Energy Consumption

Specific energy consumption of an electrochemical process relates to the electrical energy consumed per mass of product produced, and is given as follows:

$$\text{Specific energy consumption} = \frac{-nFE_{CELL}}{\phi M} \text{ (kWh/kg)} \tag{31}$$

where n is the number of electrons involved in the electrode reaction, F is the Faraday constant (96 485 C/mol), E_{CELL} is the cell voltage (V), and ϕ is the process efficiency (%) and M is the mass of product produced (kg).

3.3.5 Electro-active Area Per Unit Volume

The electro-active area per unit volume, A_s, for an electrochemical cell is given as:

$$A_s = \frac{A}{V_R} \tag{32}$$

where A relates to the cell electro-active area (m^2) and V_R the effective reactor volume (m^3).

4 EXPERIMENTAL

This section outlines the experimental design, experimental setup and experimental procedure used in this study.

4.1 EXPERIMENTAL DESIGN

Based on the literature survey it was found that a number of process parameters affect the deposition of metal powders. For the purposes of this study only metal concentration, acidity and current densities were controlled, whilst potential difference and temperature were measured. It is considered that these parameters have a large impact on the design and economics of the process. Factors such as type and size of anode or cathode, electrode distance, additional agents and removal of deposits at the electrode were considered to have a smaller impact and were not varied in this study. Based on the literature survey and fundamental of electrochemical reduction of copper, it was found that the current density should be equal or greater than 700 A/m^2 to produce granular powder. Furthermore, in order to prevent complexation of metal ions the sulfuric acid concentration should be in excess of 0.5 mol/ L.

The experimental design conditions and experimental design matrix are given in Table 3 and Table 4, respectively. The base case experimental design conditions were 30 g/L copper, 10 g/L nickel, 6 g/L iron, 2 mol/L H^+ and a current density of 1 000 A/m^2. Low and high conditions were identified for each parameter and incorporated into the experimental design matrix. Two base case runs (Run 1 A and B) were conducted to illustrate reproducibility of the experiment. This was followed by ten runs where the low and high conditions for each of the parameters were tested.

Table 3: Experimental design conditions.

Parameter	Units	Low	Base	High
Current density	A/m^2	750	1 000	1 500
Feed acidity	mol/L	0.5	2.0	4.0
Feed Cu concentration	g/L	3	30	50
Feed Ni concentration	g/L	5	10	20
Feed Fe concentration	g/L	1	6	12

Table 4: Experimental design matrix.

Run	Description	Current density (A/m^2)	Acidity (mol/L)	Feed Cu (g/L)	Feed Ni (g/L)	Feed Fe (g/L)
Run 1A	*Base Case A*	1 000	2.0	30	10	6
Run 1B	*Base Case B*	1 000	2.0	30	10	6
Run 2	*High Current*	1 500	2.0	30	10	6
Run 3	*Low Current*	750	2.0	30	10	6
Run 4	*High Acidity*	1 000	4.0	30	10	6
Run 5	*Low Acidity*	1 000	0.5	30	10	6
Run 6	*High Cu*	1 000	2.0	50	10	6
Run 7	*Low Ni*	1 000	2.0	3	10	6
Run 8	*High Ni*	1 000	2.0	30	20	6
Run 9	*Low Ni*	1 000	2.0	30	5	6
Run 10	*High Fe*	1 000	2.0	30	10	12
Run 11	*Low Fe*	1 000	2.0	30	10	1

4.2 EXPERIMENTAL SETUP

The experimental setup comprised an electrochemical reactor, direct current (DC) power supply, data acquisition system and computer to monitor experimental profiles (See Figure 15).

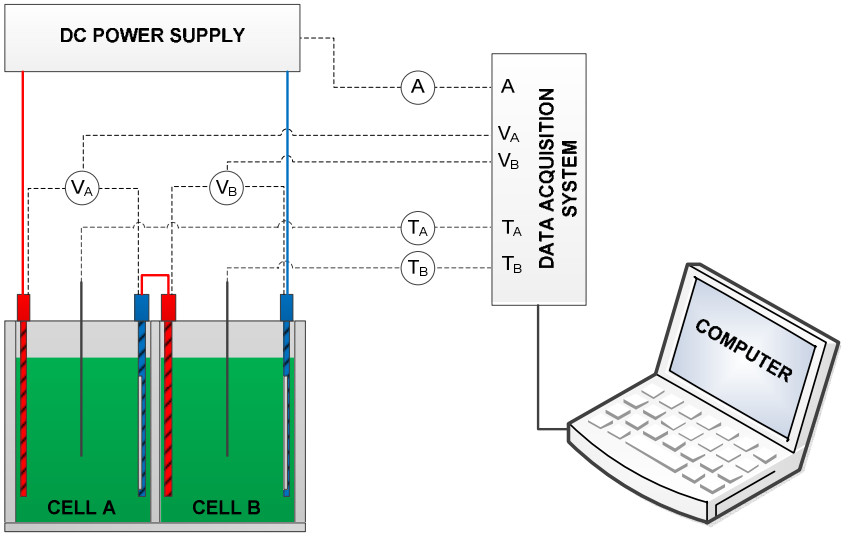

Figure 15: Experimental setup.

4.2.1 Electrochemical Reactor

The electrochemical reactor was constructed of polypropylene. It was assembled as two 4 L plate-type cells (Cell A and Cell B) to allow for two batch runs to be conducted simultaneously. The cathodes were made out of titanium sheets (225 x 175 mm) and were blanked off to an available surface area of 0.024 m^2 (only one side). The anodes were made out of titanium sheets (225 x 175 mm) that have been treated with a propriety coating of tantalum oxide and iridium oxide (dimensionally stable anodes) and had an available surface area of 0.030 m^2. The use of dimensionally stable anodes for copper electrowinning generally provides greater current efficiencies and lower specific energy consumptions than conventional lead anodes [33]. The electrodes were spaced 84 mm apart.

The positive and negative power supply connections were bolted onto the header bars of the respective anode and cathode. In order to facilitate the simultaneous operation of two cells, the cathode for Cell A was connected to the anode of Cell B (Figure 15).

Thermocouples in glass tubes were submerged in the electrolyte of each cell to measure the electrolyte temperatures. Voltage clamps were connected across the cathodes and anodes of each cell to measure the cell voltage. In order to measure current a shunt was installed in the power supply line to the electrochemical reactor.

4.2.2 DC Power Supply

The DC power supply that was used (*Agilent Technologies N5743A*) was capable providing a DC power supply within a voltage range of 0-12.5 V and a current range of 0-60 A. The unit was power-factor corrected and had functionality to operate under constant current (galvanostatic) and constant voltage (potentiostatic) operation. All experimental runs were conducted under galvanostatic conditions.

4.2.3 Data Acquisition System

The data acquisition system consisted of the *Agilent Technologies LXI 34972A* data acquisition unit with multiplex input that was connected to a computer. *Agilent BenchLink Data Logger 3* was used to log the data at predetermined intervals. For the testwork, the following parameters were logged:

i. Electrolyte A temperature
ii. Electrolyte B temperature
iii. Cell voltage A
iv. Cell voltage B
v. Current

4.3 EXPERIMENTAL PROCEDURE

Synthetic solutions were made up to the required conditions for each run using demineralised water, sulfuric acid (H_2SO_4), copper sulfate ($CuSO_4.5H_2O$), nickel sulfate ($NiSO_4.6H_2O$) and ferric sulfate ($Fe_2(SO_4)_3$). Four litres of feed solution was added to each electrochemical cell and current was applied for a duration of seven hours. Two experimental runs were conducted in parallel to demonstrate reproducibility for the base case runs. Thereafter the cells were operated independently. Samples of the electrolyte were taken at the following intervals (in minutes): 0, 60, 120, 180, 240, 300, 360, and 420. Samples were filtered via a syringe filter. After seven hours the current was stopped, the cell drained, the slurry filtered via vacuum filtration and the solids washed with demineralised water. The filtrate was sampled and all samples were analysed for total copper, nickel and iron concentrations by ICP-OES, free acid concentration by potentiometric titration and ferrous iron concentration by potentiometric titration. Figure 16 illustrates the experimental setup for two runs.

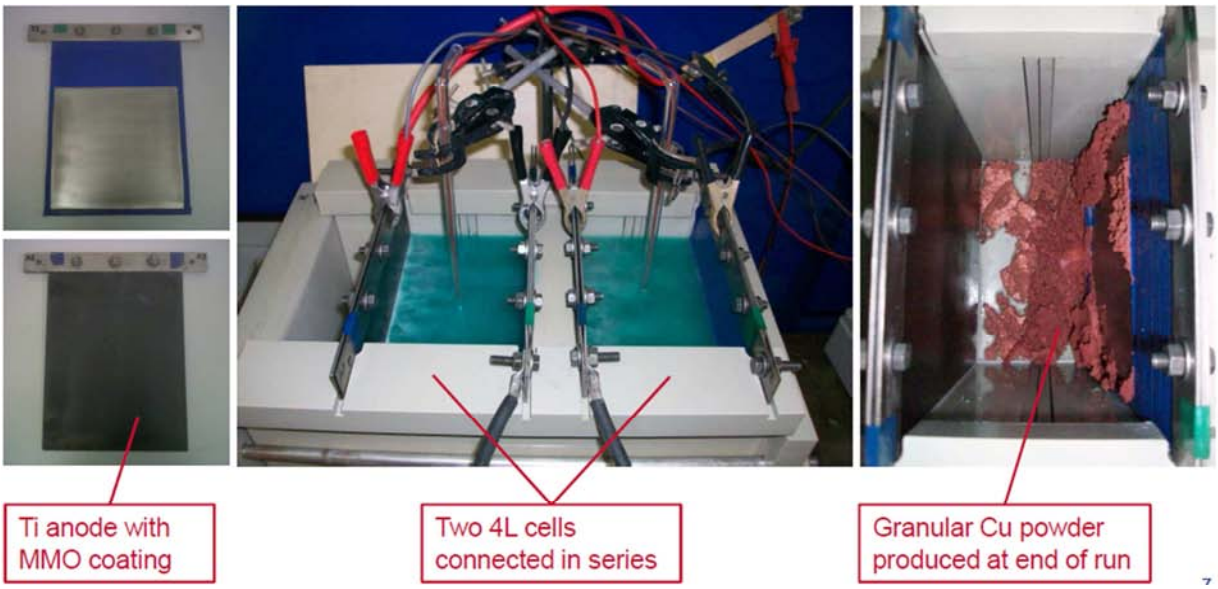

Figure 16: Experimental setup for a typical run.

Experimental work was carried out at Anglo American's Technical Solutions – Research in Johannesburg, South Africa. All runs were conducted in a walk-in fume cupboard at room temperature.

5 RESULTS AND DISCUSSION

5.1 ELECTROCHEMICAL REDUCTION TO PRODUCE COPPER POWDER

In order to characterise the electrochemical reduction of copper to copper powder under the experimental conditions, the following factors were evaluated:

i. Aqueous concentration profiles of copper, together with nickel and iron
ii. Reproducibility of the experimental method and analysis
iii. Process yield for copper
iv. Current efficiency of the process
v. Cell voltage and energy consumption
vi. Electro-active area per unit volume and process kinetics
vii. Gas evolution and solids production

5.1.1 Aqueous Concentration Profiles

The electrochemical reduction of a species is largely dependent on the thermodynamics and kinetics of the process. For a solution that contains a number of different aqueous species, the order of reducibility of species can be estimated in theory by its thermodynamic properties. However, the kinetics of the reactions taking place control what is practically probable. In order to test the hypothesis of selective recovery of copper over nickel and iron in acidic aqueous sulfate solutions, an acidic sulfate solution containing 30 g/L Cu(aq), 10 g/L Ni(aq) and 5 g/L Fe(III)(aq) was considered.

The thermodynamic order of reducibility based on the Nernst equation for this solution at 25°C is as follows: $Fe^{3+}(aq) > Cu^{2+}(aq) > H^{+}(aq) > Ni^{2+}(aq) > Fe^{2+}(aq)$. It is thus anticipated that ferric (Fe^{3+}) ions will be reduced to ferrous (Fe^{2+}) ions. This is followed by $Cu^{2+}(aq)$ reduction to Cu(s). Once most of the copper has been removed from solution it is expected that $H_2(g)$ will form. Thereafter $Ni^{2+}(aq)$ and subsequently $Fe^{2+}(aq)$ will be reduced to its solid components. Due to the reversible nature of the Fe^{3+}/Fe^{2+} reaction it is anticipated that once ferric is reduced at the cathode, some of it might oxidise at the anode, causing a mixture of ferric and ferrous species to be present in the electrolyte.

The aqueous metal concentration profiles of copper, nickel and iron under base case conditions (Run 1B) are given in Figure 17. The ratio of ferric to ferrous ions for the same run is given in Figure 18.

From Figure 17 it can be seen that the $Cu^{2+}(aq)$ concentration first decreased linearly with time, followed by an inverse exponential decrease, The nickel and total iron in solution remained constant under the experimental conditions. This illustrates that $Cu^{2+}(aq)$ was reduced to Cu(s) under the experimental conditions, without the reduction of $Ni^{2+}(aq)$ to Ni(s) or $Fe^{2+}(aq)$ to Fe(s). It furthermore illustrates that the electrochemical recovery of copper under the base case conditions was governed by two operating regimes: current limited (linear range) and mass transport limited (exponential range).

Figure 17 illustrates a linear increase and gradual flattening of the $H^{+}(aq)$ concentration profile. This corresponds with the inverse of the $Cu^{2+}(aq)$ concentration profile. The initial linear increase in the $H^{+}(aq)$ concentration was a result of the water oxidation reaction that occurred at the anode at the corresponding rate. The gradual flattening of the $H^{+}(aq)$ concentration profile indicates evolution of $H_2(g)$ by the reduction reaction of $H^{+}(aq)$. Similar aqueous concentration profiles were seen for all the experimental runs conducted (Run 1A-11). See Appendix B.

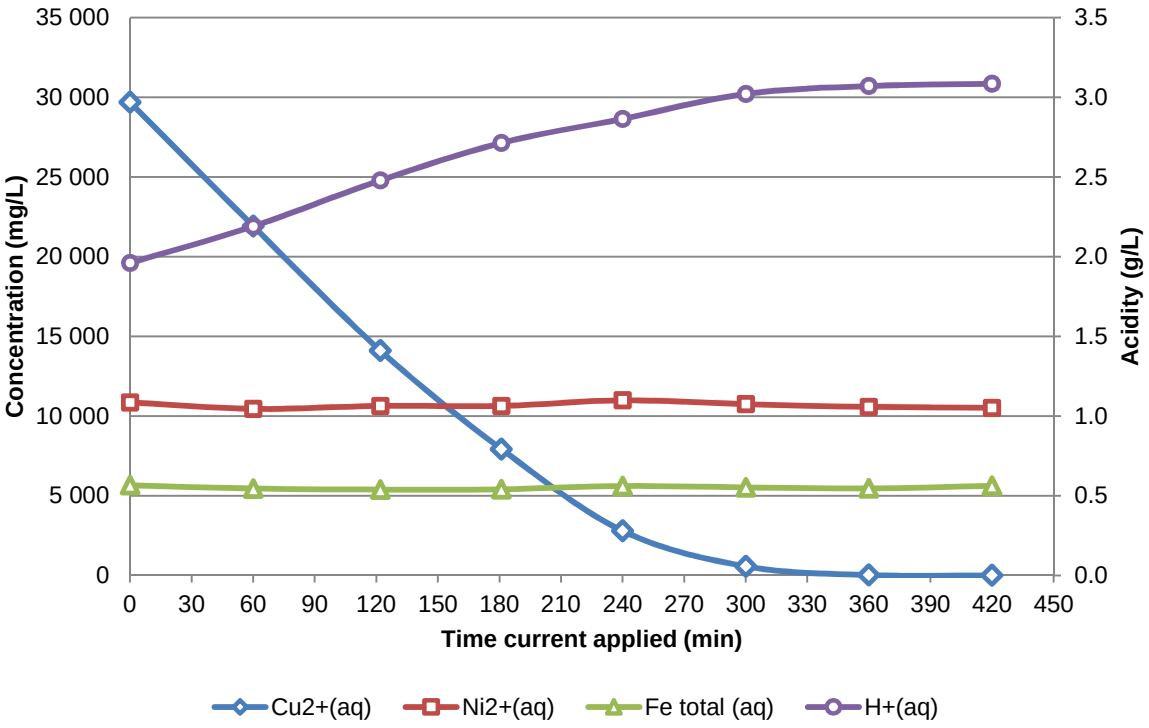

Figure 17: Aqueous concentration profiles (Run 1B).

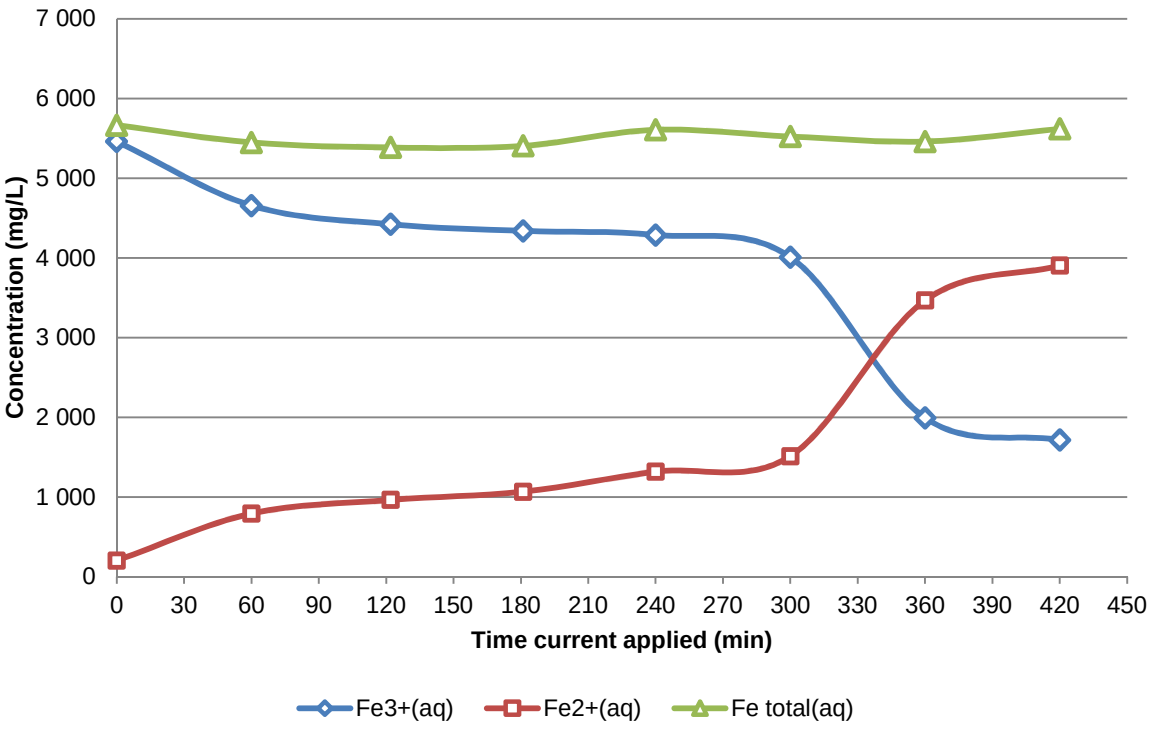

Figure 18: Aqueous Fe^{3+}/Fe^{2+} speciation profiles (Run 1B).

Figure 18 illustrates the ferric-, ferrous- and total aqueous iron concentration profiles for Run 1B. It can be seen that as the $Fe^{3+}(aq)$ concentration decreased, the $Fe^{2+}(aq)$ concentration increased to maintain a constant total aqueous iron concentration (≈ 5.5 g/L). Furthermore, it can be seen that the reduction of $Fe^{3+}(aq)$ to $Fe^{2+}(aq)$ occurred at two different rates. From 0 minutes to approximately 300 minutes the rate of $Fe^{3+}(aq)$ reduction was slow. After 300 minutes, the rate of $Fe^{3+}(aq)$ reduction increased. This corresponds to the point where $Cu^{2+}(aq)$ is depleted and $H_2(g)$ evolution is dominant. The increased rate of $Fe^{3+}(aq)$ reduction after 300 minutes is attributed to copper becoming mas transport limited.

5.1.2 Reproducibility

In order to illustrate reproducibility of the experimental method, the base case runs (Run 1A and Run 1B) were conducted using the same feed solution under the same operating conditions. Aqueous concentration profiles for Run 1A and Run 1B are compared in Figure 19 and Figure 20.

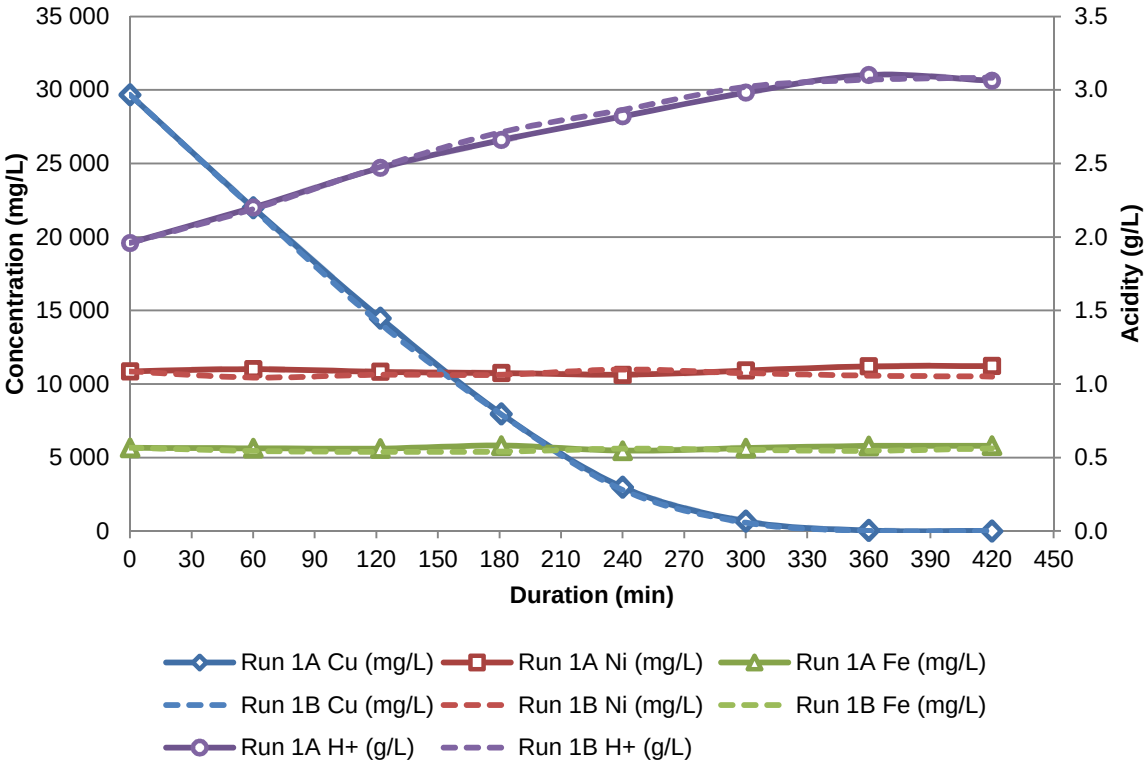

Figure 19: Aqueous concentration profiles to illustrate reproducibility (Run 1A and 1B).

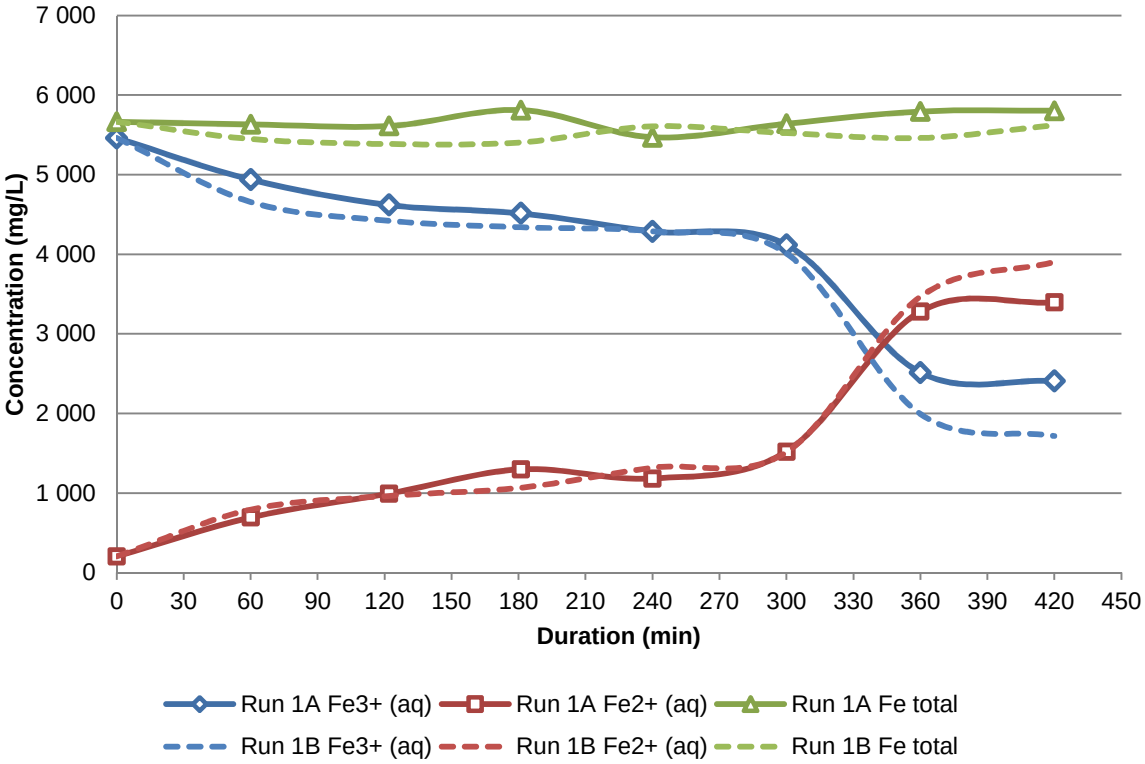

Figure 20: Aqueous Fe^{3+}/Fe^{2+} speciation profiles to illustrate reproducibility (Run 1A and Run 1B).

Figure 19 and Figure 20 illustrate very good reproducibility for the experimental method and analysis followed. The copper concentration profile and electrolyte acidity measured for Run 1A correlated well with that of Run 1B (correlation coefficients of 99.99% and 99.97%, respectively). The nickel and iron concentrations for Run 1A were found to be statistically similar to that of Run 1B at a confidence level of 92.43% and 97.36%, respectively. The ferrous ion concentration profile for Run 1A correlated well with that of Run 1B (correlation coefficient of 99.36%).

5.1.3 Process Yield

The process yield for copper (X_{Cu}) under base case conditions (Run 1A and Run 1B) are given in Figure 21. From Figure 21 it can be seen that a process yield of greater than 99.99% could be achieved after seven hours under the base case conditions. Process yield for copper increased linearly with time in the current limited regime as per Faraday's law. Once the mass transport limited regime was approached; the rate of increase was slower.

For a process yield of 95% it was required that current be applied to the electrolyte for the duration of approximately 4.5 hours.

After electrochemical reduction for seven hours and subsequent washing and filtration it was found that the Cu^{2+}(aq) concentration in the filtrate increased slightly, which resulted in a reduction in process yield. For Run 1A and Run 1B the process yields decreased from >99.99% to 99.95% and 99.93% respectively after filtration. This is attributed to the formation of very fine copper powder under mass transport limited conditions, and subsequent re-dissolution.

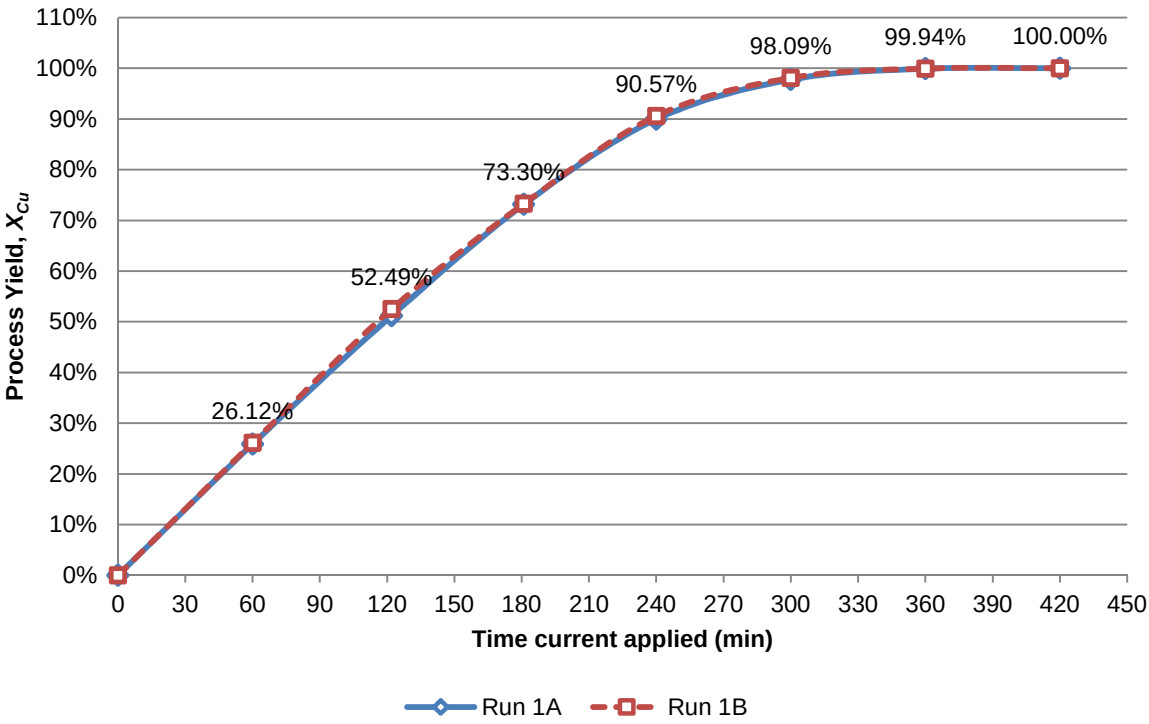

Figure 21: Process yield for copper (Run 1A and 1B).

5.1.4 Current Efficiency

The instantaneous current efficiency (ϕ_i) and overall current efficiency (ϕ) of the electrochemical reduction of copper are given in Figure 22 and Figure 23 for the base case runs. It can be seen that the instantaneous current efficiency decreased from 108% to 0% during the course of the experimental run, whilst the overall current efficiency was in the range of 108% to 58%.

As the experimental run proceeded to the point where copper was completely removed from solution (process yield of 100%), the instantaneous current efficiency and overall current efficiency decreased to 0% and 58%, respectively.

Current efficiencies greater than 100% is attributed to non-ideal mixing of the electrolyte in the absence of hydrogen evolution. It is also considered that the formation of a Cu^+ intermediate could impact the current efficiency of the process [34]. The corresponding reduction reaction is given as follows:

$$Cu^+ + e^- \rightarrow Cu \qquad (33)$$

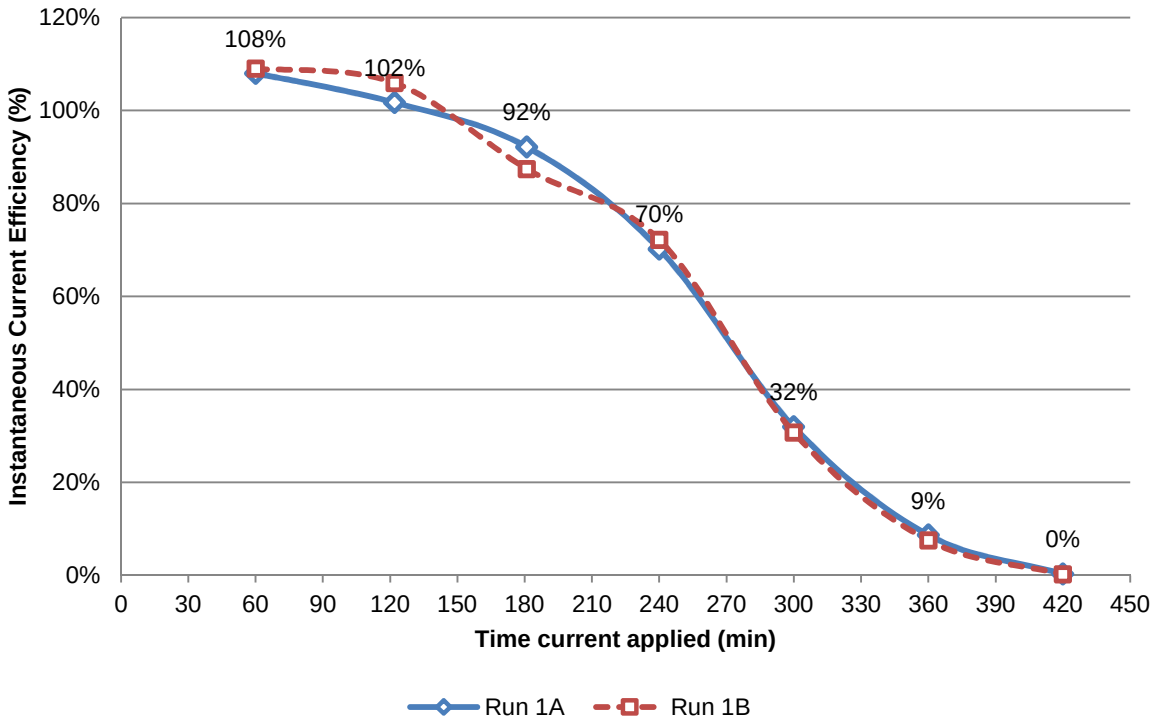

Figure 22: Instantaneous current efficiency (Run 1A and 1B).

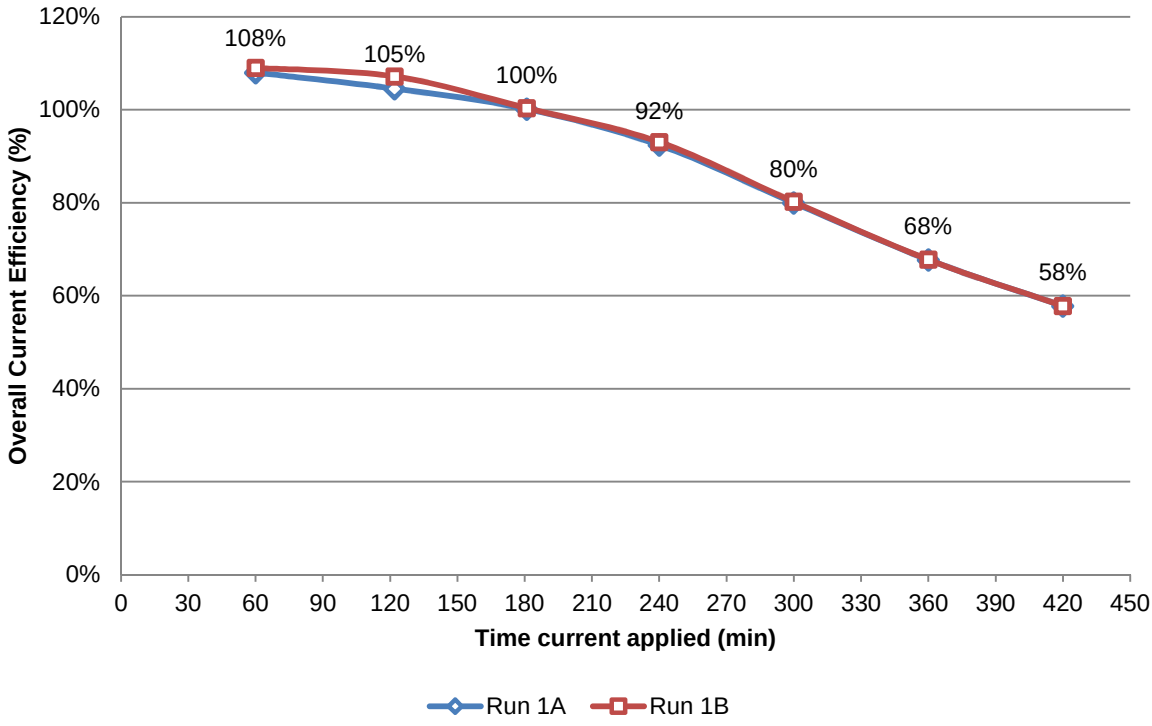

Figure 23: Overall current efficiency (Run 1A and 1B).

5.1.5 Cell Voltage and Energy Consumption

The electrical energy consumption of an electrochemical process is closely related to its cell voltage. In order to minimise energy consumption of a specific process, it is preferable to select process conditions where the cell voltage is minimised. Cell voltage and electrolyte temperature profiles for the base case runs are given in Figure 24 and Figure 25.

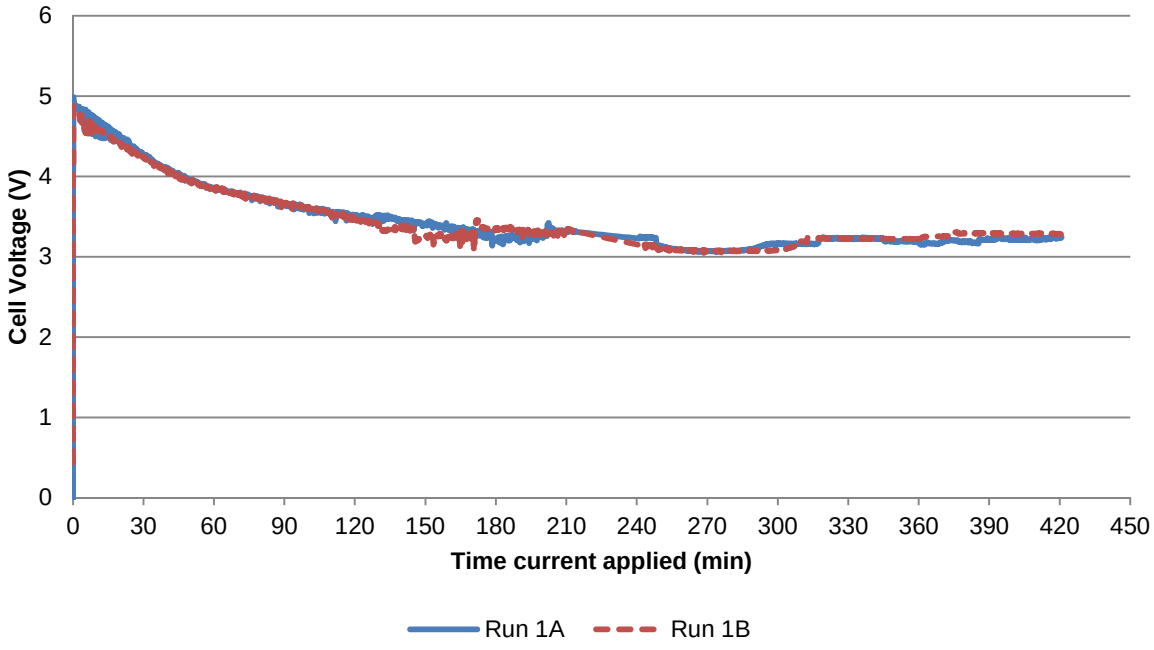

Figure 24: Cell voltage (Run 1A and 1B).

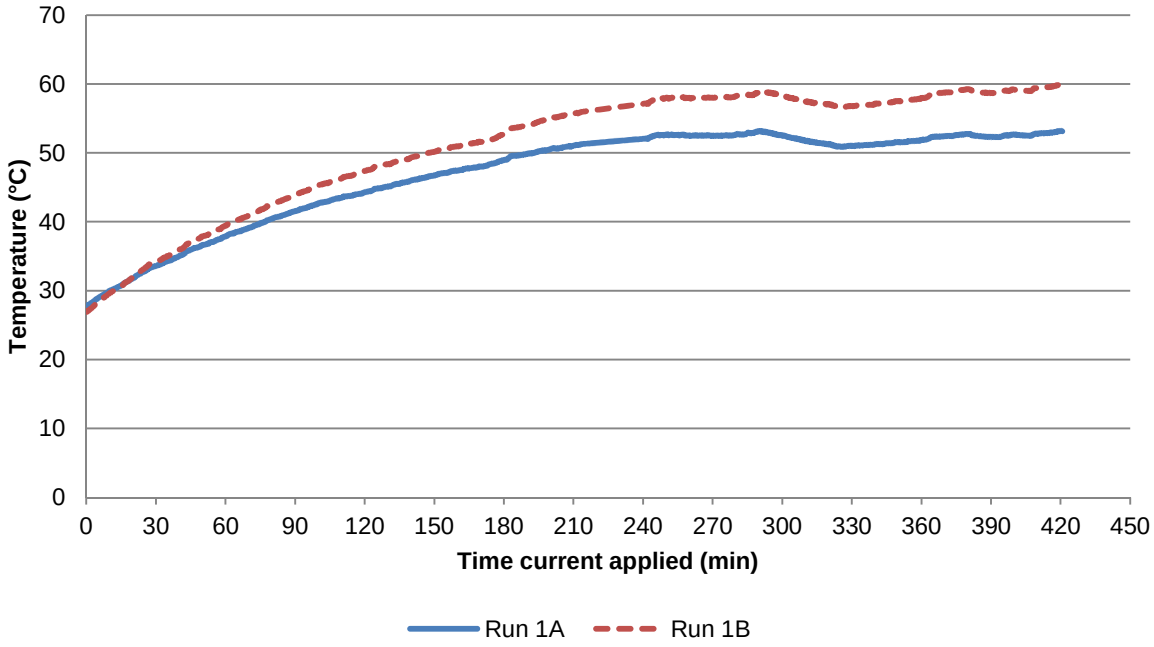

Figure 25: Electrolyte temperatures (Run 1A and 1B).

Cell voltage measurements under base case conditions (Figure 24) decreased from 5.0 V to 3.2 V over a period of seven hours. This decrease in cell voltage is attributed to a change in the electrolyte temperature from 27°C to ≈55°C (Figure 25) due to current passing between the electrodes. The increase in electrolyte temperature increases the conductivity of the electrolyte, which, as a result of its inverse proportionality, decreases the internal cell resistance (R_{CELL}).

The internal cell resistance for a given electrochemical cell can be determined by evaluating the linear relationship that exists between cell voltage (*y*-axis) and applied current (*x*-axis). This relationship is given as follows by re-arranging Equation 30:

$$\underbrace{E_{CELL}}_{y} = \underbrace{-R_{CELL}}_{m} \underbrace{I}_{x} + \underbrace{\left(E_e^C - E_e^A - \sum|\eta|\right)}_{c} \qquad (34)$$

where the internal cell resistance is determined from the slope of the line (*m*); and the sum of the anode and cathode equilibrium potentials and overpotentials by the y-intercept of the line (*c*). Cell voltage data for three runs at different applied currents (Run 1A, 2 and 3) was used in the analysis to determine the required parameters. The linear relationship between cell voltage and applied current (Equation 34) is given in Figure 26 at three different processing times.

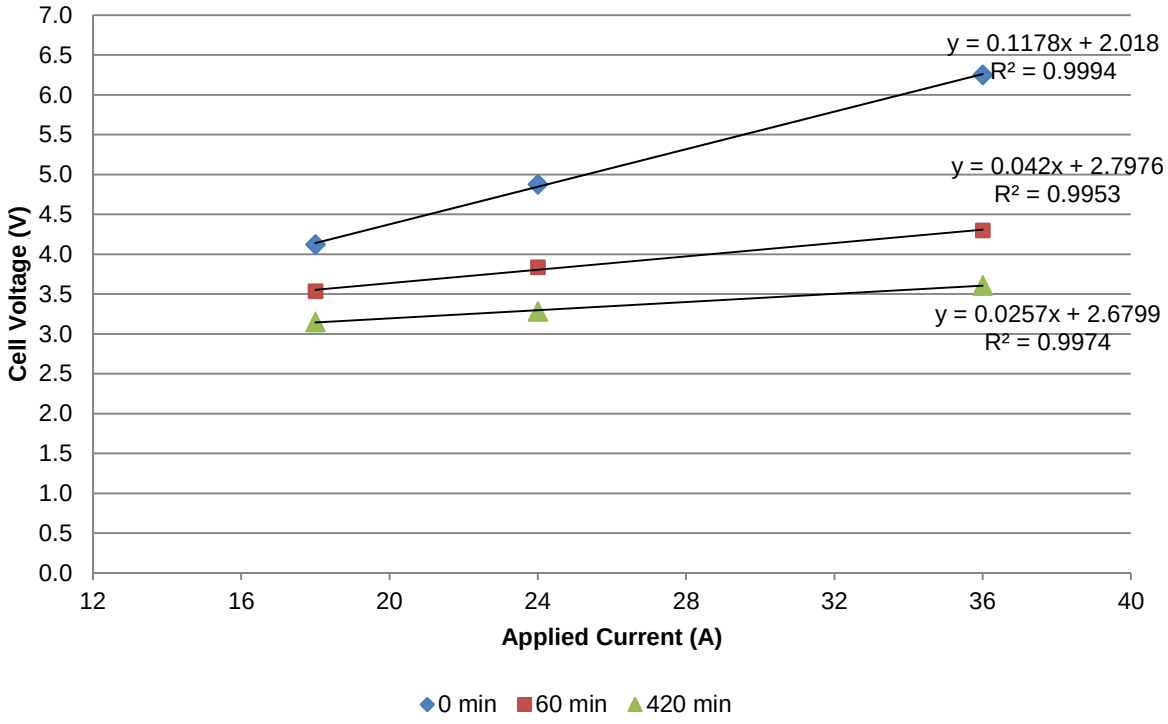

Figure 26: Linear relationship between cell voltage and applied current.

Figure 26 illustrates a decrease in the cell resistance (slope of lines) from 0.1178 to 0.0257 Ω with increasing processing time. In order to illustrate the cell resistance of the process over the full processing time, the cell resistance was calculated at 10 second intervals. This is illustrated in Figure 27.

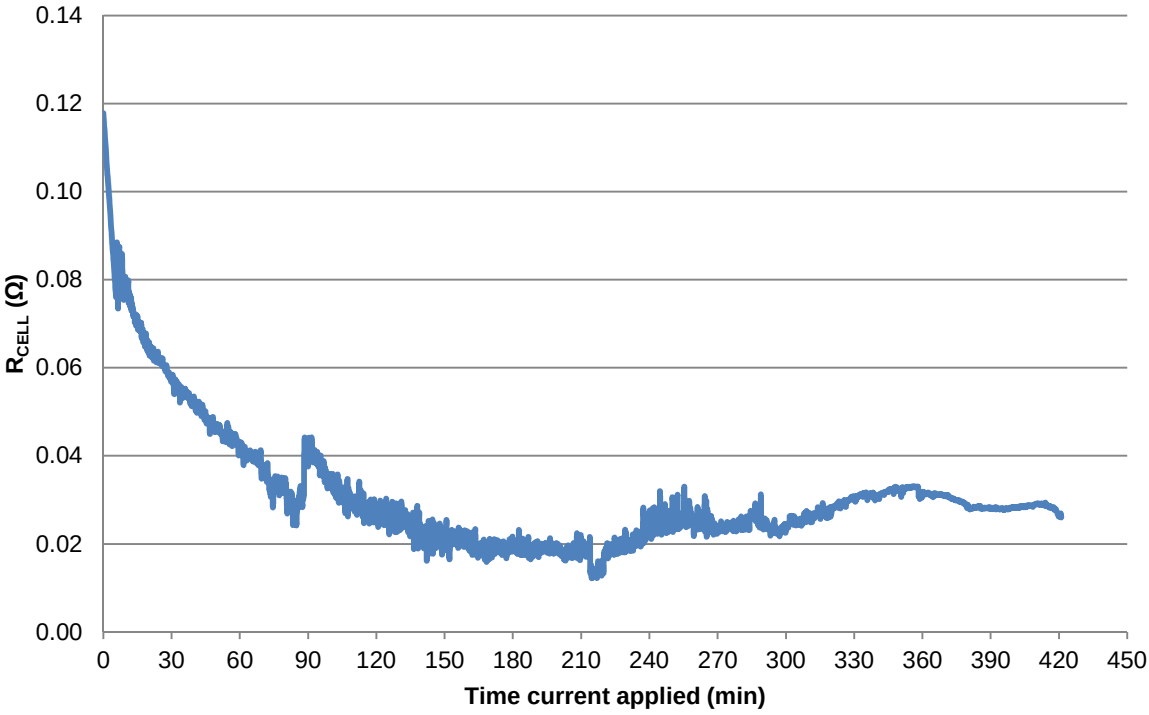

Figure 27: Calculated internal cell resistance based on Run 1-3 data.

From Figure 27 it can be seen that the internal cell resistance decreases from 0.12 to ≈0.03 Ω. This supports the notion of a decrease in cell voltage as a result of increased temperature and increased conductivity of the electrolyte.

The anode and cathode equilibrium potentials can be calculated using the Nernst equation, provided the reactions that occur at the anode and cathode; electrolyte temperature; and the molar concentrations of the relevant species are known. For the purposes of this analysis the reactions are taken as follows:

At the cathode: $Cu^{2+} + 2e^- \rightarrow Cu(s)$ E^0 = 0.340 V (16)

At the anode: $2H_2O \rightarrow O_2(g) + 4H^+ + 4e^-$ E^0 = 1.229 V (18)

Thus, the cathode and anode equilibrium potential for the considered system can be expressed as follows:

$$E_e^C = 0.340 + \frac{RT}{2F} \ln\left(\frac{1}{[Cu^{2+}]}\right) \quad (35)$$

$$E_e^A = 1.229 + \frac{RT}{4F} \ln\left([H^+]^4\right) \quad (36)$$

The difference in anode and cathode equilibrium potential under base case conditions (Run 1A and Run 1B) was calculated using Equation 35 and Equation 36. This is illustrated in Figure 28 as a function of time. From Figure 28 it can be seen that the E_e^C - E_e^A is in the order of 1.60 V and increases to ≈1.73 V with increase in temperature and decrease in Cu^{2+}(aq) concentration.

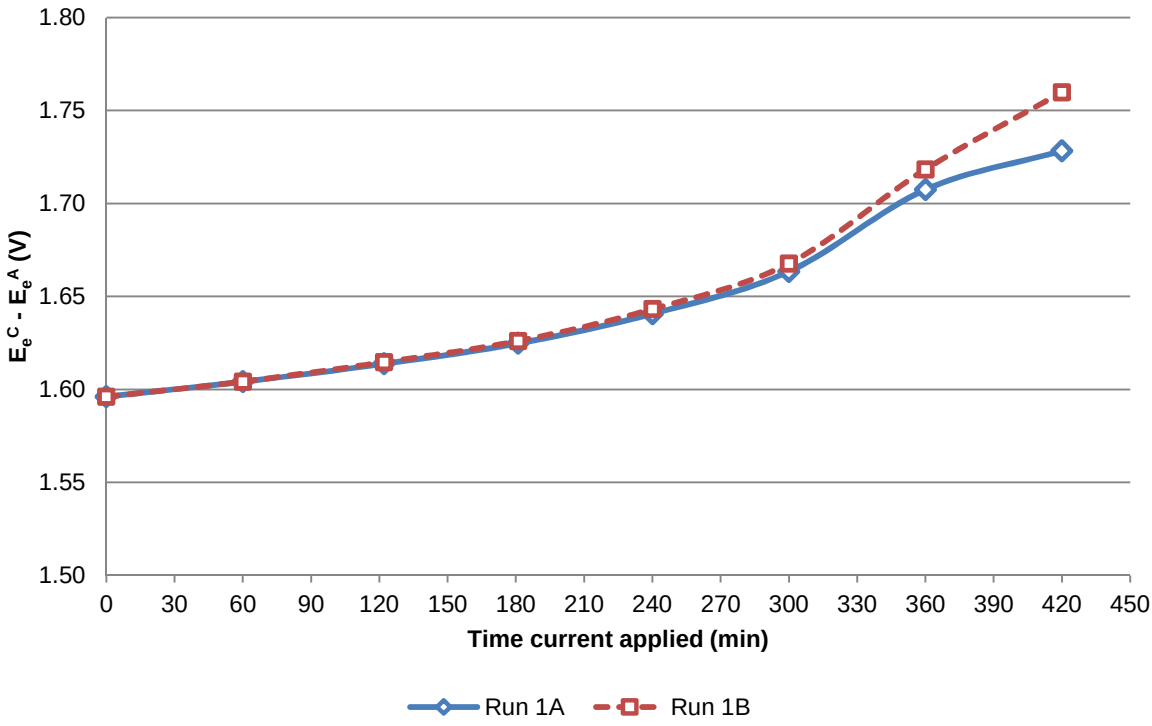

Figure 28: Difference in equilibrium potential (Run 1A and 1B).

Given the difference in equilibrium potential, the difference in overpotential can be estimated using the y-intercept (*c*) of the linear correlation (Equation 34). The sum of the anodic and cathodic overpotentials over time is given in Figure 29. This is in the order of 0.7-1.5 V.

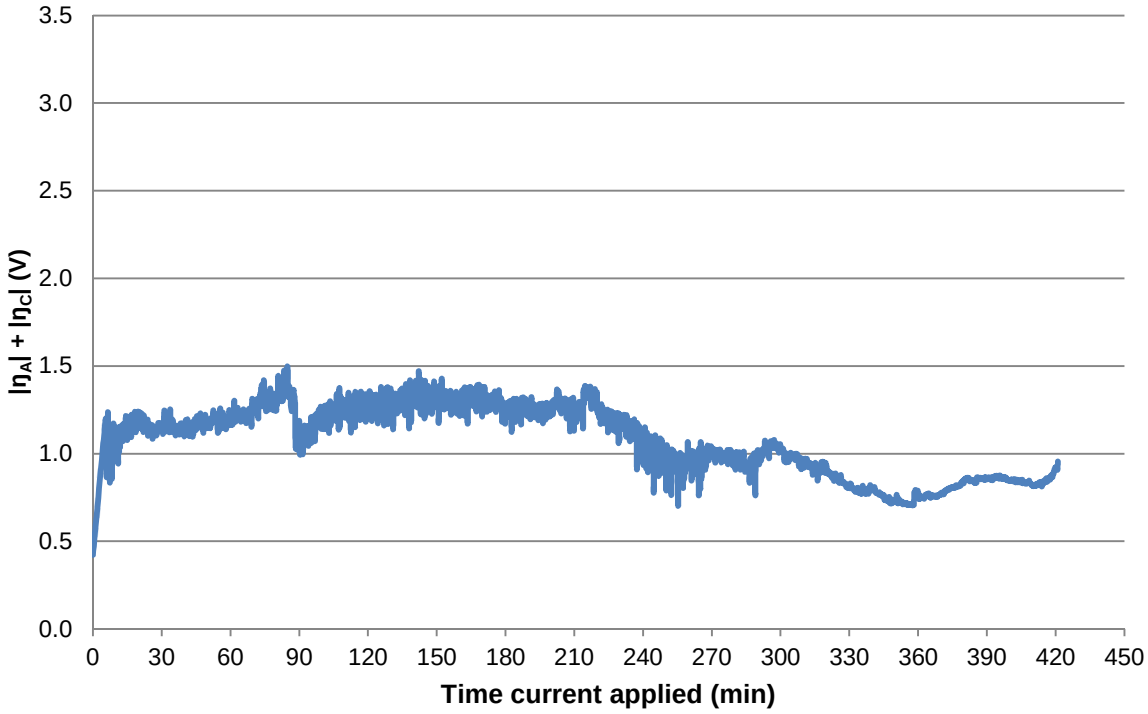

Figure 29: Sum of the anode and cathode overpotentials (Run 1A and Run 1B).

Based on the cell voltage and overall current efficiency of the electrochemical process, the specific energy consumption was determined to be in the range of 11.13-19.12 kWh/kg Cu. Figure 30 illustrates the specific energy consumption of the process relative to its process yield under the base case conditions.

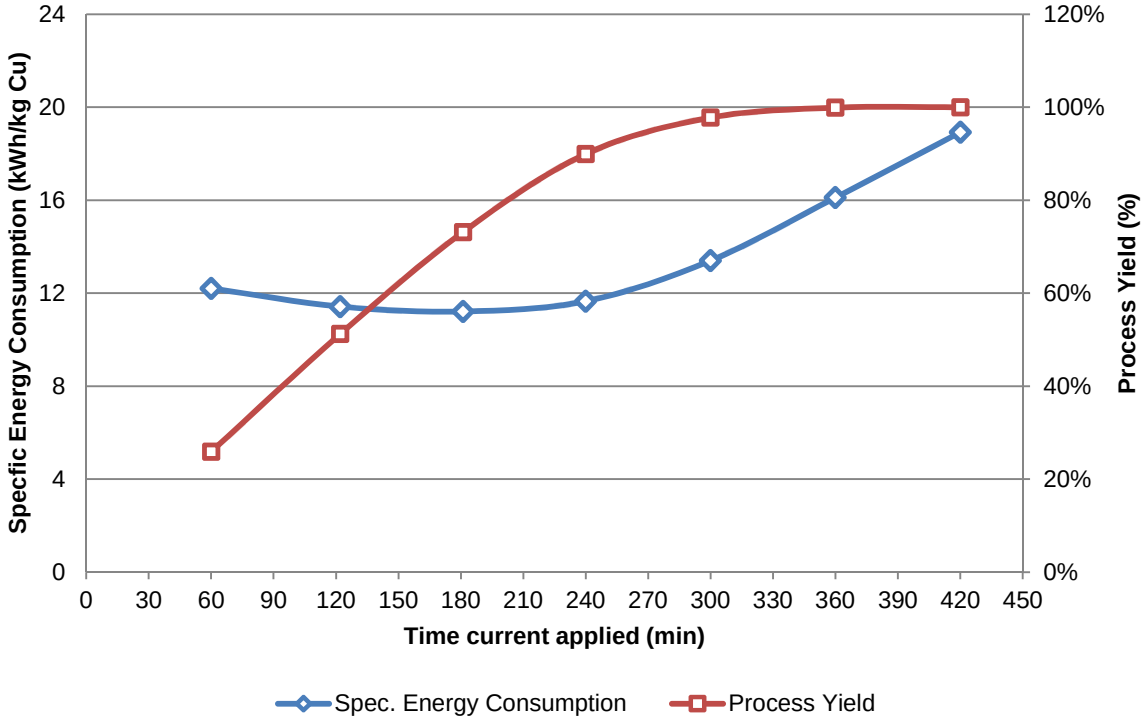

Figure 30: Specific energy consumption versus process yield (Run 1A).

From Figure 30 it can be seen that for an electrochemical process targeting a process yield of 95% the overall specific energy consumption is 12.37 kWh/kg Cu.

5.1.6 Electro-active Area and Process Kinetics

The electro-active area of the electrochemical cell was determined to be 6.00 m^2/m^3. This is based on bench-scale cathodes area of 0.024 m^2 and electrolyte volume of 0.004 m^3.

In order to illustrate the current limited and mass transport limited regimes for copper over the entire experimental range, the recovery profiles for Run 1A (*Base Case*), Run 6 (*High Cu*) and Run 7 (*Low Cu*) were combined and off-set for processing time. The combined data set is given in Figure 31.

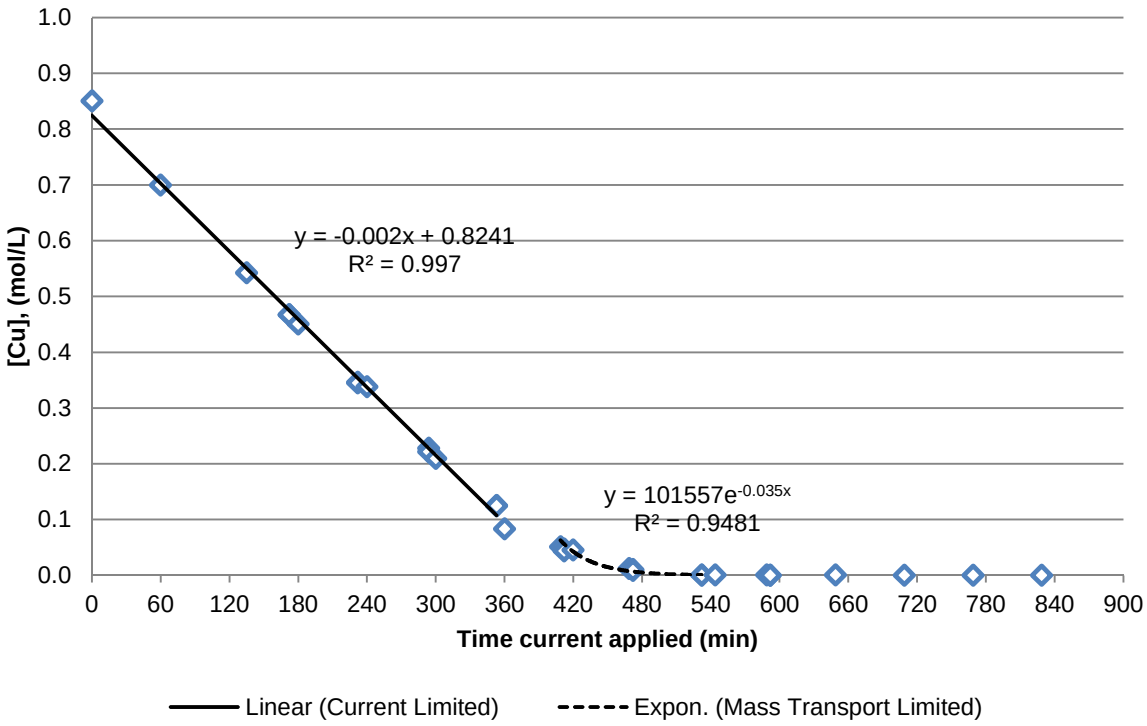

Figure 31: Current limited and mass transport limited regimes for copper.

Figure 31 illustrates a linear current limited regime where copper is electrochemically reduced at rate of 2.03×10^{-3} $mol.L^{-1}.min^{-1}$ up to a concentration of approximately 0.125 mol/L copper. Below 0.125 mol/L copper, the process undergoes a mixed zone before becoming mass transport limited below a concentration of approximately 0.050 mol/L copper.

5.1.7 Gas Evolution and Solids Formation

In order to illustrate the evolution of gases and the formation of solids, pictures were taken during various stages of the experimental runs. This is illustrated in Figure 32.

The evolution of oxygen gas at the anode under current limited conditions is illustrated in Figure 32a. During electrolysis under these conditions small oxygen bubbles are formed on the anode surface and form streaky patterns in the electrolyte. No gas evolution is observed at the cathode surface. During electrolysis the electrolyte becomes milky as a result of the oxygen bubbles and changes colour from blue to green as copper is removed from solution. The streaky patterns in the electrolyte indicate poor mixing under these operating conditions.

The initial stages of hydrogen gas evolution at the cathode between the current limited and mass transport limited operating regimes are illustrated in Figure 32b. Large hydrogen bubbles are observed at the cathode surface and small oxygen bubbles are observed at the cathode.

The evolution of oxygen gas at the anode and hydrogen gas at the cathode under mass transport controlled conditions are illustrated in Figure 32c. Small oxygen bubbles are observed at the anode with larger hydrogen bubbles at the cathode. Under these conditions the patterns formed by oxygen gas evolution at the anode are less streaky, thus indicating better mixing of the electrolyte.

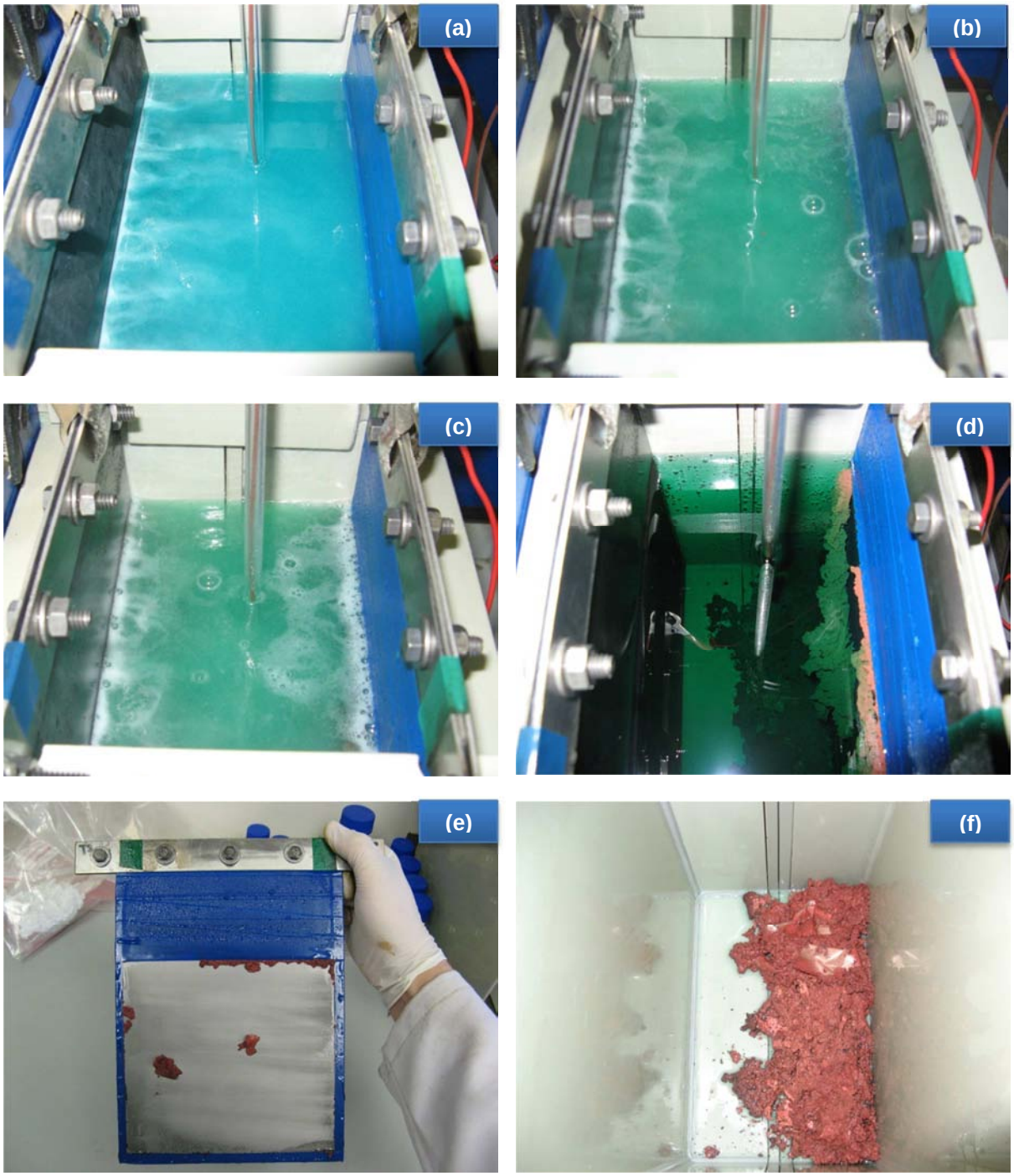

Figure 32: Pictures at various stages of the experimental run under base case conditions. (a) Evolution of oxygen gas at the anode under current limited conditions. (b) Initial stages of hydrogen gas evolution at the cathode during mixed current limited and mass transport limited conditions. (c) Evolution of oxygen gas at the anode and hydrogen gas at the cathode under mass transport controlled conditions. (d) Solids generated after seven hours of electrochemical reduction. (e) The cathode surface after seven hours of electrochemical reduction. (f) Solids remaining in the reactor after draining of the electrolyte.

The solids generated after seven hours of electrochemical reduction are illustrated Figure 32d. Once the current stopped, the electrolyte became clear. It was observed that the majority of the solids were present at the bottom of the electrochemical reactor. A small amount of solids were observed on the

cathode surface. However, these solids were loosely adhered to the cathode surface and detached on removal on cathode from the reactor.

The cathode surface after seven hours of electrochemical reduction is illustrated in Figure 32e. The cathode surface contained some copper solids, but no electroplating of copper on the surface was observed. The copper solids could be removed by washing the surface with water and the cathode could be reused in subsequent experimental runs.

The solids produced after seven hours of electrochemical reduction and draining of the filtrate is illustrated in Figure 32f. The bulk of the solids were granular. A single metal film was observed. It was considered that this was part of the solids that loosely adhered to the copper cathode surface and subsequently detached on removal of the cathode.

5.2 OPTIMAL OPERATING CONDITIONS AND IMPACT OF FEED VARIATION

In order to determine the optimum operating regime and the impact that feed variation could have on the overall process, variation of the following parameters were considered:

i. Applied current
ii. Initial acidity
iii. Initial Cu concentration
iv. Initial Ni concentration
v. Initial Fe concentration

A summary of the process yield (after electrochemical reduction and after filtration) and overall current efficiencies for all experimental runs (Run 1A-Run 11) is shown in Table 5.

Table 5: Summary of process yields and overall current efficiency for all experimental runs after seven hours of processing.

Run	Description	Process yield after reduction (%)	Process yield after filtration (%)	Overall current efficiency (%)
Run 1A	*Base Case A*	99.98%	99.53%	59.58%
Run 1B	*Base Case B*	100.00%	99.35%	59.59%
Run 2	*High Current*	100.00%	99.89%	39.51%
Run 3	*Low Current*	99.33%	98.80%	77.91%
Run 4	*High Acidity*	99.99%	99.87%	61.34%
Run 5	*Low Acidity*	99.85%	90.30%	63.68%
Run 6	*High Cu*	94.67%	90.11%	102.76%
Run 7	*Low Cu*	99.51%	93.89%	6.50%
Run 8	*High Ni*	100.00%	99.71%	59.29%
Run 9	*Low Ni*	99.99%	99.63%	61.62%
Run 10	*High Fe*	99.95%	99.36%	62.40%
Run 11	*Low Fe*	100.00%	99.87%	63.18%

From Table 5 it can be seen that the process yield after electrochemical reduction for all experimental runs varied in the range of 94.67-100.00%. The low process yield for *High Cu* (94.67%) is attributed to insufficient processing time for complete copper reduction. Under experimental conditions where sufficient processing time was allowed, the process yields after electrochemical reduction were in the range of 99.33-100.00%. The corresponding process yields after filtration and washing of the electrolyte were in the range of 90.30-99.89%. Overall current efficiencies varied from 6.50% (*Low Cu*) to 102.76% (*High Cu*). Overall current efficiencies for runs with higher and lower acidities, nickel concentrations and iron concentrations (Runs 4, 5 and 8-11) were comparable to that of *Base Case A* and *Base Case B*. Overall current efficiencies were lower than *Base Case* when higher current was applied (Run 2), and higher than *Base Case* when low current was applied (Run 3). This is attributed to a change in the rate of copper reduction – under high current conditions the rate of copper reduction increases and under low current conditions the rate decreases.

The operating and recovery profiles for all experimental runs are given in Appendix B.

5.2.1 Applied Current

Based on the operating and recovery profiles for Runs 1A (*Base Case*), 2 (*High Current*) and 3 (*Low Current*) (Appendix B) it can be seen that the rate of copper recovery, electrolyte temperature, cell voltage and acidity increased with increasing applied current. Nickel and iron recovery profiles remained unchanged. Figure 33 illustrates the rate of copper recovery in the current limited regime at various applied currents.

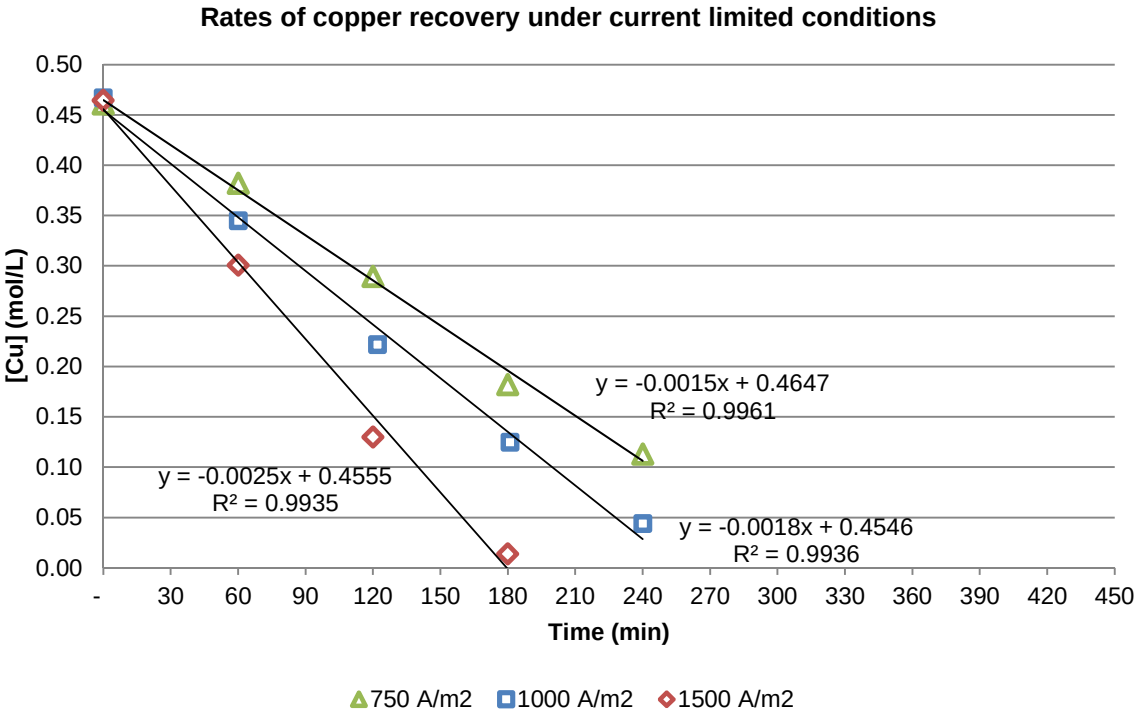

Figure 33: Rate of Cu recovery (current limited regime) at various applied currents.

From Figure 33 it can be seen that the rate of Cu recovery increases with increasing applied current.

A 50% increase in current density (from 1 000 A/m^2 to 1 500 A/m^2) resulted in a 43% increase the rate of Cu recovery (from 1.77 x 10^{-3} to 2.54 x 10^{-3} mol/(L.min)). Electrolyte temperature and cell voltage were respectively 13°C and 0.38 V higher than *Base Case* after 3 hours of processing.

A 25% decrease in current density (from 1 000 A/m^2 to 750 A/m^2) resulted in a 15% decrease in the rate of Cu recovery (from 1.77 x 10^{-3} to 1.49 x 10^{-3} mol/(L.min)). Electrolyte temperature and cell voltage were respectively 8°C and 0.06 V lower than *Base Case* after 3 hours of processing.

Figure 34 illustrates the impact of applied current on the process yield, instantaneous current efficiency, overall current efficiency and specific energy consumption of the process.

No difference in the powder production relative to the *Base Case* was observed.

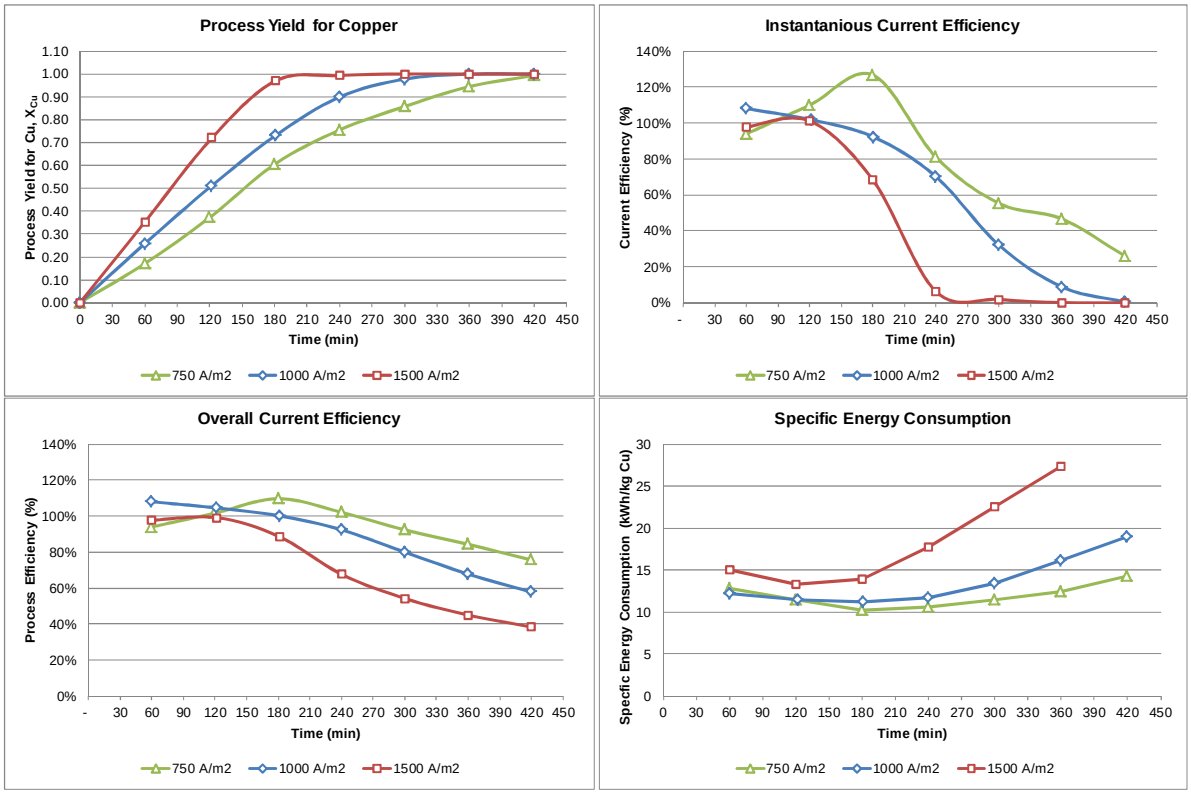

Figure 34: Impact of applied current on various process parameters.

Table 6 summarises the processing time, overall current efficiency, cell voltages and specific energy consumptions at various current densities and targeted copper extractions.

Table 6: Processing parameters at various current densities and targeted Cu extractions.

Targeted process yield (%)	Current density (A/m^2)	Processing time (min)	Overall current efficiency (%)	Cell voltage (V)	Spec. energy consumption (kWh/kg Cu)
90%	750	323	88.21%	3.10	11.96
	1 000	242	91.80%	3.16	11.72
	1 500	159	93.00%	3.70	13.54
95%	750	369	83.87%	3.07	12.48
	1 000	270	86.38%	3.14	12.37
	1 500	178	88.07%	3.62	14.02
99%	750	414	77.23%	3.13	13.82
	1 000	312	77.55%	3.15	13.85
	1 500	204	80.38%	3.55	15.06

From Table 6 it can be seen that for targeted process yields of 90%, 95% and 99% the processing time is 33-36% longer at 750 A/m^2 and 34-35% shorter at 1 500 A/m^2 (relative to *Base Case*). In general the specific energy consumption varies from 11.72-15.06 kWh/kg Cu.

The specific energy consumption together with required processing time for a targeted process yield of 95% is given in Figure 35 as a function of current density.

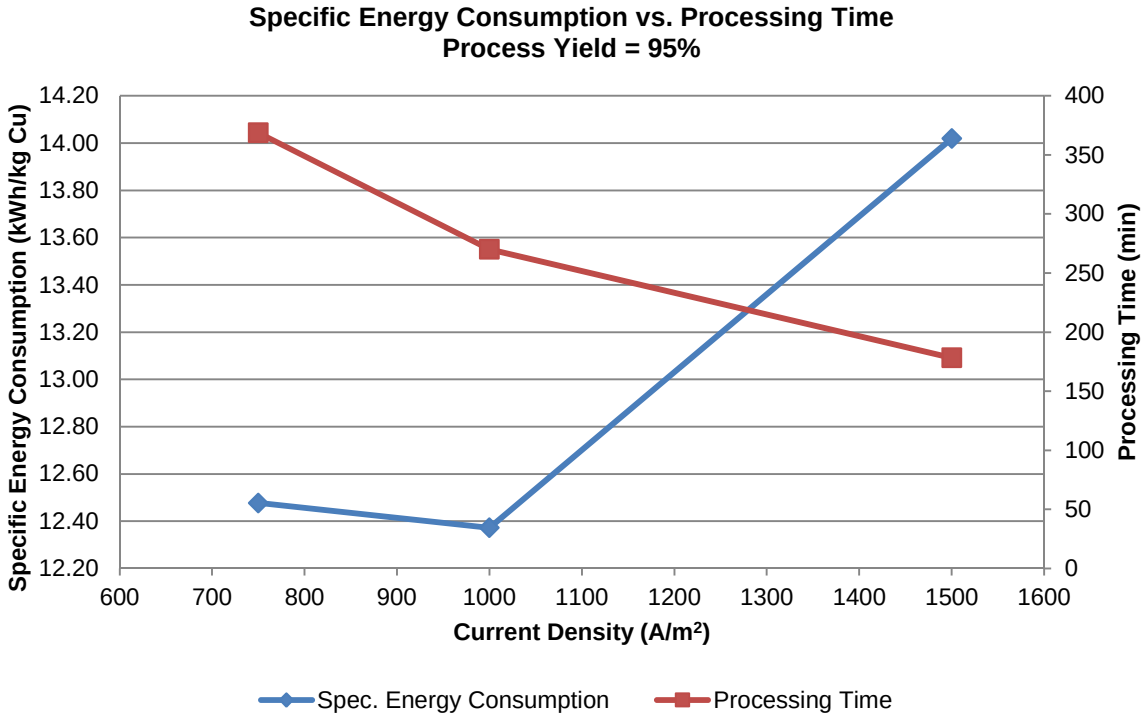

Figure 35: Specific energy consumption and processing times as a function of current density

From Figure 35 it can be seen that for a targeted process yield of 95% the optimum current density is 1 000 A/m^2 in terms of lowest specific energy consumption and processing time.

Based on this analysis it can be seen that higher applied current resulted in an increase in the rate of Cu recovery with a significant decrease in processing time. Conversely lower applied currents resulted in increased processing time, but generally have lower specific energy consumptions. For a targeted Cu recovery of 95% it was found that the optimum current density is 1 000 A/m^2 at a specific energy consumption of 12.37 kWh/kg Cu.

5.2.2 Initial Acidity

Based on the operating and recovery profiles for Runs 1A (*Base Case*), 4 (*High Acidity*) and 5 (*Low Acidity*) (Appendix B) it can be seen that the solution temperature and cell voltage increased with lower acidities. Copper, nickel and iron recovery profiles remained unchanged.

At an initial acidity of 0.5 mol/L H^+ (*Low Acidity*) the electrolyte temperature increased to 68.1°C after 4.5 hours of processing (15.6°C greater than *Base Case*). This corresponded with higher cell voltages, which reduced from 9.15 V to 3.99 V after 4.5 hours of processing (0.93 V higher than *Base Case*).

At an initial acidity of 4 mol/L H^+ (*High Acidity*), the electrolyte temperature was 4.8°C lower than *Base Case* after 4.5 hours of processing. This corresponded with lower cell voltages from 3.60 V to 2.80 V after 4.5 hours of processing (0.26 V lower than *Base Case*).

Figure 36 illustrates the impact of initial acidity on the process yield, instantaneous current efficiency, overall current efficiency and specific energy consumption of the process. In the range of 0.5-4 mol/L H^+, it was found that initial acidity of the aqueous solution did not significantly impact process yield, instantaneous current efficiency and overall current efficiency of the process. However, as a result of

the increased cell voltage at lower acidities, specific energy consumption was higher under these conditions.

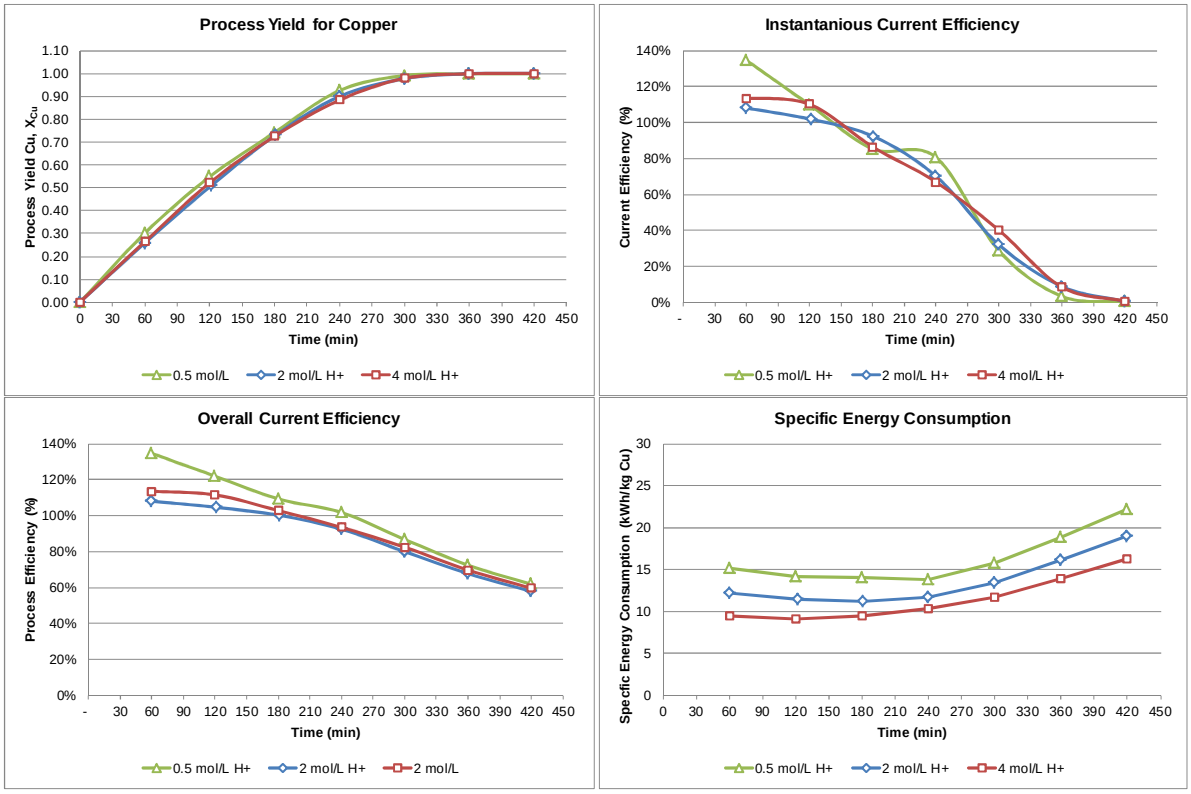

Figure 36: Impact of initial acidity on various process parameters.

The copper powder produced at an initial acidity of 0.5 mol/L H^+ (*Low Acidity)* and 5 mol/L H^+ (*High Acidity)* is shown in Figure 37a and Figure 37b, respectively.

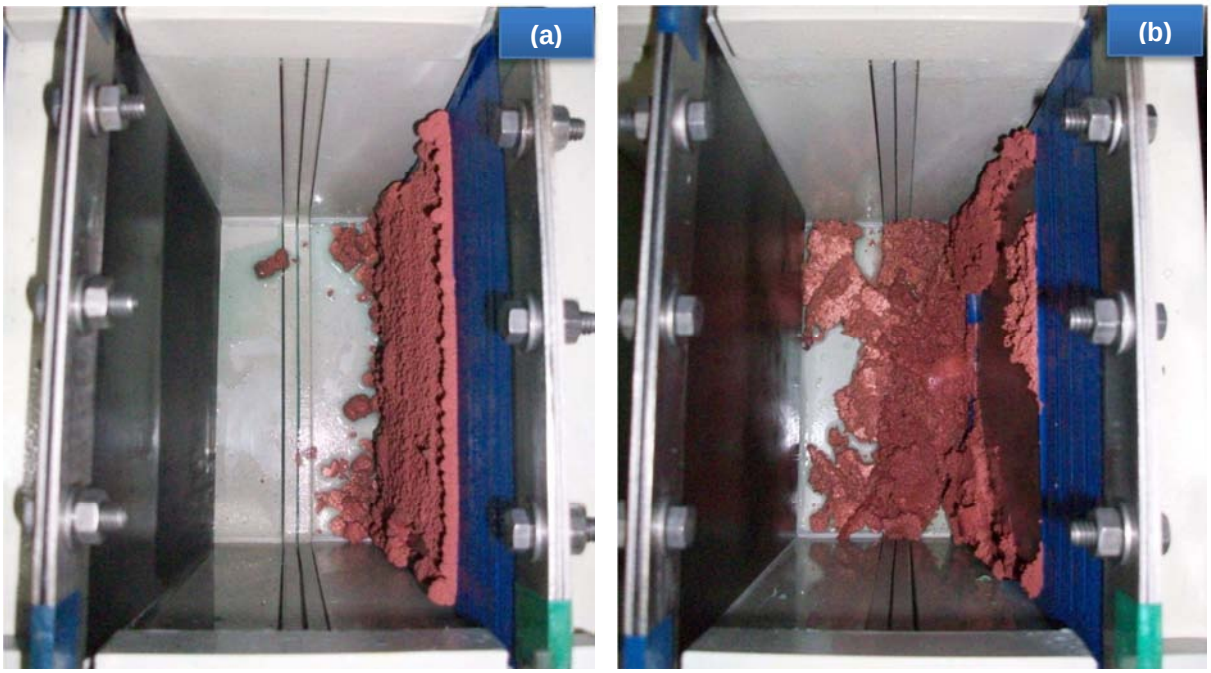

Figure 37: Copper powder produced under (a) *Low Acidity* and (b) *High Acidity* conditions.

From Figure 37a it can be seen that at the *Low Acidity* conditions the copper powder produced during the run was more adherent to the cathode surface (even after the electrolyte was drained and the cathode removed from the reactor. However, under *High Acidity* conditions (Figure 37b) similar copper powder production relative to the *Base Case* were observed.

Thus, based on this analysis it is concluded that low initial acidities in the order of 0.5 mol/L H^+ result in elevated temperatures and copper powders that adhere more strongly to the cathode surface. Given the potential impact of elevated temperature on materials of construction, and the requirement for more rigorous solids removal from the cathode, it is recommended that initial acidities be in the order of 2-4 mol/L H^+.

5.2.3 Initial Copper Concentration

Based on the operating and recovery profiles for Runs 1A (*Base Case*), 6 (*High Cu*) and 7 (*Low Cu*) (Appendix B) it can be seen that the solution temperature and cell voltage increased marginally with lower copper concentration. Slightly lower acidities were determined at lower copper concentrations. Nickel and iron recovery profiles remained unchanged.

Figure 38 illustrates the impact of initial copper concentration on the process yield, instantaneous current efficiency, overall current efficiency and specific energy consumption of the process.

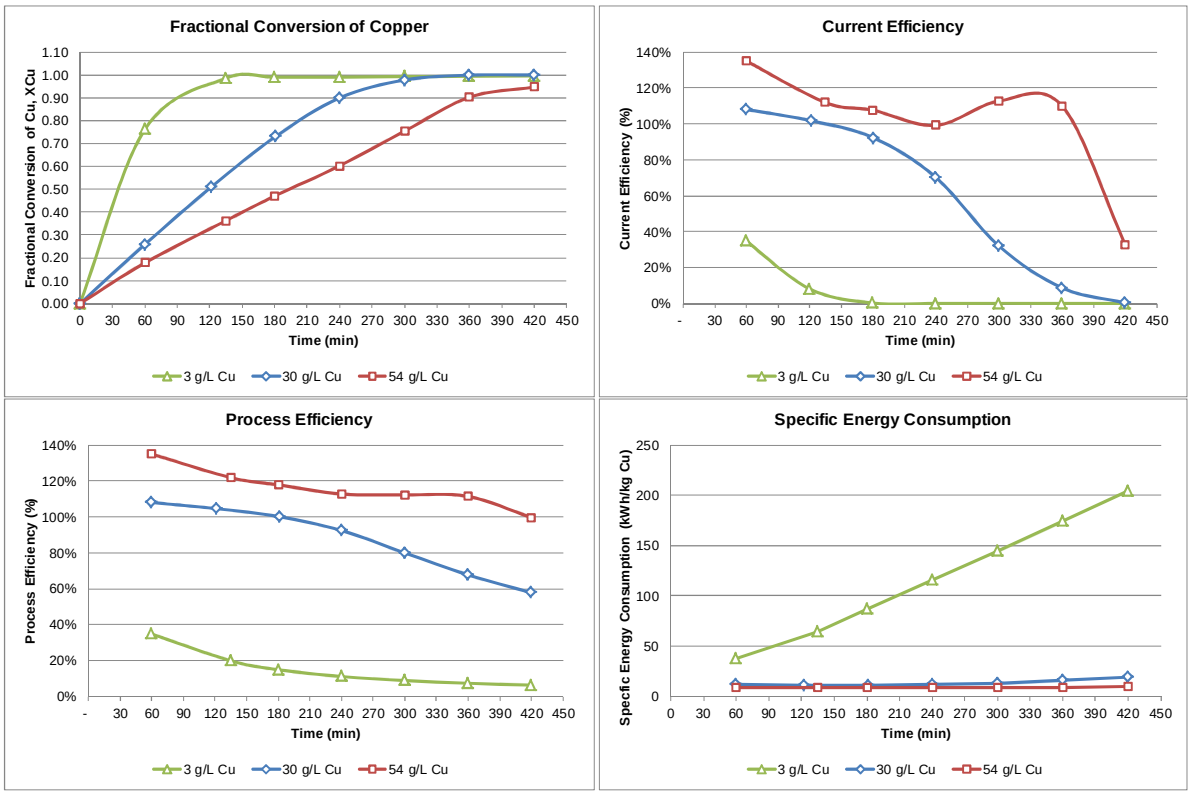

Figure 38: Impact of initial copper concentration on various process parameters.

From Figure 38 it can be seen that the initial copper concentration impacts the processing time, process efficiency and specific energy consumption. Lower copper concentrations required shorter processing times, but had lower process efficiencies and specific energy consumptions.

The copper powder produced at an initial concentration of 3 g/L copper (*Low Cu)* and 54 g/L copper (*High Cu)* is shown in Figure 39 (a, c) and Figure 39 (b, d) respectively.

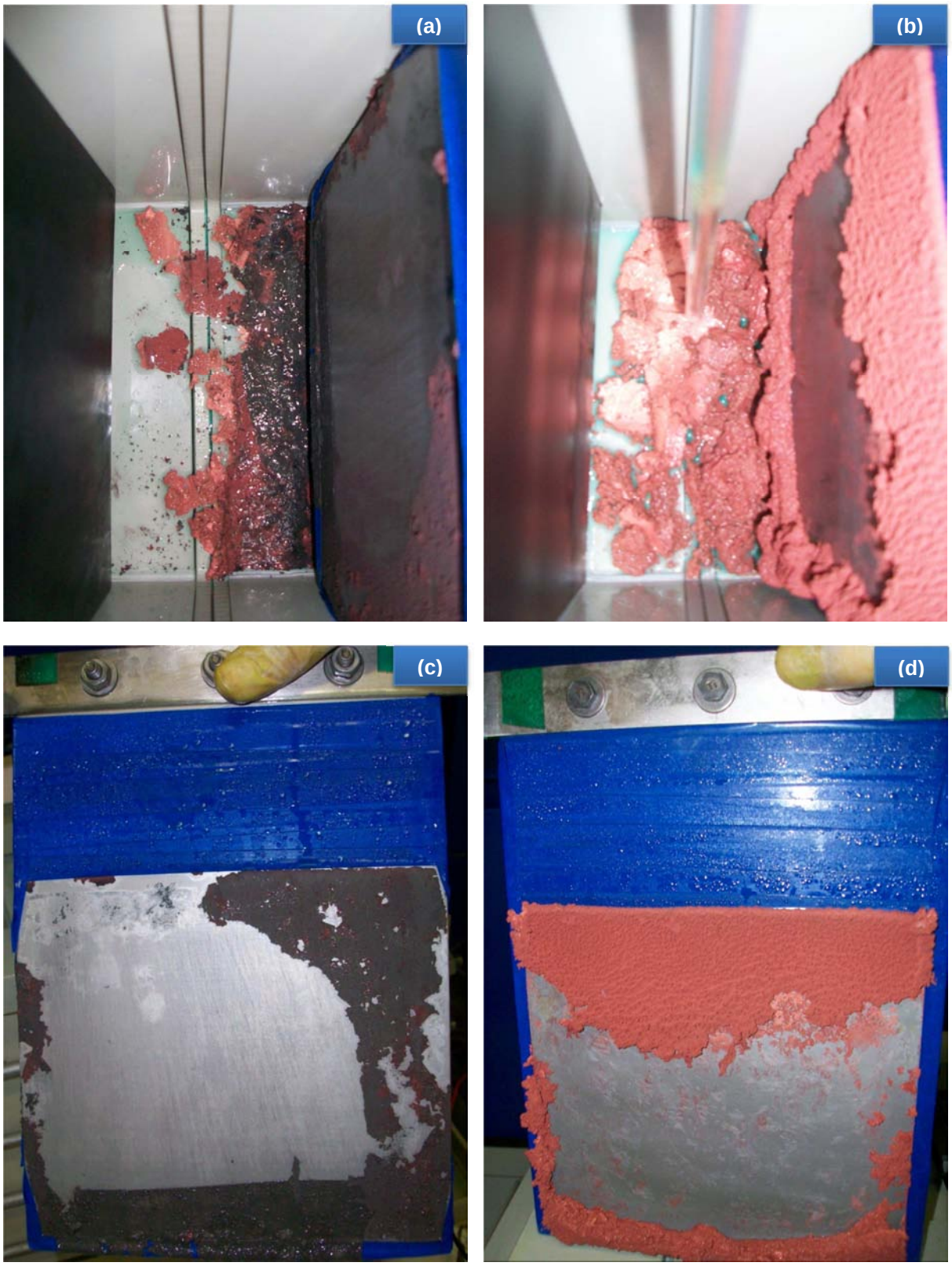

Figure 39: Pictures of the powders produced with (a,c) *High Cu* and (b,d) *Low Copper* runs.

From Figure 39 it can be seen that at the *Low Cu* condition very fine black copper powder was produced. However, at the *High Cu* condition similar copper powder production relative to the *Base Case* was observed.

5.2.4 Copper Powder Re-dissolution

The discrepancies in process yield after electrochemical reduction and process yield after filtration (Table 5) is attributed to re-dissolution of copper powder during filtration and washing. However, various degrees of copper powder re-dissolution were observed for Run 1A-Run 11. This is illustrated in Figure 40.

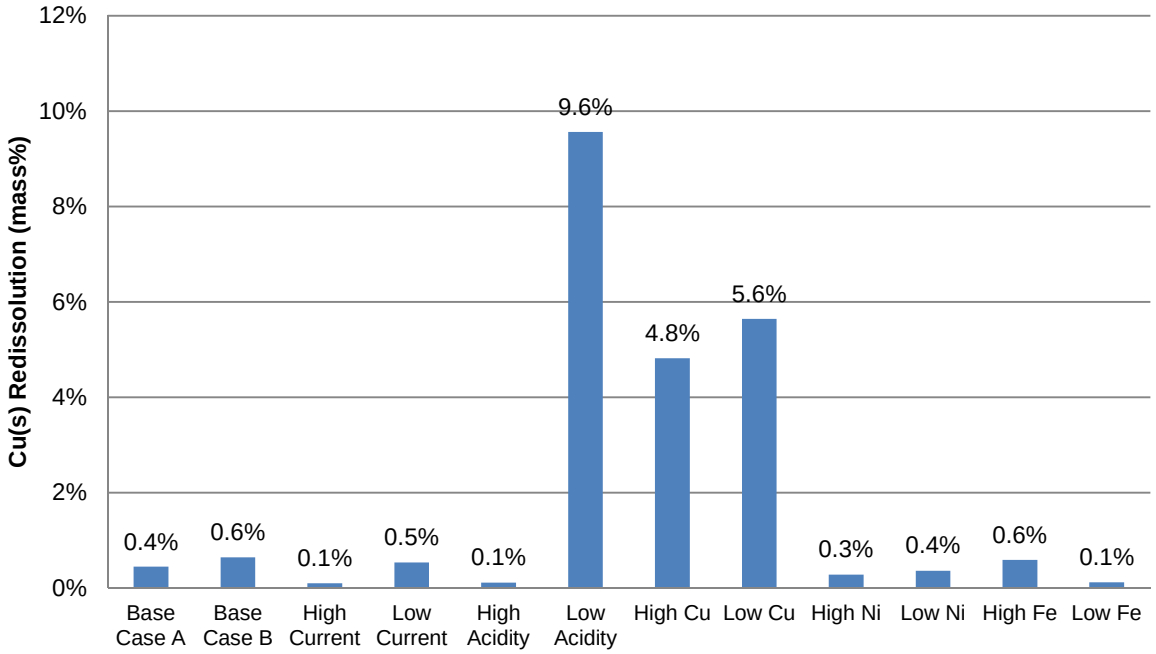

Figure 40: Degree of copper powder re-dissolution during filtration and washing.

From Figure 40 it can be seen that the re-dissolution of copper powder was significantly higher for Runs 5-7 (*Low Acidity, High Cu* and *Low Cu*). The high degree of copper powder re-dissolution for Run 5 (*Low Acidity*) and Run 7 (*Low Cu*) is attributed to higher electrolyte temperatures up to 68.1°C (≈15.6°C greater than *Base Case*) that promote the formation of smaller copper particles [14,15]. It is also considered that under elevated temperatures the leaching of copper by ferric sulfate is promoted [35]. This is given by the following reaction in sulfuric acid conditions:

$$Cu + Fe_2(SO4)_3 \rightarrow CuSO_4 + FeSO_4 \qquad (37)$$

For Run 6 (*High Cu*) the increased degree of copper powder re-dissolution is attributed to the higher mass of solids produced per cell volume (72% more solids than *Base Case*) and the associated higher degree of electrolyte entrainment.

Thus based on this analysis it is preferable for the electrochemical process to be operated at a copper concentration of 30 g/L and acidity of 2 mol/L H^+ (or greater). Nickel concentrations in the range of 5-20 g/L and iron concentrations in the range of 1-12 g/L did not significantly impact on the copper powder re-dissolution.

5.2.5 Summary

By varying the applied current, initial acidity and initial copper, nickel and iron concentrations, it was found that the optimal conditions for an electrochemical process targeting a process yield of 95% was at a current density of 1 000 A/m^2, initial acidity in the order of 1-4 mol/L H^+ and initial copper concentration of 30 g/L. At a current density of 1 000 A/m^2 an apparent optimum existed with regards to lowest specific energy consumption (≈12.37 kWh/kg Cu) and shortest processing time (≈270 min). Lower specific energy consumption directly translates to lower electrical energy consumption and operating cost, whilst lower processing time generally allow for viewer unit processes, smaller equipment, less footprint and reduced capital expenditure. An initial acidity of 2-4 mol/L H^+ promoted lower processing temperature, reduced cell voltage and lower specific energy consumption. By operating at a lower temperature the process is inherently safer and materials selection is simplified. At an initial copper concentration of 30 g/L copper the formation of fine copper powder and solids re-dissolution was minimised. These parameters have the potential to detrimentally impact the overall recovery of the process, and minimisation would improve the overall operational efficiency. Variation in the feed concentration of nickel (5-20 g/L) and iron (1-12 g/L) had no detrimental impact on the electrochemical reduction process of copper, and it is considered that feed variation within these limits would be acceptable for an industrial process. However, higher levels of iron in the form of ferric could result in increased levels of copper re-dissolution.

5.3 FLOWSHEET DEVELOPMENT

Based on the experimental base case conditions, a conceptual flowsheet was developed for an electrochemical process to recover copper from acidic sulfate solutions containing copper, nickel and iron. This conceptual flowsheet is given in Figure 41.

The process was designed to treat approximately 22.40 kg/h Cu with a plant availability of 88%. The feed electrolyte specification is 30 g/L Cu and a process yield of 95% is targeted. Based on the current London Metal Exchange price for copper [4] and a process yield of 95%, the product stream value is in the order of R 14.9 million per annum.

This section outlines the process description, process schedule, equipment sizing, capital cost estimation and operating cost estimation for the conceptual flowsheet.

5.3.1 Process Description

The conceptual flowsheet comprises a feed electrolyte holding tank (TK-001); three electrochemical cells (EC-001, EC-002 and EC-003); a tank filter for spent electrolyte filtration (FL-001); a glove box filter for solids filtration (FL-002); a vacuum receiver (VA-001); a spent electrolyte holding tank (TK-002); and cartridge filters (FL-003/4).

Feed electrolyte is transferred to the feed electrolyte holding tank (TK-001). From TK-001 the solution is transferred to one of three electrochemical cells (EC-001, EC-002 or EC-003) where it undergoes a batch electrochemical reduction process at a current density of 1 000 A/m^2 to produce Cu(s). After electrochemical reduction the slurry is drained from the cell into a tank filter (FL-002) and the cell is washed with process water to remove any residual solids. The slurry and washings are filtered under vacuum in FL-002 to remove the bulk of the solution. The filtrate from FL-002 is transferred to the spent electrolyte holding tank (TK-002) via the vacuum receiver (VA-001). The concentrated slurry from FL-001 is transferred in the glove box filter (FL-002), where it undergoes a second vacuum filtration and washing process. After filtration on FL-002 the filtrate is transferred to the spent electrolyte holding tank (TK-002) and the solids are transferred to the residues handling area. Cartridge filters (FL-003/4) are located on the spent electrolyte holding tank transfer line to capture any entrained solids present in the spent electrolyte.

Off-gas from the electrochemical cells and other process equipment is routed to the draught system for vapour scrubbing. Sample boards (SB-001 and SB-002) are located on the feed electrolyte and spent electrolyte holding tanks to monitor process performance.

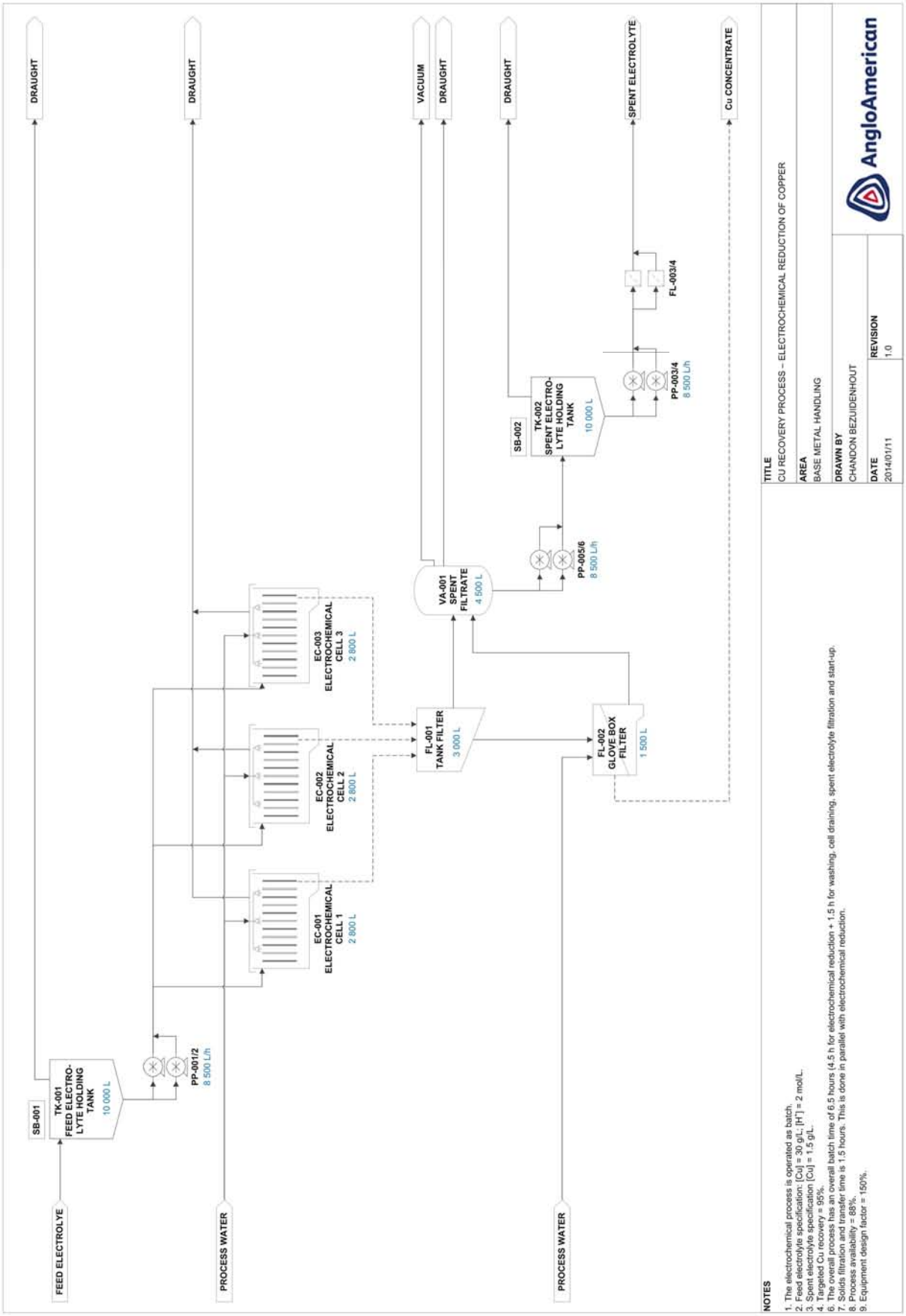

Figure 41: Conceptual flowsheet for the electrochemical recovery of copper.

5.3.2 Process Schedule

The electrochemical process is operated as batch with an overall batch time of 6.5 hours per cell. This comprises 4.5 hours for electrochemical reduction per cell followed by 30 minutes to drain and wash the cell, 60 minutes to filter the spent electrolyte and 30 minutes to fill and restart electrochemical reduction. After spent electrolyte filtration (FL-001) the slurry undergoes further filtration (FL-002) for 60 minutes. This is done in parallel with filling and start-up of the electrochemical cells.

The three electrochemical cells are operated in parallel with 1.5 hour lag in start-up. This is illustrated in the process schedule given in Figure 42

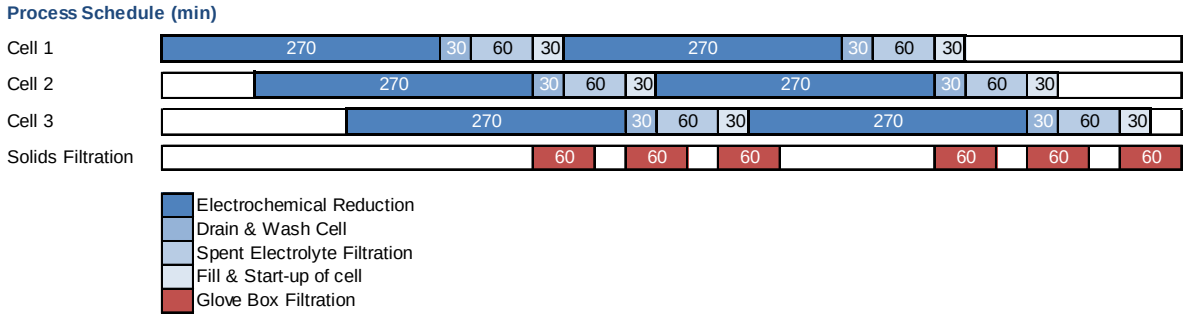

Figure 42: Process schedule illustrating parallel processing of Cell 1, 2 and 3 for six batches.

5.3.3 Equipment Sizing

For equipment sizing purposes a design factor of 1.5 has been applied. Based on three electrochemical cells operating in parallel with a batch time of 6.5 hours per cell, the effective reactor volume per cell is estimated at 2 758 L. Based on an electro-active area per unit volume of 6.00 m^2/m^3, this translates to a electro-active area of 16.55 m^2 per cell. Thus, a total of 6 cathodes and 7 anodes are required per cell with an electro-active area of 1.38 m^2 per side. Cathodes and anodes sizes were calculated to be 1.04 m (width) x 1.33 m (length) x 5 mm (thickness). At an anode-to-cathode spacing of 84 mm this translates to an electrochemical cell with the following internal dimensions: 1.09 m (width) x 1.56 m (length) x 1.62 m (height).

Additional process equipment was sized based on the anticipated volumetric and mass flowrates. Detailed calculations on equipment sizing are given in Appendix C. Table 7 summarises the equipment sizes selected for the relevant equipment.

Table 7: Equipment sizes based on a design factor of 150%.

Equipment description	Tag	Equipment size
Feed electrolyte holding tanks	TK-001	10 000 L
Electrochemical cells	EC-001, EC-002, EC-003	2 800 L
Tank filter	FL-001	3 000 L
Glove box filter	FL-002	1 500 L
Vacuum receiver	VA-001	4 500 L
Spent electrolyte holding tank	TK-002	10 000 L

5.3.4 Capital Cost Estimation

For the capital cost estimation it is assumed that the process is a brownfields installation. Infrastructure such as buildings, stores, residues handling, effluent handling, utilities (vacuum plant, compressed air, cooling water, steam, process water, centralised off-gas scrubbing) and analytical laboratories are existing.

Mechanical costs for the major plant equipment were calculated based on actual PMR stores mechanical costs that were corrected for size and time of purchase (using the six-tenth rule) [36]. These mechanical costs were then used to estimate the capital cost of the process by applying a Lang factor of 4.5. The mechanical cost calculation and capital cost estimation for the major plant equipment is given in Table 8.

Table 8: Mechanical cost calculation and capital cost estimation for the major plant equipment.

Mechanical Item Description	Original Mech. Cost	Size factor	Sized Mech. Cost	Year	Mech. Cost in 2013	No. of units	Mech. Cost	Capital Cost
GRP tank complete with lid (10000 L)	R 130 000	1.0	R 130 000	2005	R 208 256	2	R 416 512	R 1 874 303
Electrowinning cell (excl. electrodes), 600 L, PP	R 175 000	4.7	R 441 004	2011	R 489 216	3	R 1 467 647	R 6 604 412
Electrode cost (1 x 1 m)	R 9 500	1.0	R 9 500	2011	R 10 539	33	R 347 773	R 1 564 978
GRP vacuum receiver complete with dome	R 223 000	1.0	R 223 000	2005	R 357 239	1	R 357 239	R 1 607 575
Agitator shaft and blades, incl. gearbox & motor	R 29 000	1.0	R 29 000	2005	R 46 457	2	R 92 914	R 418 114
Cartridge filter (housing + cartridge)	R 2 200	1.0	R 2 200	2012	R 2 325	2	R 4 649	R 20 923
Glove box filter (double)	R 230 000	1.0	R 230 000	2012	R 243 041	1	R 243 041	R 1 093 685
Tank filter (GRP)	R 200 000	1.0	R 200 000	2011	R 221 865	1	R 221 865	R 998 391
Pump for GRP tank (100L to 20000L)	R 30 000	1.0	R 30 000	2005	R 48 059	6	R 288 354	R 1 297 594
Sample board for sample extraction from tanks	R 32 000	1.0	R 32 000	2005	R 51 263	2	R 102 526	R 461 367
Total							**R 3 542 520**	**R 15 941 342**

From Table 8 it can be seen that the estimated capital cost of the conceptual flowsheet is estimated to be in the order of R 15.9 million based on a Lang factor of 4.5.

5.3.5 Operating Cost Estimation

The direct operating cost for the conceptual flowsheet included electrical energy cost, utility cost, operating labour cost and maintenance cost. Indirect and fixed costs are not considered as part of this evaluation. It is assumed that the plant will be installed in an existing production environment.

Based on a targeted overall recovery of 95% the overall specific energy for a batch process was determined to be in the order of 12.37 kWh/kg Cu. Based on a copper feed rate of 22.40 kg/h and an electrical energy price of R 1.20 per kWh the overall electrical energy cost was estimated at R 2.8 million per annum. Utilities cost was estimated based on process water cost of R 6.29/m^3. The estimation for operating labour cost was based on the requirement of one additional operator per shift (on a 4 shift cycle). Maintenance cost was based on the replacement of 33 electrodes every a five years. To allow for miscellaneous operating costs a 10% contingency was included in the operating cost estimation. From Table 9 it can be seen that the overall operating cost is estimated to be in the order of R3.8 million per annum.

Table 9: Estimated operating costs per annum.

Operating cost component	Estimation basis	Annual operating cost (ZAR p.a.)
Electrical energy cost	*12.57 kWh/kg Cu at overall yield of 95%*	R 2 767 112
Utility cost	*Process water for washing cells and filters*	R 2 983
Operating labour cost	*One additional operator per shift*	R 600 000
Maintenance cost	*Five year lifetime of electrodes*	R 69 555
Other	*10% contingency*	R 343 965
Total		**R 3 783 614**

5.3.6 Economic Evaluation

The CAPEX and OPEX for a batch copper electrochemical reduction process to treat the anticipated feed solution of 22.40 kg/h Cu is estimated at R15.9 million and R 3.8 million per annum. Based on the current London Metal Exchange price for copper and a process yield of 95%, the product stream value is in the order of order of R 14.9 million per annum. However, in order to meet market specification additional solids handing processes are required. These potentially include treatment to prevent oxidation of the solids, annealing under reducing conditions at temperatures of 480-760°C, milling, classification and blending. The CAPEX and OPEX for solids handling processes are estimated at 20% of the electrochemical processes.

Figure 43 illustrates a cumulative discounted cash flow diagram for an electrochemical reduction process including solids handling processes. This is based on a discounted rate of 11.5%. It is assumed that commissioning will take place over a six month period and plant start-up will occur directly after commissioning.

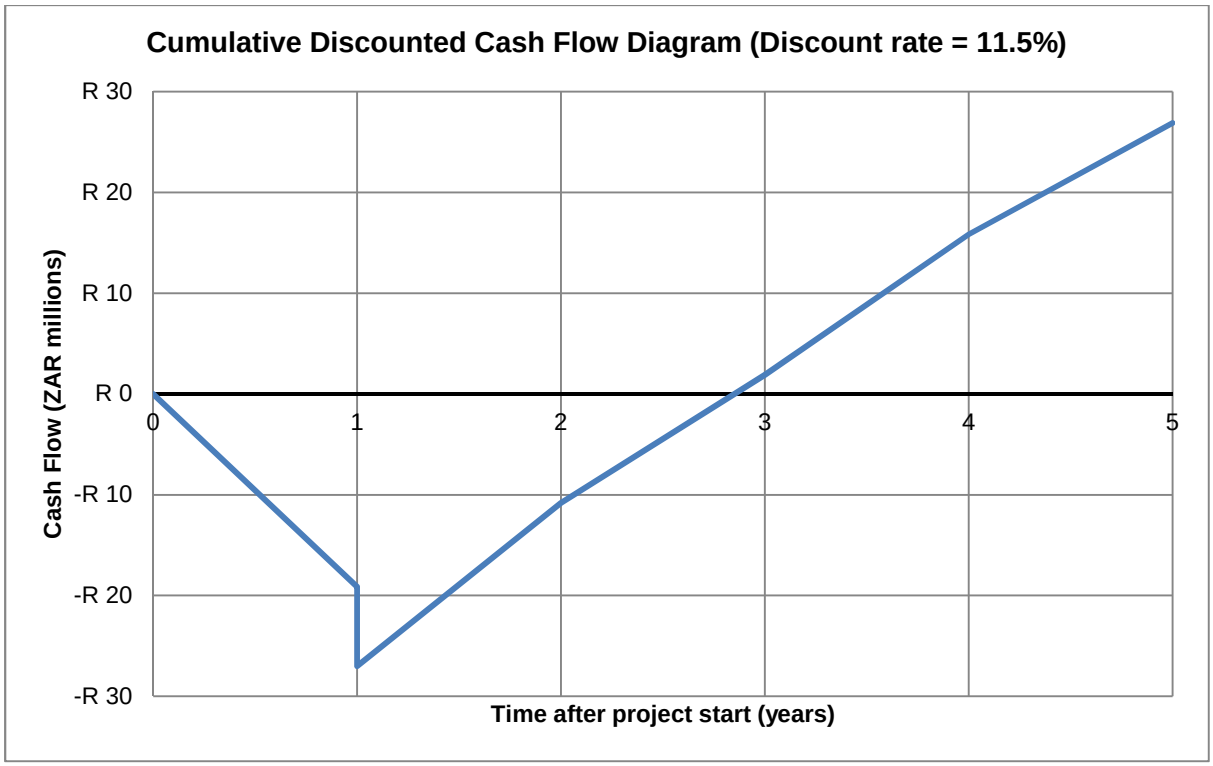

Figure 43: Cumulative discounted cash flow diagram.

From Figure 43 it can be seen that the project has a net present value (NPV) of R 26.9 million and an internal rate of return (IRR) of 37.6% over 5 years.

6 CONCLUSIONS AND RECOMMENDATIONS

The main findings from this study were:

1. **It is possible to selectively reduce Cu^{2+}(aq) to Cu(s) from a 1 mol/L sulfuric acid solution containing 30 g/L copper, 10 g/L nickel, 6 g/L iron using an electrochemical reduction process at 1 000 A/m^2.**

   The process selectively recovered 99.98-100.00% of copper from solution after seven hours of electrochemical reduction at 1 000 A/m^2. During the electrochemical process the Cu^{2+}(aq) concentration decreased linearly and then exponentially with time, thus indicating both current limited and mass transport limited conditions. The aqueous concentrations of nickel and total iron remained constant under the experimental conditions and thus did not reduce to metallic form. The acidity of the solution increased linearly at first and then remained constant, thus indicating evolution of H_2(g) by the reduction reaction of H^+(aq). O_2(g) was generated at the anode. Under mass transport limited conditions both the reduction of Fe^{3+}(aq) to Fe^{2+} and oxidation of Fe^{2+}(aq) back to Fe^{3+}(aq) occurred. The Cu(s) that formed poorly adhered to the cathode surface and gravitated to the bottom of the cell for subsequent recovery with solid-liquid separation.

2. **For a Cu electrochemical reduction process targeting a process yield of 95% at a current density of 1 000 A/m^2, the required processing time is 4.5 hours. The process has an overall current efficiency of 86.4%, cell voltage of 3.06-4.91 V and specific energy consumption of 12.37 kWh/kg Cu.**

3. **Lower feed acidity (0.5 mol/L H^+) results in higher cell voltage, elevated electrolyte temperature and higher degrees of copper powder re-dissolutions during filtration and washing. However, feed acidity in the order of 1-4 mol/L H^+ has no detrimental impact on the electrochemical reduction process for copper and copper powder re-dissolution was low.**

4. **Variation in the feed concentration of copper (3-50 g/L) impacts the electrochemical reduction processing time and also results in higher degrees of copper powder re-dissolution during filtration and washing.**

   Feed electrolyte solution with 3 g/L Cu required significantly shorter processing times than electrolyte solutions with 30g/L Cu. As a result of lower electrolyte conductivity, the cell voltages and electrolyte temperatures were higher than base case conditions. This resulted in higher levels of copper powder re-dissolution during filtration and washing.

   Feed electrolyte solutions with 50 g/L Cu required significantly longer processing times than electrolyte solutions with 30 g/L Cu. Higher degrees of copper powder re-dissolution during filtration and washing were also observed relative to base case conditions.

5. **Variation in the feed concentration of nickel (5-20 g/L) has no detrimental impact on the electrochemical reduction process of copper.**

6. **Variation in the feed concentration of iron (1-12 g/L) has no detrimental impact on the electrochemical reduction process of copper.**

7. **The current applied during the electrochemical reduction process impacts the rate of copper recovery and the specific energy consumption of the process. Based on a targeted process yield of 95% the optimum current density is 1 000 A/m^2.**

8. **The CAPEX and OPEX for a batch copper electrochemical reduction process to treat the anticipated feed solution is estimated at R15.9 million and R 3.8 million per annum. The project has a net NPV of R 26.9 million and an IRR of 37.6% over 5 years.**

   The estimated capital cost was based on a mechanical cost of R 3.9 million and a Lang factor of 4.5. It was assumed that the process is a brownfields installation – infrastructure such as buildings, stores, residues handling, effluent handling, utilities (vacuum plant, compressed air, cooling water, steam, process water, centralised off-gas scrubbing) and analytical laboratories would be existing. The estimated operating cost was based on electrical energy cost, utility cost, operating labour cost and maintenance cost. Indirect cost and fixed costs were not considered as part of this evaluation.

Based on the above-mentioned findings it is concluded that the electrochemical reduction process proposed in this study is suitable for the selective recovery of copper from a sulfuric acid solution containing predominantly copper, nickel and iron. Operating conditions (i.e. current density, initial acidity and initial copper, nickel and iron concentrations) were varied to determine the effect of each on process parameters such as process yield, current efficiency, cell voltage, temperature, specific energy consumption and processing time. An apparent optimum was determined at a current density of 1 000 A/m^2 for a process targeting a process yield 95%. Under these conditions the overall current efficiency was high (86.4%), cell voltages relatively low (3.06 – 4.91 V) and the specific energy consumption was at its minimum (12.37 kWh/kg Cu). For the proposed feed solution it was found that a processing time of 4.5 hours was required under the experimental conditions. For a batch process operating at the proposed scale of 22.4 kg/h copper and 88% availability, the above-mentioned process parameters are comparable to that of commercial processes. The number of unit processes, equipment used, equipment size and process schedule are deemed acceptable for the proposed applications within a refinery. Furthermore, given the large NPV (R 26.9 million) high IRR (37.6% over 5 years) the proposed process is considered to be a viable option for comparison with other commercially mature processes.

Given that the experimental findings from this study are based on tests with synthetics solutions, it is considered that additional work would be required on actual solutions to illustrate the effect of additional impurities on the copper product. This includes an evaluation of additional processing required to produce a saleable product in terms of purity, solids morphology and solids characteristics. Additional factors such as the hydrodynamics within a larger scale cell should alos be considered.

The main recommendations of this study are to:

1. Perform larger scale piloting and demonstration of the integrated process on actual process solutions. This includes an investigation into a suitable solids handling process to convert copper powder into a saleable product and characterisation of the morphology and quality of copper solids. A detailed costing and economic evaluation study should then be done based on the pilot plant results. The main factors to be considered during the design of the pilot plant is as follows:
   i. Batch vs. continuous operation
   ii. Optimisation of anode and cathode materials of construction
   iii. Optimisation of electrode spacing
   iv. Hydrodynamics of electrochemical cell
   v. Conditions for removing copper deposits
   vi. Solid purity
   vii. Particle size distribution

viii. Solids morphology
ix. Filtration flux

2. Perform a detailed economic evaluation to compare the OPEX and CAPEX for the electrochemical reduction process to that of the alternative hydrometallurgical processes considered. This includes further study to determine the operating conditions and economic parameters for a suitable process to recover nickel from the copper spent electrolyte.

7 REFERENCES

The following references were cited in this study:

1. Anglo American Platinum Limited Annual Report 2012, Accessed 19 January 2014, http://www.angloplatinum.com/investors/reports/2012.asp.

2. Crundwell, F.K., M.S. Moats, V. Ramachandran, T.G. Robinson and W.G. Davenport, “Extractive Metallurgy of Nickel, Cobalt and Platinum-Group Metals: Refining of Platinum-Group Metals (Chapter 37)”, *Elsevier Ltd*., 2011.

3. Anglo Platinum Management Sevices Pty. Ltd. “Upgrading of precious metals concentrates and residues”, US 2013/0177487 A1. 11 July 2013.

4. London Metal Exchange: Copper, http://www.lme.com/en-gb/metals/non-ferrous/copper/, Accessed on 8 February 2014.

5. London Metal Exchange: Copper, http://www.lme.com/en-gb/metals/non-ferrous/nickel/, Accessed on 8 February 2014.

6. Agrawal, A. and K.K. Sahu, “Problems, prospects and current trends of copper recycling in India: an overview” Resources, Conservation and Recycling, 54, pp. 401-416, 2010.

7. Agrawal A., D. Bagchi, S. Kumari and B.D. Pandey, “An overview of process options and behavioural aspects of the copper values recovered from the copper bleed stream of a copper smelter developed at the National Metallurgical Laboratory”, *Mineral Processing and Extractive Metallurgy Review: An International Journal*, 30:2, pp. 136-162, 2009.

8. Agrawal A., S. Kumari, D. Bagchi, V. Kumar and B.D. Pandey, “Hydrogen reduction of copper bleed solution from an Indian copper smelter for producing high purity copper powders”, *Hydrometallurgy 84*, pp. 218-224, 2006.

9. Agrawal A., D. Bagchi, S. Kumari and B.D. Pandey, “Hydrogen reduction of bleed stream of an Indian copper industry to produce nickel powder”, *Materials Letters 62*, pp. 2 880-2 882, 2008.

10. Production and properties of copper and copper alloy powders, *Copper Development Association Inc*. http://www.copper.org/resources/properties/129_6/production.html, Accessed on 30 January 2014.

11. Neikov, O.D., S.S. Naboychenko, I.B. Marushova, V.G. Gopienko, I.V. Frishberg and D.V. Lotsko, “Handbook of non-ferrous metal powders: Technologies and applications", *Elsevier*, pp. 181-211 2009.

12. Taubenblat, P.W., "Importance of copper in powder metallurgy", *International Journal of Powder Metallurgy and Powder Technology 10*, pp. 169, 1974.

13. “Powder metal technology and applications”, *ASM Handbook, Volume 7,* pp. 324-335, *ASM International,* 1998.

14. Orhan, G., and G.G. Gezgin, “Effect of electrolysis parameters on the morphologies of copper powders obtained at high current densities.” *Journal of Serbian Chemical Society 77 (5)* pp. 651-665, 2012.

15. Orhan, G., and G. Hapci, “Effect of electrolysis parameters on the morphologies of copper powder obtained in a rotating cylinder electrode cell.” *Powder Technology 201*, pp. 57-63, 2010.

16. Pavlović, M.G., Lj.J. Pavlović, E.R. Ivanović, V. Radmilović and K.I. Popov, “The effect of particle structure on apparent density of electrolytic copper power.” *Journal of Serbian Chemical Society 66 (11-12)* pp. 923-933, 2001.

17. Nikolić, N.D., K.I. Popov G., Lj.J. Pavlović and M.G. Pavlović, "The effect of hydrogen co-deposition on the morphology of copper electrodeposits. I. The concept of effective overpotential." *Journal of Electroanalytical Chemistry 588*, pp. 88-98, 2006.

18. Nikolić, N.D., G. Brankovic, M.G. Pavlović and K.I. Popov, "The effect of hydrogen co-deposition on the morphology of copper electrodeposits. II. Correlation between the properties of electrolytic solutions and the quantity of evolved hydrogen." *Journal of Electroanalytical Chemistry 621*, pp. 13-21, 2008.

19. Nikolić, N.D., Lj.J. Pavlović, M.G. Pavlović and K.I. Popov, "Morphologies of electrochemically formed copper powder particles and their dependence on the quantity of evolved hydrogen." *Powder Technology 185*, pp. 195-201, 2008.

20. Nikolić, N.D., G. Branković and M.G. Pavlović, "Correlate between morphology and powder particles obtained by difference regimes of electrolysis and the quantity of evolved hydrogen.” *Powder Technology 221*, pp. 271-277, 2012.

21. Pavlović, M.G., V.M. Maksimović, N.D. Nikolić and K.I. Popov, "Characterization and morphology of copper powder particles as a function of different electrolytic regimes.” *International Journal of Electrochemical Science 5,* pp. 1862-1878, 2010.

22. Nikolić, N.D. and K.I. Popov, “Electrodeposition of Copper Powders and Their Properties”, “Electrochemical Production of Metal Powders”, S.S. Djokić, *Modern Aspects of Electrochemistry 54*, pp. 125-185, 2012.

23. Wang M., Z. Wang and Z. Guo, “Preparation of electrolytic copper powder with high current efficiency enhanced by super gravity field and its mechanisms.” *Transactions of Nonferrous Metals Society of China 20*, pp. 1154-1160, 2010.

24. Schlesinger, M. and M. Paunovic, “Modern Electroplating”, 5th Ed., *John Wiley & Sons Inc.*, 2010.

25. Nicol, M., “Hydrometallurgy”, Course notes, *University of Cape Town*, 2009.

26. Das, S.C. and P.G. Krishna, “Effect of Fe(III) during copper eletrowinning at higher current density” International Journal of Mineral Processing 46, pp. 91-105, 1996.

27. Casas, J.M., F. Alvarez and L. Cifuentes, “Aqueous speciation of sulfuric acid-cupric sulfate solutions”, *Chemical Engineering Science 55*, pp. 6 223-6 234, 2000.

28. Bard, A.J., R. Parson, J. Jordan, “Standard Potentials in Aqueous Solution”, *CRC Press, Marcel Dekker Inc*.,1985.

29. Kobylin, P., “Thermodynamic modelling of aqueous metal sulfate solution”, *School of Chemical Technology, Aalto University publication series, Doctoral Dissertations* 41/2013, 2013.

30. Casas, J.M., G. Crisostomo and L. Cifuentes, “Speciation of the Fe(II)-Fe(III)-H_2SO_4-H_2O system at 25 and 50°C”, *Hydrometallurgy 80*, pp. 254-264, 2005.

31. Outokumpu HSC Chemistry 5.11.

32. Pletcher, D. and F.C. Walsh, “Industrial Electrochemistry”, 2nd Ed., *Chapman and Hall*, London, 1990.

33. Msindo, Z. S., “An investigation of the electrowinning of copper with dimensionally stable titanium anodes and conventional lead alloy anodes.”, *University of the Witwatersrand*, *Masters of Science in Engineering*, 2010.

34. Spiro, M. “A Critique of the additivity principles for mixed couples”, *Moderns Aspects of Electrchemistry 34*, Kluwer Academics, Plenum Publishers, New York, 2001.

35. Bartlett, R.W. “Solution Mining: Leaching and Fluid Recovery of Materials”, 2nd Ed. *Psychology Press*, 1998

36. Turton, R., R.C. Bailie, W.B. Whiting, J.A. Shaewitz, “Analysis, Synthesis and Design of Chemical Processes”, 2nd Ed., *Prentice Hall*, New Jersey, 2003.

APPENDIX A – THERMODYNAMICS

Appendix A – Thermodynamics contains a table of selected standard half-reaction potentials used to determine the thermodynamic order of reducibility of metal ions in solution.

STANDARD HALF-REACTION POTENTIALS IN ACID SOLUTIONS

Table A1: Selected standard half-reaction potentials in acid solutions.

Half reaction	E^0 (V)
$Ca^{2+}(aq) + 2e^- = Ca(s)$	-2.84
$Mg^{2+}(aq) + 2e^- = Mg(s)$	-2.356
$Al^{3+}(aq) + 3e^- = Al(s)$	-1.67
$Mn^{2+}(aq) + 2e^- = Mn(s)$	-1.18
$Cr^{2+}(aq) + 2e^- = Cr$	-0.90
$SiO_2(vit) + 4H^+ + 4e^- = Si + 2H_2O$	-0.888
$Zn^{2+}(aq) + 2e^- = Zn(s)$	-0.7626
$Te + 2H^+ + 2e^- = H_2Te$	-0.740
$Sb + 3H^+ + 3e^- = SbH_3(g)$	-0.510
$Fe^{2+}(aq) + 2e^- = Fe(s)$	-0.44
$Cr^{3+} + e^- = Cr^{2+}$	-0.424
$Cd^{2+}(aq) + 2e^- = Cd(s)$	-0.4025
$PbSO_4 + 2e^- = Pb + SO_4^{2-}$	-0.3505
$Co^{2+} + 2e^- = Co$	-0.277
$PbCl_2 + 2e^- = Pb + 2Cl^-$	-0.268
$Ni^{2+} + 2e^- = Ni$	-0.257
$2SO_4^{2-} + 4H^+ + 4e^- = S_2O_6^{2-} + 2H_2O$	-0.253
$As + 3H^+ + 3e^- = AsH_3$	-0.255
$Si + 4H^+ + 4e^- = SiH_4$	-0.143
$Sn^{2+} + 2e^- = Sn$	-0.136
$Pb^{2+} + 2e^- = Pb$	-0.1251
$O_2 + H^+ + 2e^- = HO_2$	-0.046
$Se + 2H^+ + 2e^- = H_2Se$	-0.028
$2H^+ + 2e^- = H_2$	0.000
$CuCl + e^- = Cu + Cl^-$	0.121
$S + 2H^+ + 2e^- = H_2S$	0.144
$SO_4^{2-} + 2H^+ + 2e^- = H_2SO_4^- + 2H_2O$	0.173
$AgCl + e^- = Ag + Cl^-$	0.2233
$HAsO_2(aq) + 3H^+ + 3e^- = As + 2H_2O$	0.248
$Cu^{2+} + 2e^- = Cu$	0.340
$2H_2SO_3 + 4H^+ + 4e^- = S + 3H_2O$	0.500
$2H_2SO_3 + 4H^+ + 6e^- = S_4O_6^{2-} + 6H_2O$	0.507
$Cu^+ + e^- = Cu$	0.520
$TeO_2(c) + 4H^+ + 4e^- = Te + 2H_2O$	0.53
$Cu^{2+} + Cl^- + e^- = CuCl$	0.559
$H_3AsO_4(aq) + 2H^+ + 2e^- = HAsO_2 + 2H_2O$	0.560
$MnO_4^- + e^- = MnO_4^{2-}$	0056
$S_2O_6^{2-} + 4H^+ + 2e^- = 2H_2SO_3$	0.569
$Sb_2O_5 + 6H^+ + 4e^- = 2SbO^+ + 3H_2O$	0.605
$PdCl_4^{2-} + 2e^- = Pd + 4Cl^-$	0.64
$Ag_2SO_4 + 2e^- = 2Ag + SO_4^{2-}$	0.654
$O_2 + 2H^+ + 2e^- = H_2O_2$	0.695

$H_2SeO_3 + 4H^+ + 4e^- = Se + 3H_2O$	0.739
$PtCl_4^{2-} + 2e^- = Pt + 4Cl^-$	0.758
$Rh^{3+} + 3e^- = Rh$	0.76
$Fe^{3+} + e^- = Fe^{2+}$	0.771
$Ag^+ + e^- = Ag$	0.7991
$OsO_4(c) + 8H^+ + 8e^- = Os + 4H_2O$	0.84
$IrCl_6^{3-} + 3e^- = Ir + 6Cl^-$	0.86
$IrCl_6^{2-} + e^- = IrCl_6^{3-}$	0.867
$Pd^{2+} + 2e^- = Pd$	0.915
$PtO + 2H^+ + 2e^- = Pt + H_2O$	0.980
$AuCl_4^{2-} + 3e^- = Au + 4Cl^-$	1.002
$Sb_2O_5 + 2H^+ + 2e^- = Sb_2O_4 + H_2O$	1.055
$H_2O_2 + H^+ + e^- = OH + H_2O$	1.14
$SeO_4^{2-} + 4H^+ + 2e^- = H_2SeO_3 + H_2O$	1.151
$ClO_3^- + 3H^+ + 2e^- = HClO_2 + H_2O$	1.181
$ClO_2 + H^+ + e^- = HClO_2$	1.188
$S_2Cl_2 + 2e^- = 2S + 2Cl^-$	1.19
$ClO_4^- + 2H^+ + 2e^- = ClO_3^- + H_2O$	1.201
$O_2 + 4H^+ + 4e^- = 2H_2O$	1.229
$MnO_2 + 4H^+ + 2e^- = Mn^{2+} + 2H_2O$	1.23
$PdCl_6^{2-} + 2e^- = PdCl_4^{2-} + 2Cl^-$	1.288
$Cl_2 + 2e^- = 2Cl^-$	1.3583
$Cr_2O_7^{2-} + 14H^+ + 6e^- = 2Cr^{3+} + 7H_2O$	1.36
$HO_2 + H^+ + e^- = H_2O_2$	1.44
$PbO_2(a) + 4H^+ + 2e^- = Pb^{2+} + 2H_2O$	1.468
$Mn^{3+} + e^- = Mn^{2+}$	1.5
$MnO_4^- + 8H^+ + 5e^- = Mn^{2+} + 4H_2O$	1.51
$Au^{3+} + 3e^- = Au$	1.52
$NiO_2 + 4H^+ + 2e^- = Ni^{2+} + 2H_2O$	1.593
$HClO + H^+ + e^- = 0.5Cl_2 + H_2O$	1.630
$HClO_2 + 2H^+ + 2e^- = HClO + H_2O$	1.674
$PbO_2(a) + SO_4^{2-} + 4H^+ + 2e^- = PbSO_4 + 2H_2O$	1.698
$MnO_4^- + 4H^+ + 3e^- = MnO_2 + 2H_2O$	1.70
$H_2O_2 + 2H^+ + 2e^- = 2H_2O$	1.763
$Au^+ + e^- = Au$	1.83
$Co^{3+} + e^- = Co^{2+}$	1.92
$S_2O_8^{2-} + 2e^- = 2SO_4^{2-}$	1.96
$Ag^{2+} + e^- = Ag^+$	1.980
$O_3 + 2H^+ + 2e^- = O_2 + H_2O$	2.075

APPENDIX B – OPERATING AND RECOVERY PROFILES

Appendix B contains operating and recovery profiles where the effects of applied current, initial acidity and initial base metal concentrations (Cu, Ni and Fe) are evaluated on the cell temperature, cell voltage and the Cu, Ni and Fe profiles during electrochemical treatment from, Run 1A-11.

APPLIED CURRENT (RUN 1A, 2 & 3)

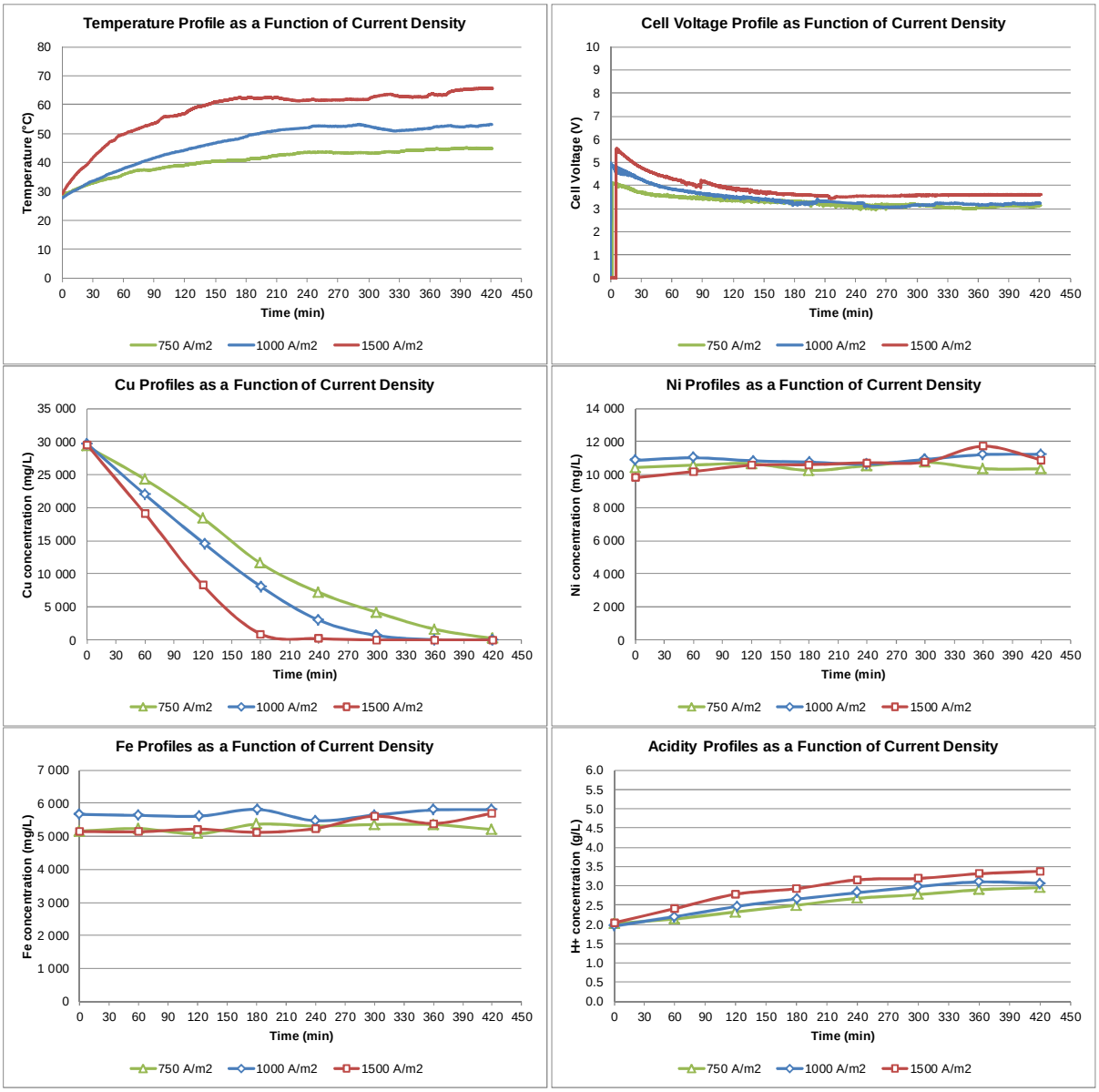

Figure 44: Operating and recovery profiles for of applied current (Runs 1A, 2 & 3).

INITIAL ACIDITY (RUN 1A, 4, 5)

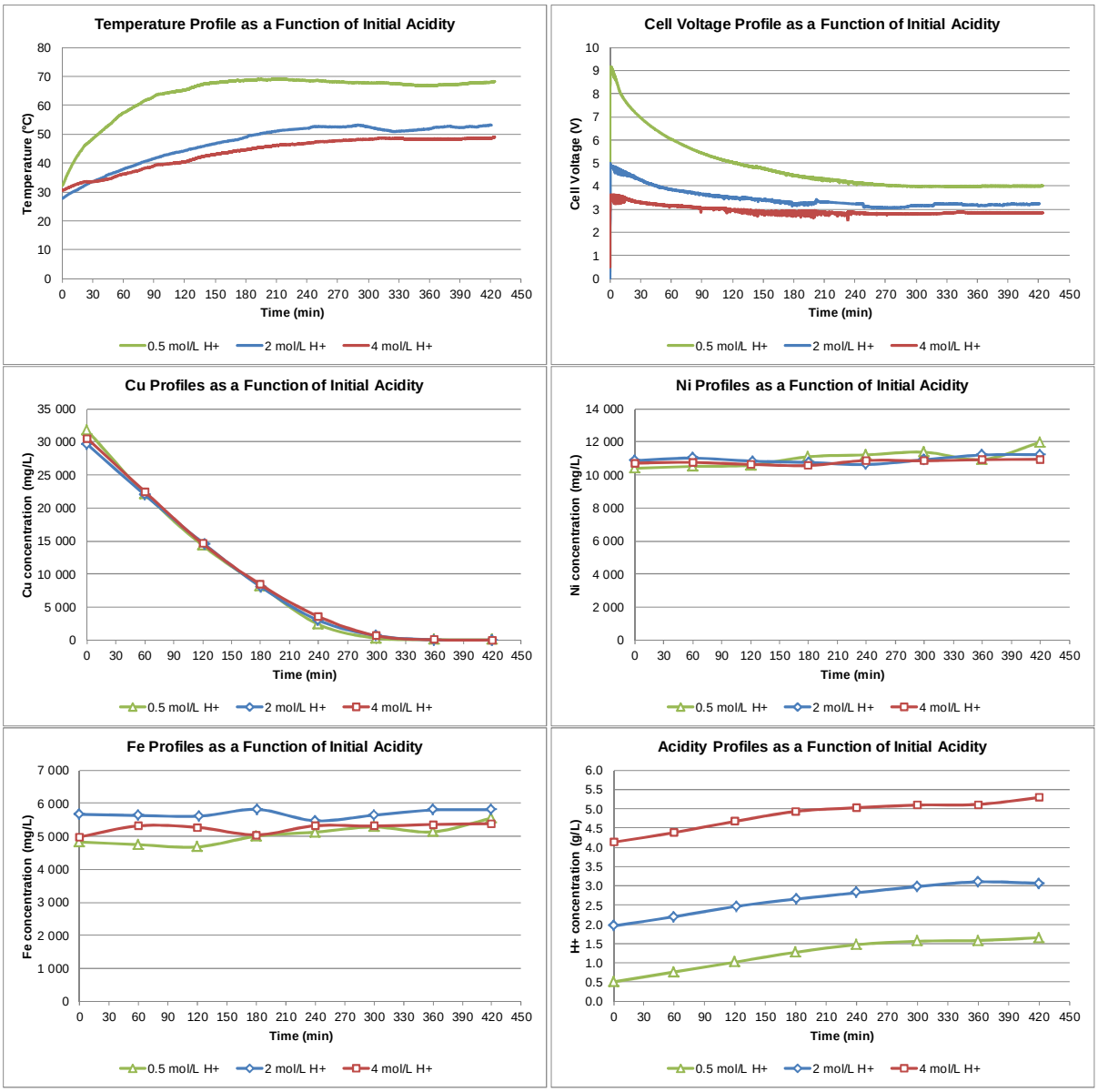

Figure 45: Operating and recovery profiles for initial acidity (Runs 1A, 4 & 5).

INITIAL COPPER CONCENTRATION (RUN 1A, 6, 7)

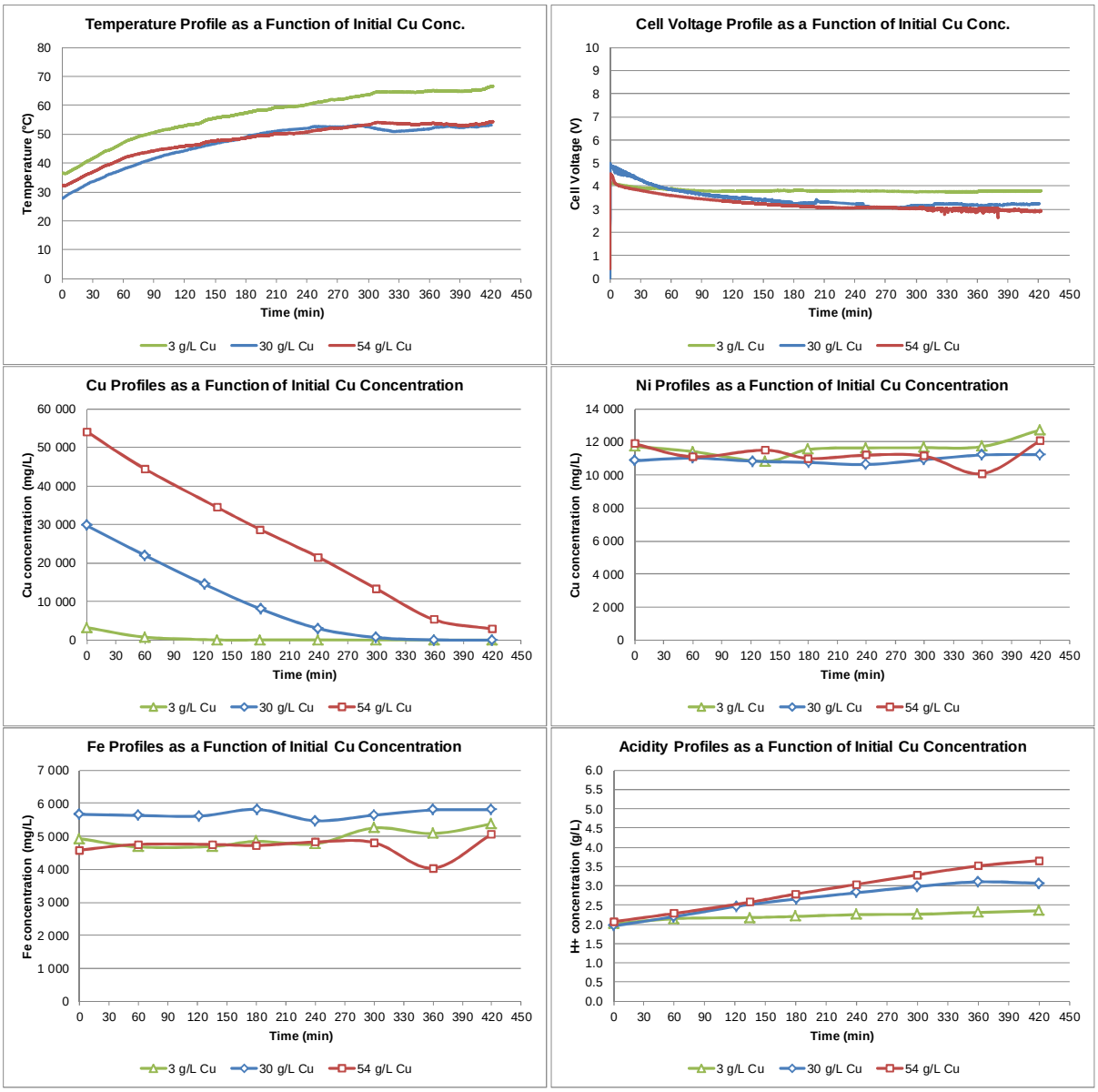

Figure 46: Operating and recovery profiles for initial Cu concentration (Runs 1A, 6 & 7).

INITIAL NICKEL CONCENTRATION (RUN 1A, 8, 9)

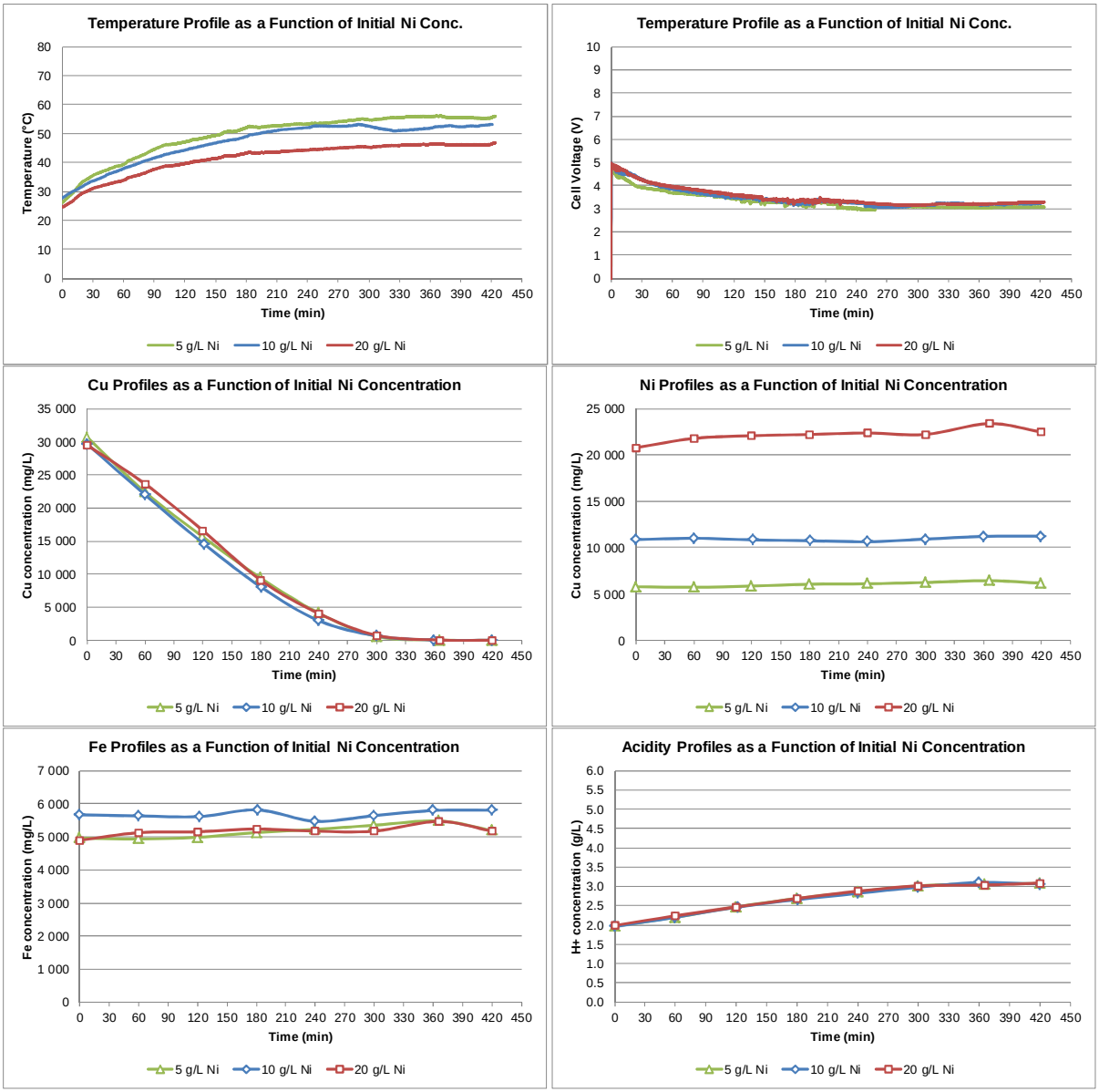

Figure 47: Operating and recovery profiles for initial Ni concentration (Runs 1A, 8 & 9).

INITIAL IRON CONCENTRATION (RUN 1A, 10, 11)

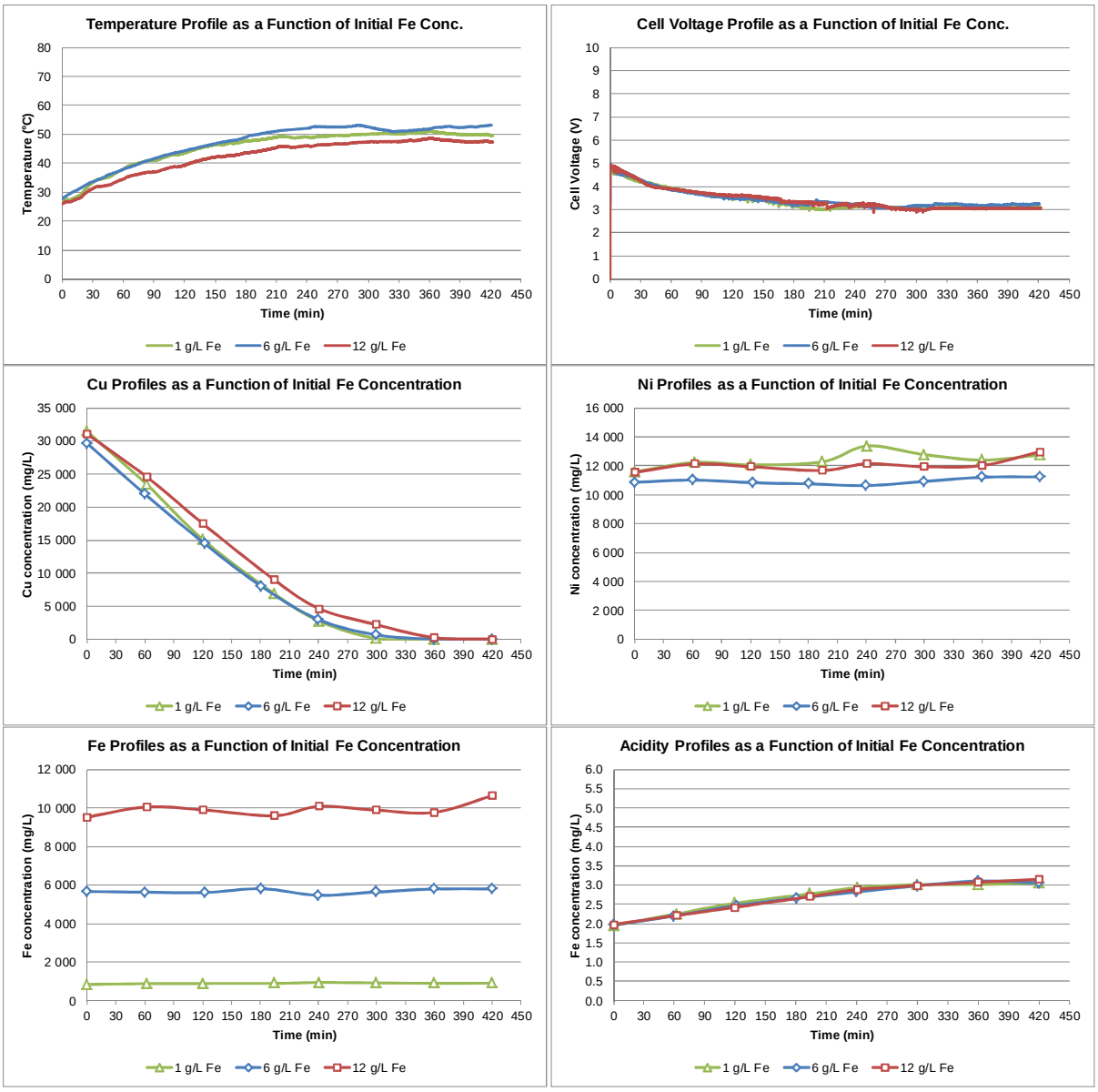

Figure 48: Operating and recovery profiles for initial Fe concentration (Runs 1A, 10 & 11).

APPENDIX C – CALCULATIONS

EQUIPMENT SIZING													
Production Requirement													
Cu feed rate	22.40	kg/h											
Plant Availability	88%												
Design Cu feed rate	25.45	kg/h											
Feed Electrolyte Specification													
Feed Cu concentration	30	g/L Cu											
Feed Ni concentration	10	g/L Ni											
Feed Fe concentration	6	g/L Fe											
Feed Acidity	2	mol/L H+											
Spent Electrolyte Specification													
Targeted Cu Recovery	95%												
Final Cu concentration	1.5	g/L											
Final Cu concentration	1500	mg/L											
Cu Recovery Kinetics													
5th order polynomial	1	2	3	4	5	6							
Polynomial coefficients	-7.30E-09	5.82E-06	-1.07E-03	1.08E-01	-1.31E+02	2.97E+04							
Targeted Final Cu concentration	1500	mg/L											
Required processing time	270.162	min											
Batch Processing Times													
Electrochemical processing time	4.50	h	*Based on experimental setup*										
Cell Washing, Tank Filtration, Shutdown & St	2.00	h	*Based on 30 min drain & wash + 60 min filtration + 30 fill & start-up for each cell.*										
Glove Box Filtration & Solids Transfer	1.50	h	*Based on solids filtration for all three cells together. Occurs in parallel with electrochemical processing.*										
Electrochemical Cell Sizing													
Volumetric flowrate	848.48	L/h					5517.442	L					
Design factor	150%		*Assumed*				1839.147						
Design volumetric flowrate	1272.73	L/h											
Mean residence time	6.50	h											
Total Effective reactor volume	8276.16	L											
No. of electrochemical cells	3.00												
Effective reactor volume per cell	2758.72	L											
Electroactive area per unit volume	6.00	m2/m3	*Based on experimental setup*										
Electroactive area per cell	16.55	m2											
No. of cathodes per cell	6.00												
No. of cathode sides per cell	12.00												
Electroactive area per cathode side	1.38	m2											
Cathode height:width ratio	1.29												
Cathode width	1.04	m											
Cathode height	1.33	m	*Based on experimental setup*										
Cathode thickness	5	mm											
No. of anodes per cell	7.00												
Anode width	1.035778	m											
Anode height	1.331715	m											
Anode thickness	0.2	mm											
Anode-to-cathode spacing	0.12	m											
Width of electrochemical cell (internal)	1.09	m	*Assumed to be 5% greater than cathode width.*										
Length of electrochemical cell (internal)	1.56	m											
Height of electrochemical cell (internal)	1.62	m											
Feed Electrolyte Holding Tank Sizing													
Volumetric flowrate of feed electrolyte	848.48	L/h											
Batch time of electrochemical process	6.50	h											
Feed electrolyte holding tank capacity	5517.442	L											
Design factor	150%												
Feed electrolyte holding tank volume	8276.163	L	*Thus an 10000 L GRP tank would be sufficient.*										
Required pumping flowrate	5517.442	L/h	*Based on 30 min filling for each cell (sequential filling, i.e. Cell1 then Cell 2 then Cell3, etc.*										
Design pumping capacity	8276.163	L/h											
Electrochemical Cell Washing													
Cu solids produced per cell	52.4157	kg											
Volume of wash water required per cell	100.00	L											
Spent Electrolyte Filtration - Tank Filter Sizing													
Volume of electrolyte per cell	1839.15	L											
Volume of wash water per cell	100.00	L											
Total volume of slurry to tank filter	1939.15	L	*Based on sequential filtration of spent electrolyte i.e. Cell 1, then Cell 2 then Cell 3.*										
Solids loading per cell	0.02703	kg/L											
Design factor	150%												
Tank filter volume	2908.72	L	*Thus a 3000 L tank filter would be suffcient*										
Cu Solids Filtration - Glove Box Filter													
Total solids on glove box (Cell 1+2+3)	157.2471	kg											
Solids %	20%	kg/L slurry											
Volume of slurry	786.24	L											
Wash water	100.00	L											
Volume of filtrate	886.24	L											
Design factor	150%												
Glove box volume	1329.35	L	*Thus a 1400 L glove box filter would be suffient.*										
Spent Electrolyte Holding Tank													
Volume of slurry from tank filter	5817.44	L											
Wash water introduced to glove box	300.00	L											
Design factor	150%												
Spent electrolyte holding tank volume	9176.163	L	*Thus an 10000 L GRP tank would be sufficient.*										
Required pumping flowrate	1272.73	L/h											

OPEX ESTIMATION				
Cu Production				
Cu feed rate	22.40	kg/h		
Targeted Cu Recovery	95%			
Cu production	186 412.80	kg per annum		
LME Cu price	$ 7 200.00	USD/t	*http://www.lme.com/en-gb/metals/non-ferrous/copper/*	
ZAR:USD exchange rate	11.08	ZAR/USD	*As on 8/02/2014*	
Cu product value	R 14 871 268	ZAR per annum		
Electrical Energy Cost				
Overall Specific Energy Consumption	12.37	kWh/kg Cu	*From experimental testwork*	
Electrical Energy Consumption	2 305 926	kWh per annum		
Electrical Energy Price	R 1.20	ZAR/kWh	*Assumed*	
Electrical Energy cost	R 2 767 112	ZAR per annum		
Utility Cost				
Volume of electrolyte per cell	1839.15	L per cell		
Volume of wash water per cell	100.00	L per cell		
Volume of wash water to FL-02	100.00	L per 3 cells		
Wash water requirement	0.0725	L/L electrolyte		
Volume of electrolyte treated	6 540 800.00	L per annum		
Volume of wash water	474 190.74	L per annum		
Process water price	R 0.00629	ZAR/L		
Process water cost	R 2 982.66	ZAR per annum		
Labour Cost				
Operators required for plant	1	operators		
No of shifts per day	4	shifts		
Operator salary + benfits	R 150 000.00	per annum		
Labour Cost	R 600 000.00	per annum		
Maintenance Cost				
Electrode cost	R 10 538.57	per electrode		
No. of electrodes	33			
Electrode lifetime	5	years		
Electrode replacement cost	R 69 554.59	per annum		
Operating Cost	ZAR per annum			
Electrical Energy Cost	R 2 767 112			
Utility Cost	R 2 983			
Labour Cost	R 600 000			
Maintenance Cost	R 69 555			
Other	R 343 965			
Total	**R 3 783 614**			

ECONOMIC EVALUATION

Cu Production				
Cu feed rate		22.40	kg/h	
Targeted Cu Recovery		95%		
Cu production		186 412.80	kg per annum	
LME Cu price	$	7 200.00	USD/t	http://www.lme.com/en-gb/metals/non-ferrous/copper/
ZAR:USD exchange rate		11.08	ZAR/USD	*As on 8/02/2014*
Cu product value	R	14 871 268	ZAR per annum	
Ni Production				
Ni feed rate		7.47	kg/h	
Targeted Ni Recovery		95%		
Ni production		62 137.60	kg per annum	
LME Ni price	$	14 105.00	USD/t	http://www.lme.com/en-gb/metals/non-ferrous/nickel/
ZAR:USD exchange rate		11.08	ZAR/USD	*As on 8/02/2014*
Ni product value	R	9 711 075	ZAR per annum	
CAPEX				
Electrochemical Process	R	15 941 342		
Solids Handling	R	3 188 268		*Assumed 20% of CAPEX for electrochemical process*
Total CAPEX	**R**	**19 129 610**		
OPEX				
Electrochemical Process	R	3 783 614	per annum	
Solids Handling	R	756 723	per annum	*Assumed 20% of OPPEX for electrochemical process*
Total CAPEX	**R**	**4 540 336**	per annum	
Discount rate		11.50%		

End of Year	Non-Discounted Cash Flow	Discounted Cash Flow	Cum. Disc. Cash Flow
0	0	0	R -
1	R -19 129 610	R -19 129 610	R -19 129 610
1	R -8 798 679	R -7 891 192.31	R -27 020 803
2	R -3 633 213.90	R -2 922 410.59	R -10 813 603
3	R 6 697 717	R 4 831 724.91	R 1 909 314
4	R 17 028 648	R 11 017 440.23	R 15 849 165
5	R 27 359 579	R 15 875 780.18	R 26 893 220

NPV	R	26 893 220	
IRR		37.6%	
Period		5	years